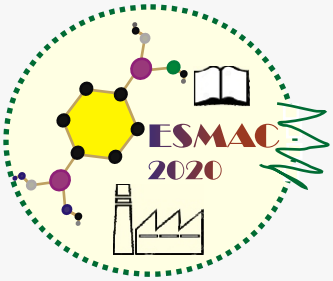

Proceedings of

International Conference

on

Emerging Smart Materials in Applied Chemistry (ESMAC-2020)

10th - 12th August, 2020

Venue:

KIIT Deemed to be University,
Bhubaneswar, Odisha, India

Editors:

Dr. Rojalin Sahu
Dr. Sanjoy Kumar Maji
Dr. Raghabendra Samantray

Advisory Committee

Chief Patron

Prof. (Dr.) Achyuta Samanta
Hon'ble Founder, KIIT & KISS

Patron

Dr. Subrat Kumar Acharya
Hon'ble Pro-Chancellor, KIIT Deemed University

Prof. H. Mohanty
Hon'ble Vice-Chancellor, KIIT-Deemed to be University

Prof. Sasmita Samanta
Hon'ble Pro-Vice Chancellor, KIIT-Deemed to be University.

Prof. J. Mohanty
Registrar, KIIT-Deemed to be University.

Organizing Committee

Convener

Dr.Rojalin Sahu, Chemistry, KIIT-Deemed to be University.

Co-Conveners

Dr.Raghabendra Samantaray, Chemistry, KIIT-DU

Dr.Sanjoy Maji , Chemistry, KIIT-Deemed to be University

Invited Speakers

Prof. S. N. Mishra, (Dean), IISER, Berhampur

Prof. Himanshu Biswal, NISER, Bhubaneswar

Suresh Dasari, Deputy General Manager, Daimler India

Prof.Indranil Bhattacharya, Director of SOLBAT-TTU Energy Research Laboratory , Tennessee Tech University, United States

Prof.Zhenxing Wang, Whuan national high magenetic field, Huazhong university of science and technology center, china

Prof. Ruey-an Doong ,National Tsing Hua University, Taiwan

Prof. Achintya Bezbaruah, Director, NAE Grand Challenges Scholars Program at NDSU,NDSU, Fargo

Prof. Anjali Pal, Professor, IIT Kharagpur

Dr Tapan Kumar Rout, Principal Scientist and Project Leader at Tata Steel, Kalinga Nagar

Dr. B. P. Biswal, Scientist, Nanochemistry, Max Planck Institute For Solid State research, Stuttgart, Germany

Prof. S. Arya, Professor, NIT, Surathkal

Dr. S. P. Mishra,Naval Materials Research Laboratory, Defence Research and Development Organisation (DRDO)

Local Organising Committee

Dr. D. Behera, KIIT Deemed to be University

Dr. J. Sinha, KIIT Deemed to be University

Dr. Samaresh Jana, KIIT Deemed to be University

Dr. Anita Pati, KIIT Deemed to be University

Dr. T. R. Sahoo, KIIT Deemed to be University

Dr. B. P. Sahoo, KIIT Deemed to be University

Dr. J. Tripathy, KIIT Deemed to be University

Dr. Sohini Sarkar, KIIT Deemed to be University

Dr. S. Singha, KIIT Deemed to be University

Dr. P. Deheri, KIIT Deemed to be University

Dr. A. Panda, KIIT Deemed to be University

Organising Secretaries

Dr. P. Rath, KIIT Deemed to be University

Dr. T. K. Bastia, KIIT Deemed to be University

Dr. B. B. Kar, KIIT Deemed to be University

Scientific Advisory Committee

Prof Gopal Kundu, Director, R&D, KIIT-Deemed to be University

Dr. Corey Thompson, Professor,Purdue University, USA

Dr. Haidong Zhou, Professor, University of Tennessee,USA.

Dr. Susan Latturner, Professor,Department of Chemistry &Biochemistry,Florida State University

Prof. J.Parida, Director, Quality Assurance Cell

Prof. T. K. Adhya, Professor, KIIT-Deemed to be University

Prof. M.Suar, CEO, KIIT TBI and Professor, KIIT-Deemed to be University

Dr. Subash Chandra Mallick
Director, LN INDTECH SERVICES PVT LTD

Dr. B. C. Tripathy
Principal Scientist, IMMT, Bhubaneswar

Dr. S. K. Tripathy, Associate Dean, KIIT Deemed to be University

Prof. A. R. Patnaik, Professor, KIIT Deemed to be University

Prof. P. Pattojoshi, Dean SAS, KIIT Deemed to be University.

Dr. K. G. Mishra, Professor, KIIT Deemed to be University

Dr. K. Parashar, KIIT Deemed to be University.

Dr. S.K.S Parashar, KIIT Deemed to be University.

Prof. S. Nanda, Professor, KIIT Deemed to be University

Prof. B.C. Guru, Professor, KIIT Deemed to be University

Prof. B. Mishra,Dean,Quality, KIIT Deemed to be University

Prof. S. Chakrabarty, KIIT Deemed to be University

International Conference on Emerging Smart Materials in Applied Chemistry (ESMAC-2020)
10-12th August 2020

10th August 2020 (Day-1)	
Technical Session-1	**Chairperson: Prof. K.G. Mishra**
9-9.30 AM	Invited Lecture-1 **Prof. Indranil Bhattacharya**, Director of SOLBAT-TTU Energy Research Laboratory , Tennessee Tech University, United States
9.30-10.00 AM	Invited Lecture-2 **Prof.Zhenxing Wang** Whuan National High Magenetic Field Huazhong University of Science and Technology center, China
10.15-10.45 AM	Invited Lecture-3 **Suresh Dasari**, Deputy General Manager, Daimler India
11-11.32 AM	**Inaugural Program**
11.35-12.05 PM	Invited Lecture-4 **Prof. S. N. Mishra**, IISER
12.05-12.35 PM	Invited Lecture-5 **Dr. S. P. Mishra**, Naval Materials Research Laboratory, Defense Research and Development Organisation (DRDO)
12.35-12.40 PM	Overview about online poster session by **Dr. A. Panda**
12.40-3 PM	Lunch break
2PM-3PM	Poster Session
Technical Session-2	**Chairperson: Dr. Samaresh Jana**
3-3.30 PM	Invited Lecture-6 **Dr. Suraj K. Tripathy**, Associate Dean, School of Chemical Technology, KIIT Deemed to be University
3.30-4 PM	Invited Lecture-7 **Dr. Tapan Kumar Rout**, TATA Steel, Kalinga Nagar
4-4.30 PM	Invited Lecture-8 **Dr. B. P. Biswal**, Scientist, Nanochemistry, Max Planck Institute For Solid State Research, Stuttgart, Germany
4.30-5 PM	Invited Lecture-9 **Dr. B. P. Sahoo**, KIIT Deemed to be University
11th August 2020 (Day-2)	
Technical Session-3	**Chair Person: Dr. Jatin Kumar Sinha**
9-9.30AM	Invited Lecture-10 **Prof. Ruey-an Doong**, NTUH, Taiwan
9.30-10 AM	Invited Lecture-11 **Dr. Prashant S. Alegaonkar** Associate Professor ,Department of Physics ,Central University of Punjab
10-10.30 AM	Invited Lecture-12

	Dr. S. Arya, Associate Professor, NIT, Surathkal
10:30-11:00 AM	Invited Lecture-13 **Dr. Asok Adak**, Associate Professor, IIEST, Shibpur
11:00-11:30 AM	Invited Lecture-14 **Prof. Anjali Pal**, Department of Civil Engineering, IIT Kharagpur
11.30-12.00 PM	Invited Lecture-15 **Prof. Himanshu Biswal**, School of Chemical Sciences, NISER, Bhubaneswar
12-2 PM	Lunch
2-3 PM	Poster
Technical Session-4	**Chair Person: Dr.Tapas Ranjan Sahoo**
3-3.30 PM	Invited Lecture-16 **Dr. Rabindra Kumar Behera**, Department of Chemistry, NIT Rourkela
3.30-4 PM	Invited Lecture-17 **Dr. Puspanjali Sahu**, Department of Materials Science and Engineering KAIST, South Korea
4-4.30 PM	Invited Lecture-18 **Dr. Kamala Kanta Nanda** Pontificia Universidad Católica de Chile
4.30-5 PM	Invited Lecture-19 **Dr.Chinmaya Mahapatra** Helmholtz zentrum Geesthach/Charité – Universitätsmedizin Berlin-BCRT
12th August 2020 (Day-3)	
Technical Session-5	**Chair Person: Dr. Kajol Parashar**
9:00-9:30 AM	Invited Lecture-20 **Prof. Achintya Bezbaruah,** Director, NAE Grand Challenges Scholars Program at NDSU, Fargo, USA
9:30-10:00 AM	Invited Lecture-21 **Dr. Partha Pratim Bag**, SRM, Sikkim
10.00-10.30 AM	Invited Lecture-22 **Dr. Jashobanta Sahoo**, IOCB, Czech Republic
Technical Session-6	**Chair person: Dr. Anita Pati**
10.30-10.45 AM	OP-1: Saismrutiranjan Mohanty
10.45-11.00 AM	OP-2: Dr. Reena Singhal
11.00-11.15 AM	OP-3: Dr. Niladri Maity
11.15-11.30 AM	OP-4: Dr. Mainak Ghoshal
11.30AM -11.45	OP-5: Amrit Kumar
11.45AM -12.00	OP-6: Kanyanjali Samal
12.00 -12.15 PM	OP-7: Dr. Naresh Kumar Sahoo
12.15 -12.30 PM	OP-8: Dr. Mukti Kant Panigrahi
12.30-1.00PM	Valedictory

Message

I am delighted to know that the Department of Chemistry, School of Applied Sciences, KIIT Deemed to be University, Bhubaneswar is going to bring out the proceedings of the International Conference on Emerging Smart Materials in Applied Chemistry (ESMAC - 2020), organised at virtual platform from 10th - 12th August 2020. I commend the Department of Chemistry, School of Applied Sciences for taking initiative to conduct this important academic meet despite a challenging situation due to the Covid-19 pandemic.

It reflects KIIT Deemed to be University's resolve to adapt to the "new normal" and continue its journey towards excellence. It is heartening that the meet was well attended by academicians, researchers, industry experts and scholars from all parts of the world. On behalf of KIIT and on my personal behalf, I express gratitude to them for making the conference a grand success. I am sure the proceedings, compiling the deliberations, will be useful for the academic community and industry alike; and pave way for future research and innovation.

I take this opportunity to congratulate the organizing team of this important event and wish them success in their future endeavours.

(Dr. A. Samanta)
Founder, KIIT & KISS

Message

I am delighted to note that the Department of Chemistry, School of Applied Sciences is organizing an International Conference on "Emerging Smart Materials in Applied Chemistry (ESMAC-2020)". It is my pleasure to welcome all the participants of this conference.

Materials, in many forms, play an important role in day to day activities of humans. Both academics and industries work relentlessly to meet these needs by designing new materials for applications. In this regard, it is much essential to create an ecosystem where researchers from academics and industries come together on the same platform with a common goal to strengthen the materials research for application in the field of environment, energy, industries and related streams, thereby, contributing to the development of the nation as well as humanity.

I wish the conference to succeed in providing a vibrant platform for the participants to brainstorm on the various thrust areas of the conference.

Prof. Hrushikesha Mohanty
Vice-Chancellor,
KIIT-Deemed to be University

Message

I am delighted to note that the Department of Chemistry, School of Applied Sciences is organizing an International Conference on "Emerging Smart Materials in Applied Chemistry (ESMAC-2020)".

I am confident that this conference will create an ecosystem where researchers from academics and industries come together on the same platform with a common goal to strengthen the materials research for the application in the field of environment, energy, industries and related streams, thereby, contributing to the development of the nation.

I congratulate the organizing team and wish the conference a great success.

Prof. Sasmita Samanta
Pro-V ice Chancellor,
KIIT-Deemed to be University

Message

It is indeed a matter of great pleasure that the Department of Chemistry, School of Applied Sciences, KIIT Deemed to be University is organized a International Conference, Emerging Smart Materials in Applied Chemistry (ESMAC)-2020 with a aim of create industry academia ecosystem towards fundamental design and application of materials.

Today when the whole world is suffering from the COVID 19 pandemic, we at KIIT Deemed to be University envisions to enrich education.
I hope this conference will act as a platform for nurturing research and academic discussion in the areas of Applied Chemistry and it will be beneficiary to the emerging Young Scientists.

I extend my best wishes to all participants for a grand success of this conference and congratulate the team for their excellent endeavour.

Wishing the team, all success.

Prof. Jnyana Ranjan Mohanty
Registrar,
KIIT-Deemed to be University

Message

I am extremely happy to note that the Department of Chemistry, School of Applied Sciences is organizing an International Conference on "Emerging Smart Materials in Applied Chemistry (ESMAC-2020)"on 10-12th August 2020.

I am very sure that this conference will inculcate the research culture among the research scholars and the faculty members of our university. It will also trigger interactions among researchers from academics and industries to exchange the ideas of recent advances in the areas of material science.

I wish the conference a grand success.

Sudarsan Nanda
Head, CIR
KIIT-Deemed to be University

Message

I am happy to know that the Department of Chemistry, SAS, KIIT University is going to organize two-day international-level conference on "Emerging Smart Materials in Applied Chemistry (ESMAC-2020)" on 10-12th August 2020.

This meet of scientists, academicians, Industry personnel, young researchers and students from allied disciplines are very crucial to solve many different challenges of Humanity as well as from socio-economic perspectives including quest of knowledge. I am confident that the deliberations will focus on smart outcomes and possibly make it an annual interaction to create that powerful mass translating to required energy to make the country self reliant.

I take this opportunity to congratulate the organizing team of this important event and wish the conference a grand success.

Dr. Puspalata Pattojoshi
Dean SAS,
KIIT-Deemed to be University

Message

Department of Chemistry, School of Applied Sciences is organizing the International Conference on "Emerging Smart Materials in Applied Chemistry (ESMAC-2020)". On behalf of the organizing committee I welcome all the invited speakers and delegates to this virtual conference.
The conference provides platform for researchers to get networked and exchange the ideas for further progress in research and development in material science. Researchers both from academia and industries come together on the same platform to share and enrich knowledge on this topic.

Our University extends helping hands for such initiatives and provides resources to make the conference a success. My sincere thanks to our Founder, Prof. Achyuta Samanta, Vice Chancellor, Prof. Hurshikesh Mohanty, Pro-Vice Chancellor, Prof. Sasmita Samanta, Registrar, Prof. Jnana Ranjan Mohanty, Dean, Prof. P. Pattojoshi and all delegates, organizers, my supportive colleagues and student members.

I wish all the conference participants and organizers a big success!

Rojalin Sahu

Dr. Rojalin Sahu
Convener
KIIT-Deemed to be University

Message

It was a proud moment for all of us to complete the international conference "Emerging Smart Materials in Applied Chemistry, ESMAC 2020", without a glitch. Heartiest congratulation for our success. I and the team of organising committee congratulate all the participants for their patient involvement in this scientific function where we cherished our effort, shared it, enriched our knowledge on materials, and much more.

Achievements in work is exciting but sharing the experience with the world is even more invigorating. In science, we realise this through publications and seminar presentations. In this regard, ESMAC 2020 was a great platform for all the material scientists and engineers from all over the world to share their hard work to almost one thousand participants.

We hope more of this in the near future, and firmly believe that more success are yet to come.

hank you for giving me an opportunity to be a part of this conference as a convener.

Dr. Raghabendra Samantaray
Asst. Professor,
KIIT Deemed to be University.

Message

It is my pleasure as a co-convenor of our first International conference "1st International Online Conference on Emerging Smart Materials in Applied Chemistry (ESMAC-2020) 10-12 August 2020" well come you all to share the novel ideas among us in the virtual platform. It gives me immense pleasure to work with Dr. Rojalin Sahu and Dr. Raghabendra Samataray. I am also happy to share my sincere gratitude to all of my colleagues of the Chemistry Department KIIT, DU for their endless support to conduct the conference.

I am also happy to share my sincere gratitude to all the respectable speakers for their delivers in the different fields in the present scenario developing the new materials/precursors and their application in the different areas of environment and medicinal fields. The achieved great success of ESMAC-2020, motivates us to continue it in future.

On behalf of organizing committee, I express my deep sense of gratitude to our Esteemed Founder, Vice-Chancellor, Pro-Vice Chancellor, Registrar, Dean (SAS), Head of the Department of Chemistry for their support to make it a successful event.

I am grateful to all the delegates, faculties, supporting staffs, students and participants for their cooperation. Wish you all have a nice time during this conference.

Dr. Sanjoy Kumar Maji
Co-convener,
ESMAC-2020

Message

It is a great pleasure for me that the Department of Chemistry, School of Applied Sciences is organizing the 1st International Conference on "Emerging Smart Materials in Applied Chemistry (ESMAC-2020)". On behalf of the organizing committee I welcome all the invited speakers and delegates to this virtual conference.

Materials are important to mankind because of the benefits that can be derived from the manipulation of their properties. Smart materials, also called intelligent or responsive materials, are designed materials that have one or more properties that can be significantly changed in a controlled fashion by external stimuli, such as stress, moisture, electric or magnetic fields, light, temperature, pH, or chemical compounds. The demand of such materials is increasing day by day.

Keeping this fact in mind, I am confident that such type of conference will bring people from both academics and industries together to conceive new ideas for development of smart materials for different applications. Being Organizing secretary, I wish a grand success of this virtual conference.

Namaskar

Prasanta Rath

Dr. Prasanta Rath
Organizing Secretary,
KIIT-Deemed to be University

Message

CONFERENCE ON EMERGING SMART MATERIALS IN APPLIED CHEMISTRY

Department of Chemistry, School of Applied Sciences, conducting a Conference of International repute with an extensive thematic area on "Emerging Smart Materials In Applied Chemistry". Chemistry has always spread its wings in all possible aspects to provide service to mankind. With the gradual advancement of scientific temperaments, smart materials are capable of solving many a problems associated with day to day life. This conference will its diversified themes will definitely provide a great platform to all academicians, industrialists, researchers and scholars to have a finite base and interactive sessions to have a solid background for research and promotion. Smart materials getting emerged to applied chemistry has generated many wonders for the recent era and this kind of a virtual interactive session will definitely bond many researchers of similar interest to have collaborative works.

This conference is the brain child of my colleague Dr. Rojalin Sahu, who initiated the theme and the programme with all possible efforts. In the present scenario, with the ongoing pandemic situation, several huddles arise to conduct such a conference in huge scale. But myself being a part of this event congratulate and extend my heartfelt thanks to my esteemed colleagues for their endless effort to make the conference successful.

Our University is always supportive for such initiatives and provides all possible means to make the program successful. My sincere thanks to our Founder sir Dr. Achyuta Samanta, Vice Chancellor Dr. Hurshikesh Mohanty, Pro Vice chancellor Dr. Sasmita Samanta, Registrar Dr. Jnana Ranjan Mohanty, all esteemed delegates, organizers, my supportive colleagues and student members.

Wish all success to ESMAC-2020!

Biswabandita Kar

Dr. Biswabandita Kar
Organizing Secretary,
KIIT-Deemed to be University

Message

It gives me immense pleasure that Department of chemistry ,School of Applied Sciences is organizing an international conference on “Emerging smart materials in applied Chemistry “(ESMAC-2020).On behalf of the organizing committee I welcome all the delegates and participants to this virtual event .

In this modern era, materials and specifically smart materials are having diversified applications .Everywhere in day to day life we come across the smart materials .So this conference is of immense justification .Again another matter of happiness is that the proceedings will be published online in scopus indexed journal .All the academicians and researchers will definitely be enlightened through this .

Being the organizing secy. ,I wish a grand success of this virtual conference .

Namaskar

Dr.Tapan Kumar Bastia
Organizing Secretary

1st International Online Conference on Emerging Smart Materials in Applied Chemistry(ESMAC-2020)
10-12 August 2020

Paper ID: 1

Quantum Yield Analysis for Hydrothermally Reduced $Cd(II)Cl_2$ doped Graphene Quantum Dots

Poonam R. Kharangarh[a*], and Vinay Gupta[a]

[a]Department of Physics and Astrophysics, University of Delhi, Delhi-110007, India,

Email: poonamkharangarh@gmail.com

***Abstract*—This paper reports about the research related to Graphene Quantum dots (GQDs) which have been attracted considerable attention in recent years due to the size, edge effects, quantum confinement and heteroatom doping. The doping of graphene based materials can effectively tune their intrinsic properties, including electronic and optical properties, surface and local chemical reactivity. Herein, we were successfully synthesized $Cd(II)Cl_2$ doped GQDs by using a facile, and environment friendly hydrothermal treatment by using less expensive $CdCl_2$ powder and Graphene Oxide (GO) as a precursor materials. All the synthesized materials were characterized by UV-Visible Spectroscopy (UV-Vis), Raman Spectroscopy, and Photoluminescence (PL). The morphological characterizations were confirmed by transmission electron microcopy images (TEM). The hydrothermally synthesized material had a size of 5-20 nm by uniform doping of $CdCl_2$ nanoparticles on graphene sheet.**

***Keywords*—Graphene Quantum Dots, Cadmium Chloride Powder, Doping, Photoluminescence**

I. Introduction

Among graphene-based two-dimensional luminescent carbon nanomaterials,GQDs has attracted tremendous research interest because of its novel potential applications from Physics to Chemistry and biology nanoelectronic devices [1]. GQDs possess band gap with strong photoluminescence (PL), due to quantum confinement and edge effects.

A lot of research has been done by using different methods including microwave-assisted hydrothermal, Hydrothermal, Solvothermal and Sol. Gel method. The low Photoluminescence quantum yield (QY) (~ 7–44%) of the GQDs has been reported so far. After a lot of trials, Li et *al.*and coworkers demonstrated highly efficient solution-processed $CsPbBr_3$ quantum dot light-emitting diodes (QLED) through balancing surface passivation and carrier injection via ligand density control. Gu et *al.* have been used glucoseas precursor material to synthesize GQDs through a one-step hydrothermal method to make an improvement in QY. The GQDs demonstrated strong green PL with FL QY (~ 44.3%). These reported methods are limited by availability of expensive materials, different color emission and accessibility of special tools. Although several efforts have been reported, a comprehensive understanding of the optical properties of GQDs is still being explored.

In this work, we have demonstrated a relationship between the defect states and the quantum yield with extensive characterization in synthesized $Cd(II)Cl_2$-GQDs.A facile hydrothermal treatment was used to synthesize $CdCl_2$doped-GQDs by combining graphite powder and $CdCl_2$ powder, The synthesized sample demonstrated excellent solubility in water, intense blue emission and high FL QY (45.8%).

II. Materials and Methods

A. Reagents

Graphite powder (Graphite India), $NaNO_3$ (98%, Sigma Aldrich), $KMnO_4$, (97%, Sigma Aldrich), KOH (≥85%, Sigma Aldrich), 30% H_2O_2 (Sigma Aldrich), and HCl ((≥99%, Sigma Aldrich), $CdCl_2$ powder (99.998%, Alfa Aesar) were used as received. Double-distilled water (ρ=18.2 MΩ·cm) was used for all experiments during the preparation of GO and $CdCl_2$ doped GQDs.

B. Preparation of GO, GQDs and Cd(II)Cl_2GQDs

For preparation of Cd(II)Cl_2-GQDs, the same procedure was used as brief in our earlier work [2-4].Graphite powder was converted into graphite oxide in accordance with the procedure described by Hummers and Offemann [5-7]. In a typical synthesis, 5.95mg of $CdCl_2$ were dissolved in 10 ml of GO solution & 10 ml of deionized (DI) water with stirring for 30 min and sonicate for another 30 min. The final solution was then transferred into a Teflon lined autoclave and heated at 150^0C for 6 h by hydrothermal treatment. Furthermore, this solution was naturally brought down to room temperature and subsequently theCd(II)Cl_2-GQDs were collected by filtration through a 0.22 μm Teflon membrane.

Results and Discussion

C. Optical Study

Raman Spectroscopy is a powerful and non-destructive tool to investigate the optical studies of GO, GQDs and Cd(II)Cl_2-GQDs. The Raman spectra of GO, GQDs and Cd(II)Cl_2-GQDs is shown in Fig. 1. The samples GO, GQDs and Cd(II)Cl_2-GQDs display a strong D peak located at 1356 cm^{-1} respectively. The G band in GO and GQDs is formed at 1590 cm^{-1} respectively; while the peak in Cd(II)Cl_2-GQDs was observed at 1609cm^{-1}.

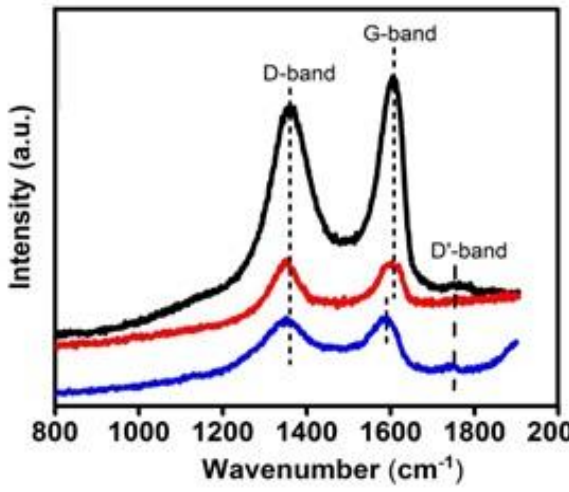

FIGURE 1.Raman spectra of GO (Black curve), GQDs (Red curve), and Cd(II)Cl_2-GQDs (Blue curve)

The shift in G band of Cd(II)Cl_2-GQDs might be due to the presence of induced defects. The observed shift in G band in Cd(II)Cl_2-GQDs towards higher frequencies compared to GO and GQDs is due to the presence of various functional groups resulting in more structural defect states. The intensity ratios (I_D/I_G) of 0.91, and 1.01, and 0.98 were observed for GO, GQDs and Cd(II)Cl_2-GQDs, respectively. The observed intensity ratio of GQDs is higher than that of GO but this ratio for Cd(II)Cl_2-GQDs is lower than that of GQDs.

III. Conclusion

In summary, we have synthesized Cd(II)Cl_2doped GQDs with tunable PL by using a facile hydrothermal method with $CdCl_2$ powder as a low-cost source material. The doped GQDs exhibit strong purple PL under the lower excitation UV light from 280nm to 340nm. It is inferred that the surface defect states that led to the band-gap variation played a significant role in the PL of GQDs with cyclic aromatic hydrocarbon-like conjugated structure. Nevertheless, the reported different synthesized methods with high quantum yield will be suitable for large-scale production.

IV. ACKNOWLEDGMENTS

The financial support for this work was provided by "Department of Science & Technology" (DST), New Delhi under "Women Scientist Scheme A" (WOS-A) (SR/WOS-A/PM-107/2017. The authors thank to EMDL Lab members in University of Delhi for facilitating us in many characterization.

References

[1] P. Tian, L. Tang ,, K.S. Teng, S.P. Lau, "Graphene quantum dots from chemistry to applications", Materials Today Chemistry, vol. 10, pp221-258, 2018.

[2] P. R. Kharangarh, S. Umapathy and G. Singh, "Effect of Defects on Quantum Yield in Blue emitting Photoluminescent Nitrogen doped Graphene Quantum Dots", Journal of Applied Physics, 122, 145107 (1-7), 2017.

[3] P. R. Kharangarh, S. Umapathy and G. Singh, "Investigation of sulfur related defects in graphene quantum dots for tuning photoluminescence and high quantum yield", Applied Surface Science, 449, 363-370 (2018).

[4] P. R. Kharangarh, S. Umapathy and G. Singh, "Thermal Effect of Sulfur doping for Luminescent Graphene Quantum Dots", ECS Journal of Solid State Science and Technology, 7(3), M29-M34 (2018)

[5] W. S. Hummers Jr and R. E. Offeman, J. Am. Chem. Soc., 80, 1339 (1958).

[6] PreetamBhardwaj, Shalu Singh, Poonam R. Kharangarh, Andrews Nirmala Grace, Surfactant decorated polypyrrole-carbon materials composites electrodes for supercapacitor, Diamond & Related Materials, 107 (2020) 107989.

[7] P.R Kharangarh, V.Gupta, A. Singh, P. Bhardwaj, A.N. Grace, Diamond and Related Materials,107913 (2020).

1st International Online Conference on Emerging Smart Materials in Applied Chemistry(ESMAC-2020)
10-12 August 2020

Paper ID: 2

An effective adsorption of Congo Red Dye from aqueous solution using TiO_2 nanoparticles: Kinetics, Thermodynamics and Isothermal Studies

B. Priyadarshini[1], T. R. Sahoo[1,*]

Department of Chemistry, School of Applied Sciences, KIIT Deemed to be University, Bhubaneswar 751024, India
** Corresponding author: Email: trsahoofch@kiit.ac.in*

Abstract. TiO_2 nanoparticles have been synthesized by co-precipitation method and are used as an adsorbent for removal of toxic Congo Red (CR) dye. The resulting adsorbent TiO_2 was characterized by X-ray powder diffraction pattern, confirming the rutile phase of TiO_2 nanoparticle. Adsorption equilibrium data were evaluated by Langmuir isotherm and Freundlich adsorption isotherm. The kinetic data were analyzed using pseudo-first order, pseudo-second order and intraparticle diffusion equations. Kinetics result revealed that the adsorption of CR is of pseudo second-order and chemisorption type. Thermodynamic parameters such as ΔG^o, ΔH^o and ΔS^o were calculated and the positive value of ΔH^o (2.64 $kJmol^{-1}$) corresponds to an endothermic nature of the adsorption process and the positive value of ΔS^o (0.162 $Jmol^{-1}K^{-1}$) reveals the increased randomness of the dye during adsorption process.

1. INTRODUCTION

Dyes are the class of coloured organic compounds which are toxic in nature as well as resistant to the action of water. A recent study shows that more than a million dyes are available in market and nearly one million ton per annum are produced, whereas 20% of dyes are released to environment through natural resources as dyes effluent [1]. The production of dyes increases day by day to fulfill the needs of growing population which also increases the release of dye stuffs as waste product. The disposal of colored wastes into water leads to think about the waste water treatment process. This is because the discharge of colored wastes is not only damaging to the aesthetic nature of the receiving streams but also toxic to aquatic life and even carcinogenic or mutagenic in nature. Congo Red dye is a benzidine based anionic azo dye which is used in dyeing cotton and other industrial purpose like it is used in rubber, paper and plastic industries [2].

Among a lot of different conventional methods, adsorption is an effective method due to the possibility of reusing the spent adsorbent via desorption [3]. Apart from this, it is also eco-friendly, simple and highly efficient. Metal oxide nanoparticles have shown a great potential for the adsorption of toxic dyes through adsorption process.

Among all metal oxide nanoparticles, titanium dioxide nanoparticles is a potential adsorbent for removal of toxic dyes due to its good surface physical and chemical property. TiO_2 nanoparticles are favorable for adsorption of toxic dyes due to the stability of its chemical structure, biocompatibility, strong oxidizing power and non-toxicity. In this article, we have studied the use of TiO_2 nanoparticles
for the removal of Congo Red (CR) dye, which is majorly used for dyeing silk, wool, nylon multi fibers etc., mainly focusing on the adsorption kinetics, thermodynamics and isotherm studies.

II EXPERIMENTAL

A. Synthesis

TiO_2 nanoparticles were synthesized by co-precipitation method. In a typical reaction 100 ml of distilled water was taken in a conical flask and it was manually cooled to 4^0C using ice around the flask with continuous stirring (400rpm). Then 3ml of $TiCl_4$ was added drop wise and the reaction was carried out while covering the flask with aluminium foil for 1 hour under constant agitation mode. Later the solution was allowed for aging of 7 days and suspension formed was centrifuged, filtered and dried in

an oven at 60^0C over night. Subsequently, the powder obtained was further calcined at 300^0C for 1 hour.

B. Adsorption experiments

The material obtained was tested for adsorption of dyes in 100ml flask containing 50ml of dye solution. The experiments were done with different operational parameter such as amount of adsorbent, agitation speed, pH, temperature and dye concentration. About 1ml of solution was pipetted out in regular interval during the experiment and centrifuged to remove the solids from solution. The clear solution was analysed using double beam UV–Vis spectrophotometer at respective absorbance maxima.

III. RESULTS AND DISCUSSIONS

A. Characterization of TiO_2

The XRD pattern of the synthesized TiO_2 nanoparticles is shown in figure 1(a). The peaks at 2θ values 27.4^0 (110), 36.1^0 (101), 54.3^0 (211) and 41.2^0 (111) confirm the rutile phase of TiO_2. The experimental XRD pattern agrees with the JCPDS card No. 76-1940 of TiO_2 nanoparticles. The intensity of the XRD peaks of the sample reflects the crystalline nature of TiO_2 particles and broad diffraction peaks indicate very small crystallite size. By using Scherrer equation, the average crystallite size of TiO_2 particles is found to be 13.34 nm, which signifies that the particles are nanoparticles. The high magnification SEM image of the prepared powder sample is displayed in figure 1(b). The average grain size is found to be in the range 30-45 nm. The sizes of the particles are fairly small which reveal the formation of uniform TiO_2 nanoparticles.

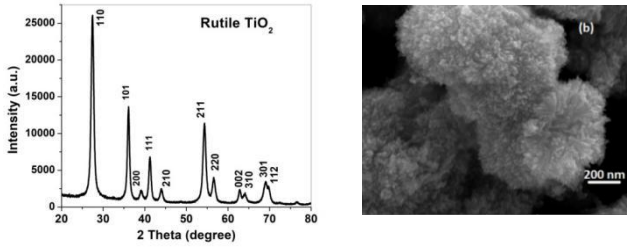

FIGURE 1. (a) XRD pattern a n d (b) SEM of TiO_2

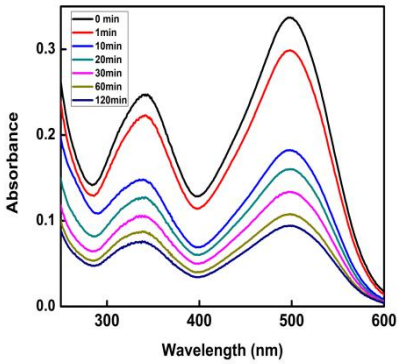

B.

FIGURE 2. Decrease in intensities of CR dye

Kinetics, Thermodynamics and Adsorption Isotherm of CR onto TiO_2

A batch of adsorption processes of CR was studied by using TiO_2 nanoparticles as adsorbents from aqueous medium, varying the adsorption parameters such as: the effect of pH, temperature, amount of adsorbent, initial concentration of dye, contact time, and shaking speed. The maximum efficiency of adsorption by TiO_2 was found to be at slightly acidic (pH~5.4) at room temperature (298K) with initial dye conc of 25ppm using 20mg of TiO_2 nanoparticle. Fig. 2 shows the decrease in intensity of the CR dye at optimum condition.

To know the mechanism of adsorption behaviour of CR with TiO_2 NPs, the pseudo–first order and pseudo–second order models have been studied. The correlation coefficient value R^2 for both the models are 0.940 and 0.982 respectively. From the study, the pseudo–second order model provides better correlation of adsorption than the pseudo–first order model.

Adsorption of CR was investigated at the temperature range of 293-333 K where other parameters were: adsorbent dose 20 mg, agitation speed 200 rpm, concentration 25 mg/L and pH 5.4. It was seen that the adsorption of dyes on TiO_2 NPs goes on increasing with increase in temperature of the solution from 293 to 333 K.

The value of ΔH^o and ΔS^o were calculated from the slope and intercept of the plot logKc Vs 1/T, based on the Vant Hoff relationship as shown in Fig 3 (a) and (b).

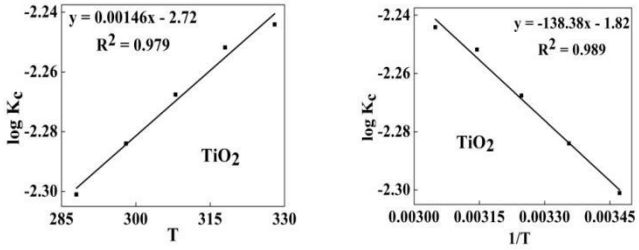

FIGURE 3. (a) Equilibrium constants for CR on TiO_2 as function of temperature (b) Van't Hoff plot for adsorption of CR with TiO_2.

The values of ΔH^o and ΔS^o were calculated from the slope and intercept, respectively. The negative value of ΔG^o (-7.15, -7.49, -7.83, -8.17, -8.51 for temperatures

293K, 303K, 313K, 323K and 333K respectively) indicates a feasible adsorption process and a spontaneous interaction of dye ion with active sites of the adsorbent. The positive value of ΔH^o (2.64kJmol^{-1}) corresponds to an endothermic nature of the adsorption process and the positive values of ΔS^o (0.162 Jmol^{-1}K^{-1}) shows the increased randomness of the dye and adsorbent at interface during adsorption process.

To determine the equilibrium behaviour between the adsorbent and adsorbate, Langmuir and Freundlich isotherm studies were performed. The correlation coefficient (R^2) of Langmuir isotherm model was found to be (0.957), not well fitted to the experimental data in comparison with Freundlich isotherm model which proves the surface of the material is heterogeneous in nature. From this experimental data, the value of 1/n (1.031) is found to be less than 10 and higher than unity, which reveals favorable condition for adsorption process.

IV.CONCLUSION

TiO_2 nanoparticles were successfully synthesized by co-precipitation method. X-ray powder diffraction pattern confirmed the rutile phase of TiO_2 nanoparticles. The positive value of the thermodynamic parameter ΔH^o (2.64 kJmol^{-1}) proves that the adsorption process was endothermic in nature and the positive values of ΔS^o (0.162 Jmol^{-1}K^{-1}) reveals the increased randomness of the dye during adsorption process. Experimental equilibrium data showed best fit with Freundlich isotherm (R^2= 0.98). The kinetics result showed that the adsorption of CR is of pseudo second-order and chemisorptions type.

REFERENCE

[1] B:Environmental, 211, 31-45 (2017).G. Akkaya Sayğılı, *J. Mol. Liq.*, **211**, 515-526 (2015).

[2] A. Ahmad, S. H. Mohd-Setapar, C. S. Chuong, A. Khatoon, W. A. Wani, R. Kumar and M. Rafatullah, *RSC Adv.*, **5**, 30801-30818 (2015).

[3] P.P.Rath, S.S.Behera, B Priyadarshini, S.R.Panda, D.Mandal, T.Sahoo, S.Mishra, T.R.Sahoo, P.K.Parhi, *Applied Surface Science* **491,** 256-266 (2019).

1st International Online Conference on Emerging Smart Materials in Applied Chemistry(ESMAC-2020)
10-12 August 2020

Paper ID: 3

Influence of Mg doping on ZnO NPs for enhanced adsorption activity of Congo Red dye

Tanaswini Patra, T. R. Sahoo'*

Department of Chemistry, School of Applied Sciences, KIIT Deemed to be University, Bhubaneswar 751024, India, trsahoofch@kiit.ac.in

Abstract. A facile microwave-assisted combustion method was adopted to synthesize pure ZnO and Mg-doped ZnO nanoparticles (NPs). The XRD pattern confirmed the presence of crystalline, cubic phase with fluorite structure of both the NPs. FESEM images revealed that the NPs are in nanoscale regime with irregular crystalline morphology having grain size ~18-45 nm. N_2 adsorption/desorption isotherms measured at -196^{o}C was of Type II, with limited hysteresis loops due to interparticle porosity. ZnO showed a good BET SSA value of 32 m^2g^{-1}. Adsorption study for removal of CR dye was done & Mg-doped NPs showed high loading efficiency than ZnO NPs. CR dye sorption follows Langmuir Isotherm with ZnO NPs whereas Freundlich isotherm with Mg-doped NPs & enhancement of sorption loading capacity (25 to125 mg g^{-1}) was observed by Mg-doped NPs. It followed pseudo second order kinetics. The negative value of ΔG^o (-6.32 to-12.26 $kJmol^{-1}$ at 288K-318K) and ΔH^o (-13.74 $kJmol^{-1}$) favours exothermic nature of adsorption.

Keywords: Congo Red; NPs; Mg-doped ZnO; Adsorption; Kinetics; Isotherm

I. INTRODUCTION

With passage of time, environmental pollution due to the contaminating industrial effluents has become a global concern. Effluents from the textile and dye industries include colored dyes having a large amount of suspended organic solid(s). The presence of these dyes even at trace concentration in the effluent (resulted from such industries) cause an increase in the COD and BOD [1], thereby affecting the metabolic processes of life including photosynthesis in aquatic systems. ZnO NPs are used for treatment of the effluent and contaminated water containing several dyes. Synthesis of ZnO and Mg-doped ZnO NPs were done through microwave-assisted combustion method, characterized by FTIR, FESEM and XRD. The process optimization and sorption chemistry for the removal of CR using both the undoped and the doped (Mg) ZnO was studied.

II. EXPERIMENTAL

C. Synthesis

Zinc nitrate ($Zn(NO_3)_2.6H_2O$) and glycine were mixed in a 100 ml beaker as per Oxidizer/Fuel ratio, in minimum quantity of distilled water. It was microwave-heated for 3 mins, at 800 Watt, frequency 2450 MHz. After 2-4 seconds ZnO was formed. In a similar way, 2% Mg-doped ZnO was synthesized using magnesium nitrate ($Mg(NO_3)_2.6H_2O$), zinc nitrate ($Zn(NO_3)_2.6H_2O$) and glycine as per O/F ratio and the resulting mixture was microwave-heated to form Mg-doped ZnO.

D. Adsorption experiments

The material obtained was tested for adsorption of dyes in 100ml flask containing 50ml of dye solution. For adsorption studies of ZnO NPs, experiments were conducted by varying agitation speed, pH, phase contact time temperature, sorbent dose and the CR concentration. Then, each filtrate sample was analysed for the CR concentration using a double beam UV-Vis spectrophotometer (Cary 60 Agilent Technology, USA) at wavelength of 496 nm. From the data adsorption isotherm, kinetics and thermodynamics were done to know the mechanism of adsorption.

III. RESULTS AND DISCUSSIONS

A. Characterization of ZnO &Mg-doped ZnO

The PXRD pattern of ZnO and its 2% Mg-doped NPs were analysed and is shown in figure 1(a). It confirmed that cubic wurtzite-type of ZnO structure which are crystalline. The average crystallite sizes of the undoped and 2% Mg-doped ZnO were found to be 38.9 nm and 24.5 nm, respectively.

In Fig. 1 (b), ZnO and 2% Mg-doped ZnO NPs had an average grain size in the range of 20–40 nm. A lower magnification image of ZnO NPs showed the formation of spongy aggregates with large alveoli (Fig. 2a), whereas Mg-doped ZnO images showed honeycomb like structure with hollow shells typical of materials obtained through combustion synthesis.

B. Application of metal oxide NPs for adsorption of CR

1. Influence of shaking speed

The CR adsorption behavior of the metal oxide (ZnO and Mg-doped ZnO) NPs were carried out by varying the shaking speed between 50 and 250 rpm. The aqueous boundary layer of the dye solution phase became thicker at

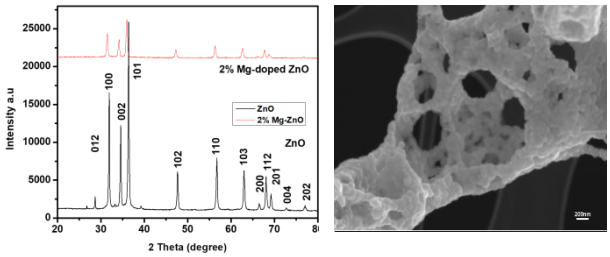

FIGURE 1. (a)XRD pattern (b) SEM of Mg doped ZnO

lower shaking speed and gradually became thinner as the rate of agitation increased. 200 rpm was found to be adequate for effective removal of CR from the aqueous phase.

2. Influence of time and CR concentration

The adsorption equilibrium of CR with ZnO NPs was attained after 300 min of contact time, whereas it was 180 min with Mg-doped ZnO NPs, a significant enhancement of reaction rate. The maximum loading capacity of both the NPs and the sorption study in the function of initial CR concentration was investigated by altering the range from 25 to 200 mg L^{-1} keeping other parameters (such as, pH 5.0, the dosage, temperature 298 K, and agitation speed 200 rpm) constant. The percent adsorption of CR with ZnO NPs followed a decreasing trend (89.99–25.76%). A similar trend (98.42–34.44%) was also observed with 2% Mg-doped ZnO NPs

3. Influence of pH

The effect of pH was studied between the acidic and alkaline range (4–11). The maximum adsorption capacity of CR at pH 5, may be attributed to the optimum dissociation of the dye CR at this acidity region (p*K*a = 4.1 at 25 ◦C).

4. Influence of doped and undoped ZnO NPs dosage

The percent sorption of CR increased while increasing both ZnO NPs and 2% Mg-doped ZnO NPs, attributable to the active and available sorption sites on the 'porous' NPs.as shown in figure 2. The adsorption efficiency as well as the rate of adsorption was relatively significantly improved in Mg-doped ZnO NPs.

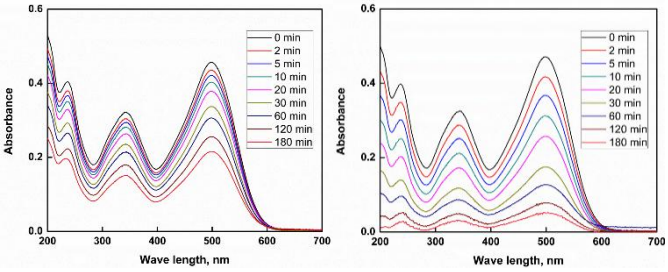

FIGURE 2. UV-Visible spectral analysis results for adsorption of CR onto the (a) ZnO NPs (b) 2% Mg-doped ZnO NPs

C. Kinetic, Thermodynamic and Adsorption studies

To establish the rate of controlling mechanism in adsorption, the kinetics of CR adsorption onto ZnO and the Mg-doped ZnO NPs are explained through two (i) pseudo-first order and ii) pseudo-second order) kinetic models [2]. The undoped and Mg-doped ZnO NPs showed strong fit to the intraparticle diffusion model ensuring multiple layer sorption mechanism.

The thermodynamic behaviour was investigated at varied temperatures (288–318K) at a constant pH. With an increase in temperature of the CR solutions from 288 to 318K, the adsorption capacity of NPs decreased (Fig. 3a,b). The value of Kc increased with increasing temperature (288–318 K). Thermodynamic parameters ΔG^o, ΔH^o and ΔS^o were calculated to determine the spontaneity of adsorption.

In this study, the R_L value for the adsorption of CR onto the undoped and Mg-doped ZnO NPs were found to be 0.299 and 0.996 respectively, for a CR concentration of 50 ppm at temperature 303 K, indicating that CR adsorption onto ZnO NPs phase is favorable [3]. The experimental data validated with the Freundlich isotherm model. The R^2 values for the adsorbent of Mg-doped ZnO NPs was found to be 0.999 indicating the best-fit for Freundlich adsorption model.

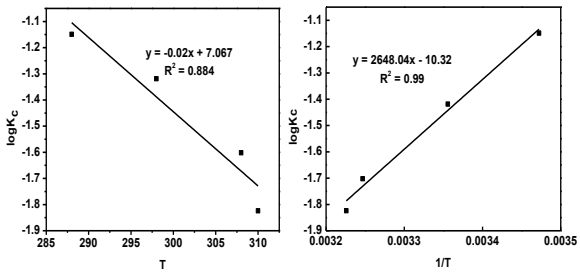

FIGURE 3. (a) Equilibrium constants for CR on Mg-ZnO as function of temperature (b) Van't Hoff plot for adsorption of CR with TiO_2.

IV.CONCLUSION

The ZnO NPs were synthesized by microwave-assisted combustion method. There is a stronger adsorption of the CR with 2% Mg-doped ZnO NPs. The CR adsorption was found to be efficient at pH 4.5 at a maximum loading capacity of 125 $mg.g^{-1}$. The CR adsorption study with both the NPs followed a pseudo-first order kinetics. Experimental equilibrium data best-fit with the Freundlich isotherm model indicating a multilayer adsorption of CR. Thermodynamic parameter ΔH^o (+13.74 and 50.7 KJ/mol) was determined confirming about the endothermic nature of adsorption using both the NPs. A positive ΔS^o (0.0614 and 0.198 $Jmol^{-1}K^{-1}$) value suggested an increased degree of freedom of adsorbed species. Mg-doped ZnO NPs can be applied as

a green pollutant abatement strategy for contaminated wastewaters in general.

REFERENCE

1.Bensalah, N., Alfaro, M.Q., Martínez-Huitle, C.A., Electrochemical treatment of synthetic wastewaters containing Alphazurine; A dye. *Chemical Engineering Journal*, *149*(1-3), pp.348–352.

2. Weber, W.J. and Morris, J.C., 1963. Kinetics of adsorption on carbon from solution. *Journal of the Sanitary Engineering Division*, *89*(2), pp.31–60

1st International Online Conference on Emerging Smart Materials in Applied Chemistry(ESMAC-2020)
10-12 August 2020

Paper ID: 4

Interaction of nano-carbons with transonic shock waves

Prashant S. Alegaonkar *

Department of Physics, School of Basics and Applied Sciences, Central University of Punjab, City Campus, Mansa Road, Bathinda 151 001, PB, India, E-mail:prashant.alegaonkar@cup.edu.in

***Abstract*—Interactions of transonic shock waves (speed ~ 1.1 Mach, pulse pressure > 1.5 GPa, duration ~ µs) with nano–carbons (NC) is reported. NC, grown via chemical vapour deposition technique, were die molded into cylindrical-form (thickness ~ 5 mm). These samples were subjected to variable–strain–rate (VSR) measurements by split Hopkinson pressure bar technique. Time variations in stress, strain, and strain rates were recorded to extract number of constructive parameters like sonic/shock impedance, work–hardening coefficient, elasto–plastic time, Hugoniot elastic limit, force movement, dislocation speed, shock damping coefficient, etc., usingnon-equilibrium-statistical–Hugoniot hydrodynamic model. Impacted NCs were examinedusing optical, electron microscopy, and Raman imaging. Broadly, incident strain energy disseminated by ~ 60-80% absorption loss and ~ 40-20 % transmittance with chemical modifications in NC. At molecular level, dynamic deformation dramatically modified the force constants with bond elongation @ –C–C– (by ~ 80%), and @ –C=C– (> 150%) compared to pristine. Details are presented.**

***Keywords*—Dynamic deformation, dislocation dynamics, phonon dispersion, signal processing, shock wave, nano–carbon**

V. Introduction

In strategic sector, the term shock waves from the blast is an important example of destructionyielding deformation in a medium. After the World War II, dynamic events in a medium have been extensively investigated. Time varying pressuresubjected onto a body is a dynamic process that leads to dynamic deformation that generates mechanical disturbance.Such stress wave propagates with characteristic velocities and amplitudes. Theyhave elastic, plastic, and shock characterstics depending uponamount of dynamic force and type of medium. Among them, shock waves, generated oblast, are lethal, capable to introduce shear instabilities, dynamic fracture, blast, fragmentation, perforation, and even explosion on their interaction with materials, however, have constructive aspect too! and capable of making chemical changes in certain materials (like graphite to diamond). Split Hopkinson pressure bar [SHPB] is an important experimental tool to simulate shock waves, at the laboratory level. [1] In this study, we addressed the questions: how shock waves interact with nano-carbon materials, what is structure and hydrodynamic changesin nano-carbons? And this is the central part of the discussion. Nano-carbons (NCs), after fabricating by chemical vapour deposition, were subjected to SHPB studies to obtain stress, strain, and strain rate parameters. Impaccted NCs were investigated using number of characterization studies. Collected shock wave signals after processing indicated variations and inter–dependence of shock parameters and provided insight into processes involved like flow hardening, phase transformation, physicochemical modifications, shock damping, phonon drag, etc. Details are presented.

VI. Materials and Methods

Synthesis of NCs was done bychoosing sugar cane waste; as precursor and subjected to chemical

vapour deposition (CVD), equipped with rapid thermal reactor. Precursor was covered intometallic enclosure, kept intoCVD reactor ata base pressure ~ 2 Torr with argon flow ~ 15 sccm with initial riseupto 200^{0}C finally to ~ 600^{0}C. The obtained carbon power was post treated to obtain final NC product [2].For HSR measurements, Al base (dim.: 10 (dia.) mm, ~ 5 (h.) mm) was fabricated on which NC samples were mounted.Specimenswere sandwiched between the bars. The projectile, which is a striker bar, is propelled towards the incident bar by the gas gun. Stresses generated are derived by measuring the strains produced by elastic wave at any point, as it propagates along the bars, using semiconductor strain gage rosettes bonded to both incident and transmitted bar. The gages are, electronically, connected to sensor instrument, data acquisition unit and processing system. NCs were recovered and subjected to characterizations.The sonicated samples along with the pristine NCs (termed as NCs) samples were subjected to various characterization techniques.The optical imaging was carried out at 100x magnifications in the transmission Fraunhoffer diffraction limited geometry in order to obtain information about thinnest specimen event at one atom layer thick. More than hundreds of images were taken together for NCs and HSR NCs, at various sites to collect damage statics.Raman measurements were performed at 532 nm photo-excitation, over region 200–3000 cm-1, at room temperature. Fourier transformed Infrared (FTIR) measurements were carried out over 400–4000 cm-1. Uv–visible spectroscopic investigations were done over 200–700 nm.

VII. Results and Discussion

A. Equation of state: Hugoniot constructionfor NCs(GNF and CNS)

In general, σ–ε curve is represented by a bilinear function in which first stage is elastic and second plastic. Figure 3(a) shows dynamic work hardening in elastic region in which CNS strength is high compared to GNF. σ, ε and strain rate, $\dot{\epsilon}$, dependent. For metal–like response, σ–ε is a power function shown in figure.

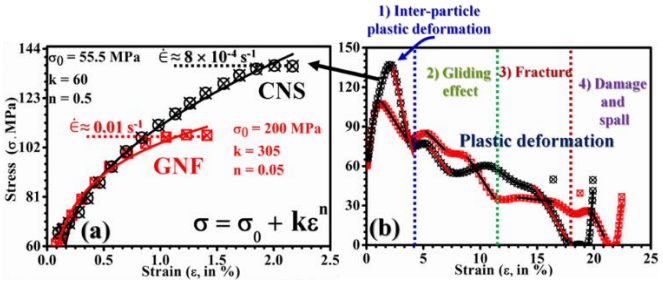

Fig.3: Stress (σ) vs strain (ε) curve for nano-carbons (a) elastic region showing power law based uniaxial extension and (b) plastic deformation. Liner fittings at various regions of curves are dσ/dε for evaluation of hydrodynamic parameters.

B. Signal Processing Study

The areal force is distributed, mostly, with non-uniformity. The distribution is obtained from force-time curve. In this, the force is appropriately transformed into F⁄A← P, where, A, is cross-section area for CNS ~ 100 nm^2 and GNF ~ 106 nm^2. The temporal variations are obtained through velocity estimations. For CNS low pressure areas are seen in discrete fashion with prominence. At some portions of CNS, high pressure regions (grey shed) are aligned in the direction of shock propagation followed by, gradient, appeared low magnitude pressure zones.

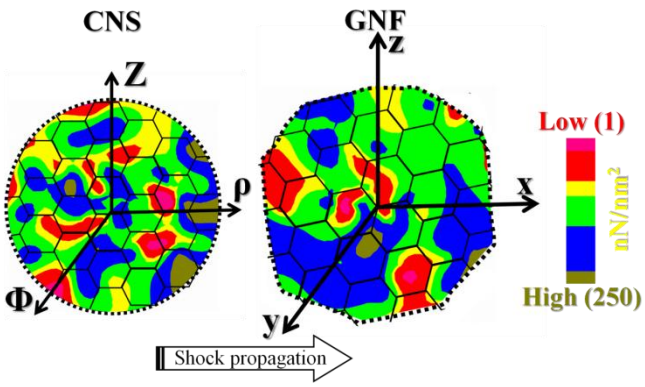

Fig. 4: Cross-section of the volumetric force distribution NCs (with color scale bar) indicating nature of shock propagation.

For GNF, the scenario is distinctly different, there are very few high force area seen. Moderately high (blue code) amount of force is seems to be spread over the graphene flake. The strain volume non-uniformity is the major common feature, due to in-homogeneous compression wave propagation through in both the nano-carbons [3].

VIII. Conclusion

We have studied the effect of shock waves on NCs such as GNF and CNS, prepared using chemical vapour deposition. The waves, typically, with velocity > 1.1 Mach, peak pressure > 1.2 GPa, and pulse width ~ μs duration were simulated experimentally by split Hopkinson pressure bar and impart onto NCs. Variations in strain, strain rate with time and stress, strain rate vs strain were measured to extract number of dynamic mechanical parameters. Incident shock with speed ~ 5.0×10^3 m/s dispersed into NCs with average magnitude ~ 2.5×10^3 m/s. The stress (σ)–strain (ε) curve, bi–linearly showed parabolic work hardening with coefficient, n, ~ 0.40 and elasto–plastic time parameter, t, ~ 2.0×10^{-5} s^{-1}. The volumetric stress rise rate which was much higher, under elastic behavior, imposed Hugoniot elastic limit (HEL) ~ 9.13 GPa. Interestingly, at the interface of elasto–plastic stage the behaviour of GNF was insulator(ceramic)–like. Overall all structural reduction was ~ 50%, specifically, eliminating corners, and edges. Incident elastic energy ~ 3.6×10^5 is reduced to ~ 2.8×10^5 N/m^2 by 30 % reduction while propagation within GNF. The velocity is reduced almost by 50 % showing shock damping by GNF.

References

[1] Meyers, M. Dynamic Behavior Of Materials; 1st ed.; John Wiley & Sons Inc: New York, 1994; pp. 01-117.

[2] S. Chink, I. P. S. Sandhu, D. R. Saroha, P. S. Alegaonkar "Dynamic deformation in graphene nano–flakes bytransonic shock waves," ACS Applied Nano Materials, vol.01, pp. 10–16, March 2018.

[3] M.S. Mahmoud, J.Y. Farah and T.E. Farrag, "Ballistic Impact Behavior of Carbon Nanotube And Nanosilica Dispersed Resin And Composites," Journal of Applied Physics, vol. 22, pp. 211-216, 2013.

1st International Online Conference on Emerging Smart Materials in Applied Chemistry(ESMAC-2020)
10-12 August 2020

Paper ID: 5

Growth of $(Co_{1-x}Ni_x)Cr_2O_4$ (x = 0, 0.5 and 0.25) Spinel Nanoparticles and Epitaxial Thin Films: Structure and Magnetism

P. Mohanty, C.J. Sheppard and A.R.E. Prinsloo

Cr Research Group, Department of Physics, University of Johannesburg, Johannesburg, PO Box 524, Auckland Park, South Africa

Multiferroic materials, having coexistence of magnetic and ferroelectric order, are of current interest because of the complex interplay between various order parameters [1]. Multiferroic $CoCr_2O_4$ single crystals demonstrate a conical-spiral ordering temperature (T_s) and a lock-in transition temperature (T_L) below the ferrimagnetic Curie temperature (T_c), which is unconventional when compared to other spinel oxides, such as ferrites [1, 2]. Experimental evidences show that the observed spiral component induces the electric polarization [2].Substituting Ni at Co site can substantially influence the magnetic transitions because of the change in magnetic exchange interactions amongst the neighboring cations [3]. In nano-scale the hysteresis loop demonstrates a wasp-waist feature not observed in the bulk [3]. In addition, the magnetic transitions are found to be influenced by the dopant ion and the repercussions thereof are observed utilizing temperature depend dc-magnetization and neutron diffraction techniques [3, 4]. In furtherance of these studies, work was extended to include thin films of $(Co_{1-x}Ni_x)Cr_2O_4$ (x = 0, 0.5 and 0.25) deposited on $MgAl_2O_4$ (100) and MgO (100) substrates, by means of pulsed laser deposition (PLD) techniques [4]. The impact stress in epitaxial grown thin films on the physical properties was explored. The possible role of cationic site substitution on structural, magnetic and electronic properties will be discussed.

[1] D. Khomskii, Physics 2, 20 (2009).
[2] Y. Yamasaki *et al*., Phys. Rev. Lett. 96, 207204 (2006).
[3] P. Mohanty *et al*., J. Magn. Magn. Mater, 498, 166217 (2020).
[4] P. Mohanty *et al*., Nanotechnology**,** 31, 285708 (2020).

1st International Online Conference on Emerging Smart Materials in Applied Chemistry(ESMAC-2020)
10-12 August 2020

Paper ID:6

A Chemical Analysis Study onthe Improvementof Durability of Cement Concrete by Self-Healing Nano-TiO_2

Chakraborty A[b] *and* Ghosal M[a*]

[a]Jt.Secretary, Coal Ash Institute of India, Sethbagan, Dum Dum, Kolkata-30, India, mainakghosal2010@gmail.com
[b] Associate Professor, IIEST, Shibpur,India,arun_besu_civil@yahoo.com

Abstract—Durability of a concrete is defined as its ability to resist aggressive chemical attacks, weathering actions, abrasion or any other process of deteoriation.Inadequate durability leads to many negative impacts - loss of strength and serviceability, corrosion, increased cost of repairs etc. While there are many factors affecting durability, the main being cement and water quantity/quality, sulfate and chloride attacks, permeability etc.Sulfate attack originates from the presence of sewage in soil or soil-foundation containing excessive fertilizers or industrial wastes or automobile exhausts while chloride attacks arises from the salty sea environment within 100Kms from the coast. India has a huge coastline of more than 7500Kms witha harsh marine climate while out of 30 most polluted cities in the world,21 were in India[1].So,the durability study of concretedemands the need for the hour. This paper discusses the effect of adding nano-sized TiO_2 particles both in cement and concrete composites alongwith its self-healing effect on concrete from the hostile attacks of sulfates and chlorides.

Cement comprise of four principal clinker mineral phases: tricalcium silicate (Ca_3SiO_5),di calcium silicate(Ca_2SiO_4),tri calcium aluminate($Ca_3Al_2O_6$) & tetra calcium alumino ferrite($Ca_4Al_2Fe_2O_{10}$)[2].Cement gets its strength from its reaction with water to form two products, viz. (1) Calcium-Silicate-Hydrate(C-S-H) gel which is responsible for its strength gain and (2) CalciumHydroxide (Ca $(OH)_2$).This reaction also known as hydration reaction due to hydrated product formation is given below.

Cement + H_2O = C-S-H (Calcium Silicate Hydrate) + Ca $(OH)_2$

Calcium Hydroxide is treachrous as it serves the main culprit for strength loss in the cement concrete matrix, through its reaction with outside chemical agents containing sulfate or chlorides.
In sulfate attack which is characterised by whitish apperaence on the concrete surface,this calcium hydroxide is converted to calcium sulfate or secondary gypsum causing internal pressuures in the cement concrete matrix due to its expanded volumes.Gypsum in turn reacts with hydrated calcium aluminates of cement to form ettringite which is known for its extensive cracking and expansion.This results in loss of cohesion and crack formation,thus making the concrete more porous and permeable.The reaction mechanism is shown below.

Ca $(OH)_2$ + Mg/Na_2SO_4 = $CaSO_4.2H_2O$(secondary gypsum)
$CaSO_4.2H_2O$ + $2Ca_3Al_2O_6.12H_2O$(tri calcium aluminate) = $3CaO.Al_2O_3.3CaSO4.3H_2O$(Ettringite)

Sulfate attacks the cement concrete matrix while chloride attack is characterised by corrosion on the steel reinforcements.Here calcium hydroxide is converted to soulble calcium chloride which in turn reacts with hydrated calcium aluminates of cement to form calcium chloro aluminates.The reaction mechanism is shown below.

Ca $(OH)_2$ + 2NaCl = $CaCl_2$ (soluble calcium chloride)+ 2NaOH
$CaCl_2$ + $2Ca_3Al_2O_6$ $.12H_2O$(tri calcium aluminate) = $3CaO.Al_2O_3.CaCl_2.10\ H_2O$(calcium chloro aluminates)

Cement hydration attains more than 90% at 28 days but continues to hydrate in the long-terms i.e.1 year(365 days) albeit at a very small rate[3].So in our tests we have considered results both at 28 days and at long terms,i.e.365 days. Optitmized addition of nano-TiO_2 having mean particle size diameter in the range of 30-40nm has a distinctive self-healing capacity whereby it increases the mechanical strength of cement composites and also concrete composites w.r.to the controlled samples as shown in Fig.1[4,5].Also the concrete samples casted with these nanomaterials resulted in more workability and whitish appearences.However, this self-healing capacity of nano-TiO_2 is more evident when it successfully wards of the aggressive chemical attacks of sulfate/chlorides as shown in Fig.2.

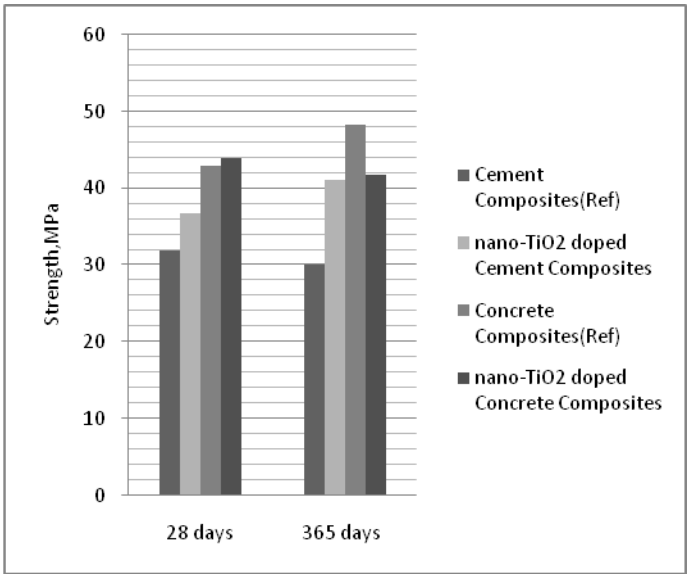

Fig.1: Strength variations of cement & concrete composites with & without nano-TiO_2

It is to be noted from both the figures i.e. Fig.1 & Fig.2 that nano-TiO_2 performs better in aggressive environments like $MgSO_4$/ $MgCl_2$ than ordinary exposures, which may be attributed to its self-healing characteristics.

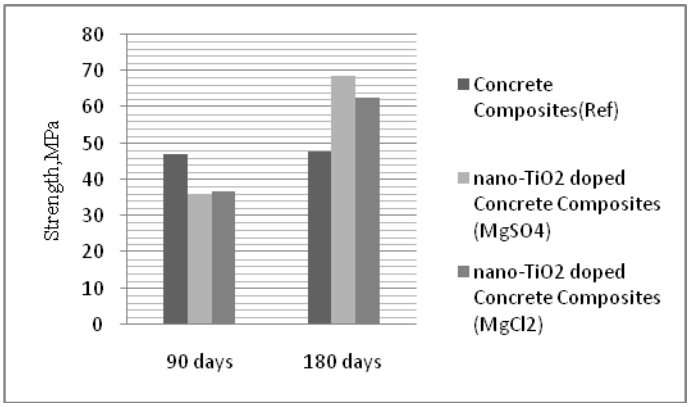

Fig.2: Strength variations of cement & concrete composites with & without nano-TiO_2in aggressive ($MgSO_4$/$MgCl_2$) exposures

So, nano-TiO_2could help in manufacturing high strength concrete which in turn helps to make the concrete more durable, causing it to be more workable or flowable which is the main reason for its increased resistance to chemical attaks like $SO4^{-2}$/Cl^{-1}hence with smoother exterior fnish resulting in more deletrious substances decomposition thus making the end product greener as shown in Fig.3.

The compound Titanium was found in 1791 by William Gregor, in England and has applications in wide range of industries from food coatings to construction to paints to sunscreen lotions.Its nano dimensions have proved to have more novel unique photo-catalytic properties than its parent bulk material as our Paper reports.This is due to the fact that when sunlight falls on nano-TiO_2doped concrete, electrons are released which combines with O_2 in the atmosphere creating "O^{2-}" (Superoxide anion).As a result of these release of electrons,nano-$TiO_2$and takes electrons from moisture of the air and then return to its original state. On the other hand, the moisture that lost the electron becomes a hydroxyl radical (•OH) resulting in a loss of moisture from the cement matrix system.As a result, chemical attacks of sulfate and chlorides could not be continued in the second stage, when the involvement of hydrated tri calcium aluminates from cement matrix comes into picture.Hence, hydrated products is not being attacked and the cement matrix continues to grow in strength.

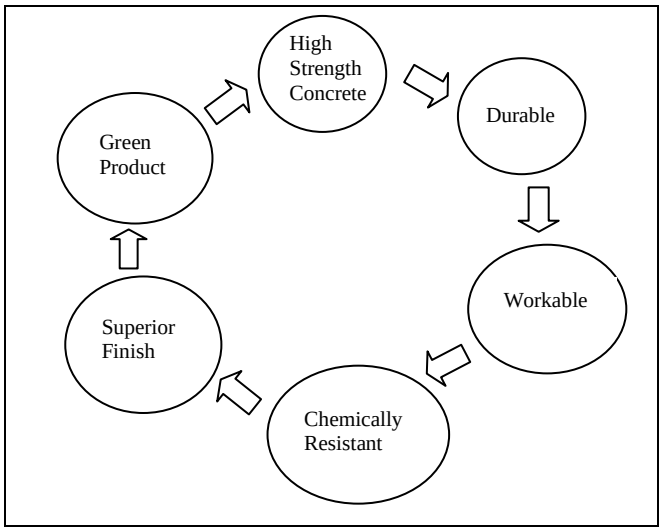

Fig.3: Relationship among various parameters in nano-TiO_2 doped cement concrete composites

References

[1]https://en.wikipedia.org/wiki/Air_pollution_in_India.
[2]https://en.wikipedia.org/wiki/Portland_cement
[3]Price, W.H., *ACI J.*, 22(6), 417–432, 1951
[4] Martins T,et al.An experimental investigation on nano- TiO_2 and fly ash based high performance concrete, *The Indian Concrete Journal*,Jan.2016,Vol 90,Issue 1,pp23-31.
[5]Ghosal et al "A Comparative Assessment of Nano-SiO2 & Nano-TiO2 Insertion in Concrete", *European Journal of Advances in Engineering and Technology*, (2015), pp. 44-48.

1st International Online Conference on Emerging Smart Materials in Applied Chemistry(ESMAC-2020)
10-12 August 2020

Paper ID:7

Layered crystalline inorganic ion exchangers for separation of Sr^{2+} ions from nuclear waste

SamathaBevara[a*], PremaGiri[b], S. NagabhusanAchary[c], Raman K. Mishra [b] and Amar Kumar [b]

[a]Chemistry Division, Vignan's Foundation for Science, Technology and Research, Vadlamudi, Guntur, Andhra Pradesh, 522213, India, samathahcu@gmail.com
[b]Waste Management Division, Bhabha Atomic Research Centre, Mumbai 400085, India
[c]Chemistry Division, Bhabha Atomic Research Centre, Mumbai 400085, India

Abstrcat: Nuclear fuel reduces the cost of nuclear waste managementand the radionuclides separated from nuclear waste could be used as radiopharmaceuticals. In view of this, inorganic ion exchangers have been synthesized for the separation of ^{90}Sr ions from liquid nuclear waste. $K_2Zr(PO_4)_2$ and $Na_{0.5}Mn_2O_4$-$0.96H_2O$ (Na-Birnessite) are the two layered inorganic ion exchange materials were compared for their activity as ion exchangers for ^{90}Sr separation from liquid nuclear waste. $K_2Zr(PO_4)_2$ is a complex, layer structured phosphate synthesized by solid state synthesis route and crystallizes in rhombohedral lattice. Synthetic birnessite mineral ($Na_{0.5}Mn_2O_4$-$0.96H_2O$) with Na^+ ions as exchangeable ions has been synthesized by the oxidation of $Mn(OH)_2$. Distribution coefficients for these materials for ^{90}Sr separation from nuclear waste have been calculated in wide range of pH medium and for various equilibration times.

***Keywords*—Radioactive nuclear waste, Ion exchangers, $K_2Zr(PO_4)_2$, Birnessite**

IX. INTRODUCTION

Nuclear energy is an alternate energy source for many developing countries at present. Cost of the nuclear energy could be minimized by the effective management of nuclear waste. ^{90}Sr, ^{137}Cs and ^{106}Ru are the radionuclides generated in high concentrations as fission products due to nuclear fission of ^{235}U. Separation of these long lived radionuclides not only reduces the nuclear waste management cost but also possess many technological applications. Among various radionuclides present in nuclear waste, ^{90}Sr is of major concern due to 28.8 y of long half life and high specific activity 1.5×102 Ci/g.[1]. Selective separation of radionuclides from nuclear waste is tedious because of high salt concentration, low pH and temperature due to radioactive decay. Framework inorganic materials are promising ion exchangers for separation of ^{90}Sr from nuclear waste because of their high thermal, chemical and radiation stability.[2, 3]In this study we have investigated the ion exchange properties of two layer structured crystalline inorganic materials namely $K_2Zr(PO_4)_2$ and Na-Birnessite ($Na_{0.5}Mn_2O_4$-$0.96H_2O$), and their ion exchange behaviors were compared.

X. MATERIALS AND METHODS

$K_2Zr(PO_4)_2$ and Na-Birnessite were synthesized by solid state synthesis and by oxidation of $Mn(OH)_2$ respectively as earlier reported by us.[4, 5]$K_2Zr(PO_4)_2$was synthesized by the solid state reactions of $KH_2(PO_4)_2$ and ZrO_2 at 750°C. Na-Birnessite was synthesized by the oxidation of $Mn(OH)_2$ in presence of excess NaOH. $Mn(OH)_2$ was obtained by the hydroxylation of $MnCl_2$.[5, 6]

Structural characterization of the $K_2Zr(PO_4)_2$ and Na-Birnessite was carried out by powder X-ray diffraction, the details of the structural characterizations were presented in the earlier reports.[4, 5]Crystal structures of both the materials have been analyzed by using Fullprof-2K software.The ion exchange characteristics of both $K_2Zr(PO_4)_2$ and Na-Birnessite were studied by using ^{85}Sr tracer solutions. ^{85}Sr has half-lifeof 64.8 d, specific activity = 2.4 × 104 Ci/g and it is a γ-emitter, and can provide similar chemical properties as that ^{90}Sr. The distribution coefficient K_d is measured as K_d (mL/g) = [(Ai - Af) / Af] × V/M, where Ai = counts before equilibration, Af = counts after equilibration, V = volume of solution in mL, M = mass of the ion exchanger in gram.

XI. Results and Discussion

A. Structural characterization

As mentioned, both the materials$K_2Zr(PO_4)_2$ and Na-Birnessite have layered structure, where the structure is formed with negatively charged phosphate ions in case of $K_2Zr(PO_4)_2$and manganate ions in case of Na-birnessite.K^+ or Na^+ ions were present to maintain the charge neutrality in between the layers. The flexibility of ZrO_6 and PO_4 connections in $K_2Zr(PO_4)_2$ render flexibility of the structure, while the structural diversity of Na-Birnessite is mainly controlled by the stacking of the rigid sheets of MnO_6 in it. This difference is reflected in the crystal structure of these two, thus $K_2Zr(PO_4)_2$ crystallizes in a higher symmetric lattice compared to Na-Birnessite. In the present studied samples, $K_2Zr(PO_4)_2$ has rhombohedral unit cell with space Group: P-3 (a = 5.1965(1) Å, c = 9.0422(1) Å, V = 211.456(1) $Å^3$**)** and Na-Birnessite has a monoclinic unit cell with space group C2/m (a = 5.147(7) Å, b = 2.851(4) Å, c = 7.309(6) Å, β = 102.9(2)°, V = 104.6(2) $Å^3$**)**.[4, 5] Further it can be mentioned here that the interlayer distance in the $K_2Zr(PO_4)_2$ is more due to larger negative charge of the sheets, which require more positive charge in between the layers compared to the Na-Birnessite.[6, 7]The interlayer distances of $K_2Zr(PO_4)_2$ and Na-Birnessite are 9.04 and 7.14 Å respectively, which can be attributed to larger ionic radii of the K^+ compared to Na^+. In the Na-Birnessite case, significant amounts of empty spaces are present in between the layers thus incorporation of neutral molecules like water in between the layers takes place. However, in both cases the interlayer cations are labile and thus amenable to exchange with other cations of similar size and charge. Thus cation exchange properties in both the materials are possible under nuclear waste conditions.

B. Ion exchange characteristics

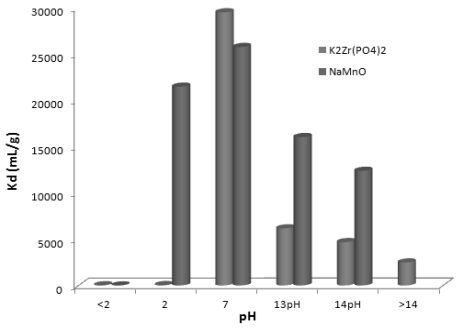

Fig. 1 Variation of distribution coefficient (K_d) with pH for $K_2Zr(PO_4)_2$ and Na-Birnessite.

The structural stabilities of both $K_2Zr(PO_4)_2$ and Na-Birnessite materials were examined by treating them with solutions of various pH. The effect of pH over distribution coefficient (K_d) was examined by equilibrating 0.05g of sample in 5mL of ^{85}Sr tracer prepared by different pH solutions. A constant equilibration time of 3 h was maintained for all the batch experiments. The radioactivity of the tracer solution was measured before and after ion exchange. The maximum distribution coefficient (K_d) ~ 30,000 mL/g for $K_2Zr(PO_4)_2$ and K_d ~ 26,000 mL/g for Na-Birnessite was observed at pH=7. The distribution coefficient value is constant for a wide pH range in case of Na-birnessite compared to $K_2Zr(PO_4)_2$ indicating the higher structural stability and ion exchangeability in large pH window. The variation of K_d with change in pH medium is shown in Fig. 1.

XII. Conclusion

In summary, ion exchange characteristics of two layered crystalline inorganic ion exchangers namely $K_2Zr(PO_4)_2$ and Na-Birnessite ($Na_{0.5}Mn_2O_4$-$0.96H_2O$) were compared. Both $K_2Zr(PO_4)_2$ and Na-Birnessite ($Na_{0.5}Mn_2O_4$-$0.96H_2O$) were crystalline in nature and stable in liquid nuclear waste conditions. Ion exchange characteristics of both $K_2Zr(PO_4)_2$and Na-Birnessite reveal that the distribution coefficient (K_d) value is higher in case of $K_2Zr(PO_4)_2$compared to Na-Birnessite. The higher distribution coefficient (K_d) in case of $K_2Zr(PO_4)_2$indicates that the structure is more flexible and number of K^+ ions present are more compared to Na-Birnessite and readily available for exchange with ions of similar size and charge.The distribution coefficient (Kd) value for Na-Birnessite is constantly high over wide range of pH compared to $K_2Zr(PO_4)_2$ indicating, more stability of Na-Birnessite in nuclear waste conditions compared to $K_2Zr(PO_4)_2$.In view of these ion exchange characteristics, it could be concluded that $K_2Zr(PO_4)_2$ is a better ion exchanger due to higher number of K^+ ions presence and large inter layer spacing compared to Na-Birnessite. The distribution coefficient (K_d) in acidic medium is higher and stable in wide pH range for Na-Birnessite compared to $K_2Zr(PO_4)_2$.

References

[1] N. Momoshima and E. A. Bondietti, "The radial distribution of ^{90}Sr and ^{137}Cs in trees," J. Environ. Radioact.,vol. 22, pp93-109, 1994.

[2] S. N Achary, B. Samatha and A. K. Tyagi, "Recent progress on synthesis and structural aspects of rare-earth phosphates," CoordinChem Rev., vol340, pp266-297. 2017.

[3] B. Samatha, S. N. Achary, S. J. Patwe, A. K. Sinha and A. K.Tyagi, "Preparation and crystal structure of K 2 Ce (PO 4) 2: a new complex phosphate of Ce (iv) having structure with one-dimensional channels," Dalton Trans.,vol 45, pp980-991, 2016.

[4] B. Samatha, P. Giri, S. J. Patwe, S. N. Achary, R. K.Mishra, A. Kumar and A. K. Tyagi, "Separation of 90Sr from nuclear waste by crystalline complex phosphates of Ce (IV) and Zr (IV)," J. Environ. Chem. Eng., vol6, pp2248-2261, 2018.

[5] B. Samatha, P. Giri, S N. Achary, G Bhallerao, R. K. Mishra, A. Kumar, C. P Kaushik and A. K. Tyagi, "Synthetic Na/K-birnessite for efficient management of Sr (II) from nuclear waste," J. Environ. Chem. Eng.,vol 6,pp 7200-7213, 2018.

[6] J. Cai, J. Liu and S. L. Suib, "Preparative Parameters and Framework Dopant Effectsin the Synthesis of Layer-Structure Birnessite by AirOxidation," Chem. Mater., vol145, pp2071-2077, 2002.

[7J. Cai, J. Liu and S. L. Suib,"Synthesis and X-ray Crystal Structures of the New, Three-Dimensional Ethylenediphosphonates [$A\{HO_3P(CH_2)_2PO_3H_2\}$] (A = Alkali Metal, Tl, or NH_4): Solid," Chem. Mater., vol2006, pp813-819, 200.

1st International Online Conference on Emerging Smart Materials in Applied Chemistry (ESMAC-2020)
10-12 August 2020

Paper ID:8

First Principle Calculation on Co−TCNQ monolayer as Bi-functional single atom Electrocatalyst

Biswanath Mukherjee*

Department of Physics, Sidho-Kanho-Birsha University, Ranchi Road, Purulia, 723104, India
E-mail: biswanath.mukh@gmail.com; biswanath-mukherjee@skbu.ac.in

***Abstract*—First principle based density functional theory (DFT) computations have been applied to investigate cobalt-tetracyanoquinodimethane (Co–TCNQ) monolayer as stable bi-functional electrocatalyst in both ORR and OER for sustainable energy production. DFT calculation showed that Co−TCNQ monolayer possesses excellent catalytic activity towards ORR and OER, following 4-electron reduction pathways. The free energy portraits of Co-TCNQ monolayer in alkaline media measures an overpotential of 0.6 V (*vs* RHE) for OER and onset potential of 0.32 V (*vs* RHE) for ORR. The excellent catalytic activity of two dimensional Co-TCNQ monolayer has been explained in terms of Bader charge analysis which revealed a net transfer of 0.27|e| charges from Co centre to the OO* adsorbates in Co-TCNQ-OO* composite.**

***Keywords*— Bi-functional electrocatalyst, first principle calculation, DFT, Co-TCNQ, fuel cells**

I. Introduction

Fuel cells have been introduced as novel energy conversion devices [1] in past decades because of its capability of producing sustained energy through two redox reactions, namely, oxygen reduction reaction (ORR) and oxygen evolution reaction (OER). However, the sluggish reaction kinetics of ORR at cathode greatly limits the large scale application of fuel cells. Additionally, the platinum (Pt), which has been used as highly effective ORR catalyst [2], suffers from a number of shortcomings, including, lower abundance, higher cost, and poor durability, which fatally inhibit its wide commercialization [3]. In case of OER, the noble metal oxides, like, ruthenium (Ru) and iridium (Ir) were identified as the best catalyst [4], which are not only highly precious, but, scarce too, hindering its widespread scalable applications. Therefore, the development of cost-effective, earth-abundant, and non-noble metals based ORR/OER electrocatalysts with low onset/overpotential is highly essential for further progress of fuel cell technology. Specially, the designing of stable bifunctional electrocatalyst for ORR and OER will be a key step towards solution of future energy catastrophe [5].
Recently, the family of 2-D transition metal–tetracyanoquinodimethane (TM-TCNQ) have been explored by different groups due to their promising catalytic properties [6]. However, the potential of these TM-TCNQ composition till remains unexplored, especially their possible extent as bifunctional electrocatalyst is largely unknown [6]. Herein,

DFT calculations on 2-D cobalt-TCNQ (Co–TCNQ) monolayer were carried out to explore as bi-functional electrocatalyst. The study revealed that Co−TCNQ monolayer can act as a promising bi-functional catalyst with overpotential (η) of 0.6 V (*vs* RHE) towards OER and onset potential of 0.32 V for ORR in alkaline media (pH = 14). The Bader charge analysis dictated that a net charge of 0.27|e| transferred from

Co atom towards O atoms in the Co-TCNQ-OO* composite due to the strong hybridization between Co-*3d* with O-*2p* orbitals.

II. DFT Calculation Methods

All computations have been carried out with Vienna Ab-initio Simulation Package (VASP) with Projector Augmented Wave (PAW) potential coupling PBE-type generalized gradient-corrected functional [7] with exchange-correlation potential. Energy correction has been done using Grimme's DFT-D2 dispersion interactions. For geometry optimization, a 5×5×1 mesh and for electronic structure calculations, a 11×11×1 grid have been used. The unit cell of Co-TCNQ was taken parallel to the x-y plane with a vacuum of 20 Å along z-direction to avoid any interlayer interactions.

III. Results and Discussion

The optimized geometry of a Co-TCNQ unit cell and that under O_2 adsorption as obtained from DFT calculation are presented in Figure 1(a) and (b), respectively. One unit cell of Co-TCNQ monolayer consists of one Co atom at the centre, four nitrogen (N) atoms, twelve carbon (C) atoms and four hydrogen (H) atoms. The optimized lattice parameters for the structure $a = 6.87$ Å, and $b = 11.13$ Å with a vacuum of 20 Å along c axis.

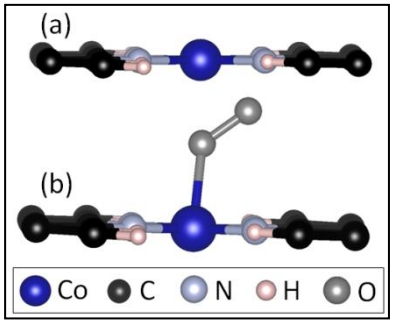

Fig. 1: Optimized geometry of (a) Co-TCNQ unit cell (b) Co-TCNQ-OO*.

The general equation which governs the ORR/OER mechanism in alkaline medium is as follows:

$$O_2(g) + 2H_2O\ (liq) + 4e^- \rightleftarrows 4OH^-$$

The reduction of O_2 in $4e^-$ pathway consists of adsorption of intermediate products, *viz*, *OOH, *O and *OH followed by the desorption of OH^-. The adsorption of O_2 molecule is energetically favorable on the Co-TCNQ substrate as it shows downhill in the free energy diagram in ORR at zero cell potential (Figure 2a). The first hydrogenation process requires an energy of 0.5 eV (uphill in the diagram), resulting in the formation of *OOH with O-O bond length elongated by 0.14 Å (from 1.27 to 1.41 Å). As found from the free energy diagram (at U = 0.4 V) in Figure 2(a), the onset potential for ORR on Co-TCNQ is 0.32 V (RHE). The consecutive hydrogenation steps are exothermic in nature which favours the dissociation of O-O bond. This validates the proposition of ORR reaction mechanism to proceed along $4e^-$ pathway. On the other hand, the adsorbed free energies of reactions intermediates in case of OER are depicted in Figure 2(b). The free energy profile of Co-TCNQ catalyst for OER illustrates that at equilibrium potential (U = 0.4 V), the OOH* formation step is endothermic by 0.6 V, which is the required external potential (overpotential) for OER to proceed.

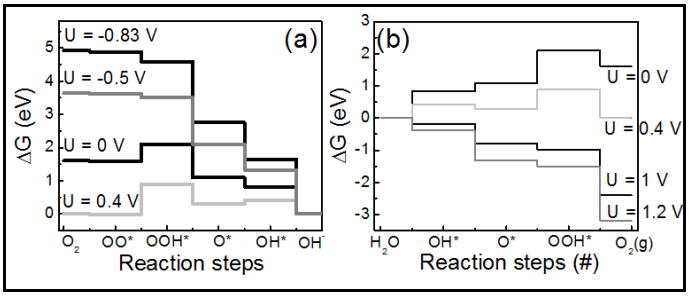

Fig. 2: Gibbs free energy profile of Co-TCNQ catalyst in alkaline medium for (a) ORR (b) OER.

To evaluate the charge transfer between central Co-core in Co-TCNQ and OO* adsorbate due to the interlayer interaction during ORR, the charge density difference $(\Delta\rho)$ between the composite and the individual components was calculated, i.e.,

$$\Delta\rho = \rho_{Co-TCNQ-OO^*} - \rho_{Ni-TCNQ} - \rho_{OO^*}$$

The optimized geometry of $Co-TCNQ-OO^*$ composite and the charge re-arrangement in different atoms is displayed in Figure 3(a). It is seen that there is depletion of charges in central Co atom (green), and a net accumulation of charges (yellow) around two O-atoms. The exact distribution of charges due to interaction between adsorbate and substrate have further been computed by Bader charge analysis, the summary of which is displayed in Figure 3(b). It is observed that the central Co-atom is susceptible to lose electrons, while two O-atoms in OO^* adsorbate are more liable to gain electrons. This analysis further shows that a net 0.27|*e*| charges migrated from the central Co-atom to O-atoms in $Co-TCNQ-OO^*$ composite leading to the elongation of O–O bond length from 1.23 Å to 1.27 Å. This facilitates adsorption of O_2 molecule on Co-TCNQ monolayer to favor ORR.

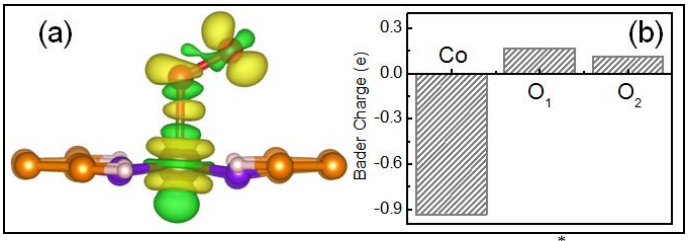

Fig. 3: (a) Charge re-distribution in Co-TCNQ-OO* optimized structure. Yellow and green colours indicate respectively accumulation and depletion of charges. (b) Bader analysis.

IV. Conclusion

The promising performance of Co-TCNQ monolayer towards bi-functional electrocatalysis shows the potential to overcome the challenge towards the development of cost-effective, durable and high-efficiency single-atom electrocatalyst for future metal air batteries and fuel cell technology.

References

[1] E. Antolini, J. Power Sources, vol. 170, pp. 1-12 2007.

[2] (a) M.K. Debe, Nature, vol. 486, pp. 43-51 2012; (b) J. Qu, F. Ye, D. Chen, Y. Feng, Q. Yao, H. Liu, J. Xie and J. Yang, Adv. Colloid Inter. Sci., vol. 230, pp. 29-53, 2016.

[3] P.C.K. Vesborg and T.F. Jaramillo, RSC Advances, vol. 2, pp. 7933-7947, 2012.

[4] (a) T. Reier, M. Oezaslan and P. Strasser, ACS Catalysis, vol. 2, pp. 1765–1772, 2012; (b) N.T. Suen, S.F. Hung, Q. Quan, N. Zhang, Y.J. Xu and H.M. Chen, Chem. Soc. Rev., vol. 46, pp. 337–365, 2017.

[5] Z.F. Huang, J. Wang, Y. Peng, C.Y. Jung, A. Fisher and X. Wang, Adv. Energy Mater., vol. 7, pp. 1700544-1700564, 2017.

[6] (a) Y. Ma, Y. Dai, W. Wei, L. Yu and B. Huang, J. Phys. Chem. A, vol. 117, pp. 5171–5177, 2013; (b) Q. Deng, J. Zhao, T. Wu, G. Chen, H.A. Hansen and T. Vegge, J. Catal., vol. 370, pp. 378–384, 2019.

[7] J.P. Perdew, K. Burke and M. Ernzerhof, Phys. Rev. Lett., vol. 77, pp. 3865-3868, 1996.

1st International Online Conference on Emerging Smart Materials in Applied Chemistry (ESMAC-2020)
10-12 August 2020

Paper ID:9

Physio-chemical Impact over Outdoor Solar PV Module by Atmospheric Aerosols Absorption and Deposition

Ayan Banik[1a*]

[a] Department of Electrical Engineering
Cooch Behar Government Engineering College
**Corresponding author: ayanbanik97@yahoo.com*

***Abstract*—Natural atmospheric airborne aerosols or commonly dust exhibit a wide range of sizes from nanometers to few micrometers with different size and configuration. It is composed of both organic and chemical composition and significantly affect air quality index with much destruction in the environment and human livelihood. In recent times it has been observed that Solar rooftop PV has gained huge popularity and has been installed throughout India to priorities and encourage sustainable green energy generation. As per standard test condition, a photovoltaic cell operates with [15-25] % efficiency under adverse physical condition i.e. temperature, irradiance, humidity, etc. [1]. A recent study shows that atmospheric particulate matter (PM) i.e. dust outbreak and free aerosols deposition over the encapsulant surface of Solar PV modules possesses serious threat in power generation and optimization capability of Solar PV in turn drastically reduces the power output and efficiency. Moreover, it has also been responsible for alteration in physiochemical properties of PV after long exposure. In this work, an effort has been made to present a synopsis of aerosol observations, source inventories, characterization, energy metrology and the theoretical understanding required to enable an assessment of radiative forcing from aerosols. An investigation has been made over aerosol science more precisely aerosol chemistry to study its typical chemical properties, estimate unique potential impact, assess the influence over solar panel feasibility, sensitivity and transmittance [2].**

***Keywords*—Aerosols, Energy metrology, Efficiency, Particulate matter, Sensitivity**

Fig. 1 (A) Partially cleaned solar panels representing accumulation of Particulate Matter for 28 day

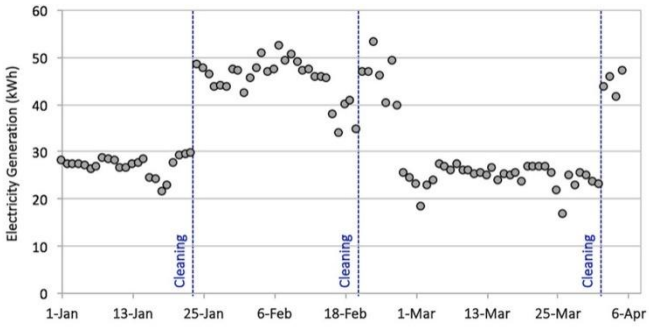

Fig.1 (B) the change in measured solar energy production after several solar panel cleanings

1st International Online Conference on Emerging Smart Materials in Applied Chemistry(ESMAC-2020)
10-12 August 2020

Paper ID:10

Preparation, Characterization and Soxhlet Leaching Studies of Some Uranium Doped Borosilicate Simulated Nuclear Waste Glasses with Different Modifiers

Malik P. P.[a], Hazra G.[b*]

[a] Department of Chemistry, B.B. College, Asansol, West Bengal, India, patitbu99@rediffmail.com
[*b] Department of Chemistry, Kalna College, Kalna, West Bengal, India, goutamhazra1@gmail.com

***Abstract*— In the present work we have been developed the borosilicate glasses loaded with uranium for immobilization of high level nuclear waste at much lower temperature (from 800°C – 900°C) with a soaking period of 90 minutes to achieve homogeneity of the glass. The determination of pH ranging from 6.18 up to 7.45 of the leachate solution at ambient temperature under varying time intervals shows interesting and regular variations. Leaching study of these glasses was conducted with the help of Soxhlet distillation apparatus with distilled water with a maximum time period of 200 hours. Weight losses were measured with respect to time of leaching. Residual activities were followed by 'Radiotracer technique' with respect to cumulative time period of leaching. The results are reported in the range 1.34×10-4 g.m-2.hr-1 and 8.26×10-3 g.m-2.hr-1 respectively at 90°C. The findings have been corroborated in terms of ionic size, ionic radii and hence ionic potential of the modifier ions incorporated into the glass structure.**

***Keywords*— Nuclear waste, Glass, modifier, leaching, vitrification, ionic potential**

I. Introduction

The threaten problem of global warming and climate change have allowed the benefits of nuclear power. Uranium is a fuel that does not release carbon dioxide and so it seems to be a promising candidate to displace fossil fuels to generate electricity. The nuclear power has serious problem of disposal of radioactive waste. The future development of nuclear energy depends largely on the successes of programmes and management of radioactive waste generated at various stages of the nuclear fuel cycle1. Glass are the first materials developed as a host for high level waste via melting vitrification technology. Glass offers a medium for waste containment since it has the ability to dissolve most of the

elements of the periodic table. The fission product constituents thus become a part and parcel of the glass structure as compared to any other mechanical entrapment. Glass can be considered as a truly 'secular' matrix, imbibing in one melt all the elements contained in the waste. This results in a permanent and irreversible fixation of the nuclides in the various matrixes. Glass has very high leach resistance, i.e., it does not dissolve easily in water. High leach resistance is one of the most desirable properties of the solid matrix used to immobilize the fission product.

In this present work, the preparation and characterization of borosilicate glasses of different composition loaded with simulated nuclear waste and doped with uranium were studied. The chemical corrosion in water of these glasses was measured in terms of leaching study.

II. Materials and Methods

a. Reagents

After dry and wet mixing (in acetone medium) the ingredients were dried and taken in alumina crucibles and fired

in a muffle furnace fitted with programmer in the range 800^0 C – 900°C for soaking periods of 90 minutes in air. In considering that the glass will be utilized to incorporate nuclear waste with some of the fission fragment like RuO which is highly volatile, the lower the glass processing temperature the better will be the glass melt. The glass batches used in the present work were prepared from the AR grade ingredients. The oxides SiO_2 and B_2O_3 (borax) act as the glass former while PbO act as intermediates and BaO, SrO and CeO_2 act as modifiers. The compositions used in the present work as well as melting point and density of the melted glasses are shown in Table 1.

Table 1: Compositions (wt. %), Melting point and Density of the prepared glasses

Glass ID	SiO_2	$Na_2B_4O_7$	PbO	BaO	CeO_2	SrO	Uranyl aceatate	M. P. (± 2°C)	Density (g/cm^3)
BS9	**39.6**	**20**	**30**	**5.0**	**-**	**-**	**5.4**	**800**	**5.2413**
BS10	**39.0**	**20**	**30**	**5.0**	**-**	**-**	**6.0**	**850**	**5.3241**
BS11	**39.0**	**20**	**29.5**	**5.0**	**-**	**-**	**6.5**	**900**	**5.3725**
BS12	**39.0**	**20**	**25**	**5.0**	**-**	**5.0**	**6.0**	**850**	**5.2939**
BS13	**39.0**	**20**	**25**	**5.0**	**5.0**	**-**	**6.0**	**900**	**5.0825**
BS14	**39.0**	**20**	**21**	**5.0**	**5.0**	**5.0**	**5.0**	**900**	**4.8962**

B. Experimental Studies

To determine the pH of the leachate solution with the help of Systronics digital pH meter (Model 335), the glass sample was grinded and mess through to achieve 0.300 – 0.425 mm size. Then one (1) gm of the specified sized glass powder was taken in a beaker containing 40 ml distilled water. For leaching study, about 0.5 gm of glass powdered sample of the specified sized were accurately weighed and was taken in a nylon net through which glass powder did not pass out. Nylon net containing the sample was placed in a Soxhlet apparatus with a round bottom flask (500 ml capacity) fitted with condenser and distilled water was used as medium. The distillation was carried out for varying period up to 24 hrs. The heating being done by a heating mantle [ASTM: C1285-02(2008)]. Since U is α/β active, the leaching behavior can be studied by 'radiotracer technique' with the help of a Geiger-Muller counter by measuring the net counts per sec (cps) and it was done up to 200 hrs.

III. Results and Discussion

The effect of different modifier ions like $Ba^{2+,}$ Pb^{2+}, Ce^{4+} and Sr^{2+} is quite evident on the melting points and time of melting. Here the mechanism is that the modifier ion (M^{n+}) dissociates a Si-O or B-O bond of net work and generates anionic O sites (O^{-}) and gets attached to such sites ionically. The ionic potential increases as following order Ba^{2+} (1.48) < Pb^{2+} (1.5) < Sr^{4+} (1.54) < Ce^{4+}< (3.39). A metal ion having greater ionic potential will attract more OH^{-} ions to form the corresponding hydroxides $M(OH)_n$. The consumptions of hydroxide ion increases the dissociation of H_2O in the forward direction, releases more number of H^{+} ion in the medium. The resulting solution becomes acidic giving rise to low pH value. The leach rates (LR) for BS9, BS10 and BS11 are determined from surface area analysis after measuring the leaching. These values are obtained as 1.34×10^{-4} $g.m^{-2}.hr^{-1}$, 6.26×10^{-4} $g.m^{-2}.hr^{-1}$and, 8.26×10^{-3} $g.m^{-2}.hr^{-1}$ respectively. Presence of CeO_2 in the glass batches shows the more leach resisting property as Ce ion act as good a binder due to its higher coordination number.

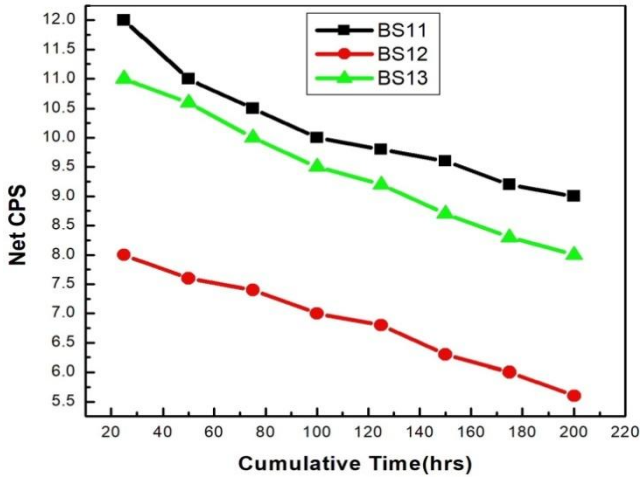

Figure 1: Plot of Net cps Vs Cumulative leaching Time for Borosilicate glasse

From the Fig. 1(net cps vs. cumulative time) it is observed that with increasing cumulative time, the net cps (for alpha & beta) has decreased in an exponential way. This signifies that with increasing leaching time, the release of uranium along with other constituents becomes slower and slower until getting stopped. This indicates that the glass becomes resistant to leaching and is a better choice for the disposal of nuclear waste.

IV. Conclusion

Borosilicate can be used as potential solid matrix for immobilization of high level radioactive waste. Addition of PbO improves the low melting temperature of glasses which significantly reduces the volatilization of ruthenium and cesium. The durability and the chemical resistance properties are improved with addition of intermediate oxides like CeO_2.

References

[1]G. Hazra, P. Mitra and T. Das, "Preparation and Properties of Lead-Iron-Phosphate Nuclear Waste Glasses" *Trans. Ind. Ceram. Soc.*, vol. 78, no. 2, pp. 1-9, 2019.

[2] A. Ghosh, G. Hazra, P Mitra and T. Das, "Incorporation of Nuclear Wastes in Lead Iron Phospate and Uranium containing LIP Glasses", *Orient. J. Chem*, vol. 30, no. 1, pp.87-94, 2014.

[3]P.P. Malik, G. Hazra, P Mitra and T. Das, "Role of Different Modifiers on Melting Points, pH under Leaching and Leaching Rates in Nuclear Waste Glasses" *Progress in Theoretical and Applied Physics*, Vol. 1, no. 1, pp.1-10; 2013.

1st International Online Conference on Emerging Smart Materials in Applied Chemistry(ESMAC-2020)
10-12 August 2020

Paper ID:11

Genetic variation of Pkinase domain of check point kinase 2 protein involved in Invasive ductal carcinoma: An *In silico* study

Satya Narayan Sahu [a], Biswajit Mishara [a], Rojalin Sahu [a*], Subrat Kumar Pattanayak [b,*]

[a] *School of Applied Sciences, Kalinga Institute of Technology (KIIT) Deemed to be University, Bhubaneswar -751024,India*
[b] *Department of Chemistry, National Institute of Technology ,Raipur -492010,India*
[*]*Corresponding authors: rsahufch@kiit.ac.in, skpiitbbs@gmail.com*

***Abstract*— Identification of diseased non-synonymous single nucleotide polymorphisms (nsSNPs) is crucial to characterize the genetic basis of diseases, access individual susceptibility to disease and determination of molecular and therapeutic targets. In the present study we discussed about the Invasive Ductal Carcinoma (IDC) and biomarker prediction through computational. IDC is a type of breast cancer, which is a most common cancer in worldwide and is the second leading cause of cancer related mortality in women after lung cancer. The check point kinase 2 (CHEK2) is a family of protein kinase super family , which regulates the checkpoint capture through phosphorylation in cell cycle and inhibit the activity of CDC25A , CDC25B and CDC25C genes . In the present work , we have studied the structural stability of mutant Pkinase domain of CHEK2 encoded protein as well as binding mechanism with theaflavic acid and quercetin by molecular docking interaction . Here, we have analyzed the molecular dynamics properties of both native and mutant (Y390C) models of Pkinase domain of CHEK2 encoded protein to predict the stability of the structure. To proceed further we have analyzed the binding site and binding energy of the protein with different phytochemicals. From the molecular docking study phytochemicals have found highest binding energy with mutant Pkinase domain of CHEK2 encoded protein. All the studied phytochemicals showing inhibitory effects against mutant CHEK2 encoded protein.**

***Keywords*— Molecular Dynamic Simulation, AutoDock, Invasive ductal carcinoma, CHEK2, Protein, Mutation**

The checkpoint kinase 2 (CHEK2) is a family of protein kinase super family , which regulates the checkpoint capture through phosphorylation in cell cycle and inhibit the activity of CDC25A , CDC25B and CDC25C genes [1]. It has been also named as moderate penetrance breast cancer (BC) susceptibility gene, which is responsible for invasive ductal carcinoma (IDC) [2-3]. Invasive ductal carcinoma is a type of brest cancer, which is a most common cancer in worldwide and is the second leading cause of cancer related mortality in women world after lung cancer [4]. There are different types of mutations and various aberrations are found in the CHEK2 gene like I157T, R117G, I160M, G167R, and G167A etc. Y390C and I157T are the well-studied and have been coherence with risk susceptibility to cancer [5]. It was found moderate risk (20–25%) of developing breast cancer for female mutation carriers [6]. It is considered as a tumor suppressor gene.

Here we analyzed the molecular dynamics properties of both native and mutant (Y390C) models of Pkinase domain of CHEK2 encoded protein to predict the stability of the structure, which mutation is responsible for IDC. To further proceed we analyze binding site and binding energy of the protein with different phytochemicals. From the molecular docking study phytochemicals have found highest binding energy with mutant Pkinase domain of CHEK2 encoded protein.Our main focus in this study is the evaluation of the energy of interaction between the mutant model of Pkinase domain of CHEK2 gene encoded protein with the above mentioned phytochemicals. Formerly molecular docking has

been utilised to recognise the binding affinity of the compounds [7-8].The molecular docking or molecular interaction analysis is proceeded to calculate the binding energy of receptor and ligand. To compute the key features of binding performance between mutant (Y390C) CHEK2 protein with theaflavic acid and quercetin molecular docking was performed. The binding performance between mutant model of studied protein at Y390C with theaflavic acid resulting the binding energy -6.8 kcal/mol , in which the residues GLY315, SER428 and VAL314 are binds in hydrogen bonding ,where as TYR424 and PRO425 residues are interact in hydrophobic interaction and the detail schematic representation is shown in Fig 1 .

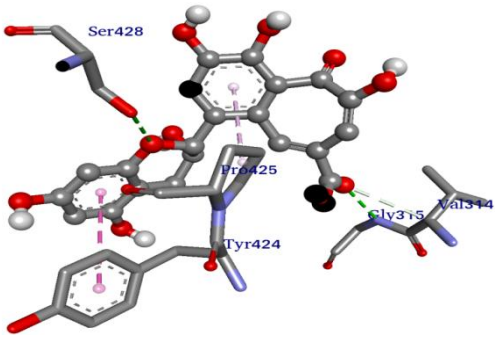

Fig. 1: Diagrammatic representation of docking interaction of theaflavic acid with mutant model of Pkinase domain of CHEK2. Where the ball and stick model is represent to theaflavic acid and stick models are represent to interacting amino acid residues . The pink dotted lines are hydrophobic interactions and green dotted lines are hydrogen bonds.

In overall the native model is more stable than compared mutant model of the studied domain of the protein. The mutant model of protein has more number of hydrogen bonds as compared to native model of protein, which is resulted from hydrogen bond number analysis. From molecular docking study we can find out the interaction between protein and ligand. Here we studied mutant Pkinase domain of CHEK2 gene encoded protein with above said different phytochemicals to predict the binding performance of diseased protein. From detail study of molecular interaction study Pkinase domain of CHEK2 gene encoded protein at Y390C with different molecules shows that the phytochemical theaflavic acid having the best binding performance as compare to quercetin, because the number of hydrogen bonding.

References

[1] J. Abud, JC. Prolla, P. Koehler-Santos, P. Ashton-Prolla,"CHEK2 1100DELC germline mutation: a frequency study in hereditary breast and colon cancer Brazilian families," Arquivos de gastroenterologia, vol. 49, pp. 273-278, 2012.

[2] S. Guauque-Olarte, AL. Rivera-Herrera, L. Cifuentes-C "Mutations of the CHEK2 gene in patients with cancer and their presence in the Latin American population,"*F1000Research*, vol. 5, pp . 2791, 2016.

[3] J. Yang, J. Zhu, K. He, et al.,"Proteomic profiling of invasive ductal carcinoma (IDC) using magnetic beads-based serum fractionation and MALDI-TOF MS," *J Clin Lab Anal*, vol. 29(4), pp. 321–327, 2015.

[4] C. Liu, Y. Wang, QS. Wang and YJ. Wang, "The CHEK2 I157T variant and breast cancer susceptibility: a systematic review and meta-analysis," *Asian Pac J Cancer Prev*, vol. *13*(4), pp.1355-1360, 2012.

[5] N. Wang, H. Ding, C. Liu, X. Li, L. Wei, J. Yu, M. Liu et al, "A novel recurrent CHEK2 Y390C mutation identified in high-risk Chinese breast cancer patients impairs its activity and is associated with increased breast cancer risk,"*Oncogene* , vol. *34*(40), pp. 5198-5205, 2015.

[6] S. Seal, D. Thompson, A. Renwick, A. Elliott, P. Kelly, R. Barfoot, T. Chagtai, H. Jayatilake, M. Ahmed, K. Spanova and B. North,"Truncating mutations in the Fanconi anemia J gene BRIP1 are low-penetrance breast cancer susceptibility alleles," *Nature genetics*, vol. *38*(11), pp.1239-1241, 2006.

[7] SN. Sahu, and SK. Pattanayak, "Molecular docking and molecular dynamics simulation studies on PLCE1 encoded protein," Journal of Molecular Structure, vol. 1198, pp. 126936, 2019.

[8] SN. SAHU, M. MOHARANA,, R. SAHU, AND SK. PATTANAYAK, "IMPACT OF MUTATION ON PODOCIN PROTEIN INVOLVED IN TYPE 2 NEPHROTIC SYNDROME: INSIGHTS INTO DOCKING AND MOLECULAR DYNAMICS SIMULATION STUDY,"JOURNAL OF MOLECULAR LIQUIDS, VOL.281, PP.549-562,2019.

1st International Online Conference on Emerging Smart Materials in Applied Chemistry(ESMAC-2020),10-12 August 2020

Paper ID: 12

Nanoceramics in CAD-CAM Dentistry: An Overview

Aswini Kumar Kar[1], R.Padmini Rani[2], Lokanath Garhnayak[3], Angurbala Dhal[4], Mirna Garhnayak[5]

[1] Professor, Department of Prosthodontics, KIDS, KIIT Deemed to be University, Bhubaneswar, Odisha, India, Email id: bapujikar@gmail.com
[2] MDS, Department of Prosthodontics, KIDS, KIIT Deemed to be University, Bhubaneswar, Odisha, India, Email id:dryuvrani17@gmail.com
[3] Associate Professor, Department of Prosthodontics, SCB Dental College & Hospital, Cuttack, Odisha, India Email id: drloknath@gmail.com
[4] Professor, Department of Prosthodontics, SCB Dental College & Hospital, Cuttack, Odisha, India Email id: drangurbaladhal@gmail.com
[5] Professor, Department of Prosthodontics,Institute of Dental Sciences,SOA University,Bhubaneswar,Odisha, India Email id: mirnagarhnayak@gmail.com

Abstract: Lava Ultimate Resin Nano Ceramic (RNC) blocks are innovative new CAD/CAM materials that make it possible to achieve superior esthetic results in easy steps. The blocks are made of nano ceramic particles embedded in a highly cured resin matrix. Therefore, composite materials can be used to characterize and adjust resin nano ceramic restorations after milling. The milled RNC restorations can be individualized intra-orally or extra-orally, either before or after insertion. Unlike conventional ceramic restorations, customization and glaze firing is neither necessary nor possible with RNC restorations. This opens up the opportunity for intraoral individualization and adaptation of the restorations.

Keywords: CAD/CAM, Nanoceramics, Hybrid

CAD/CAM systems are widely popular in contemporaryprocedures. There are many products and materials touse with different cases and indications in the market.In the current study, most current materials, mainlyNano ceramics and hybrid ceramics are investigated,their advantages and disadvantages are evaluated, andthe current products in the market are listed.

* **Corresponding Author** : DR ASWINI KUMAR KAR
Professor, Department of Prosthodontics
KIDS, KIIT, Bhubaneswaswar
Email id: bapujikar@gmail.com

Currently, various restorative materials are used with CAD/CAM systems. Glass ceramics are often preferred especially in anterior restorations according to their high aesthetic characteristics. The mechanical properties of glass-ceramics can be improved using different methods. Furthermore, alternative materials that have proper characteristics of ceramics are also improved. Nano ceramics and hybrid ceramics were developed to combine the favourable properties of ceramics and composites. The aim of this review is to give information about newly developed Nano ceramic and ceramic hybrid materials used with CAD/CAM systems.

The science of controlling matter on the atomic and molecular level is named as nanotechnology. Particle size of the materials and chemical properties can be changed by nanotechnology.28 The chemical reactivity of the material increases whenever the particle size of materials reduced to nanoscale dimensions. Nano ceramics are comprised of Nano-sizedceramic particles, Bis-GMA, UDMA, Bis-EMA and TEGDMA containing resin matrix.

The structure of the matrix consists of 20 nmin diameter silica nanomers and 4-11nm in diameter zirconia nanomers. Silane moleculejoined in the structure during production of theblocks and provides the formation of chemicalbonds between the resin matrix and the nanostructure.Silane is a bifunctional molecule andcapable of forming chemical bonds betweenthe organic (resin based materials) andinorganic (ceramic and oxidized metal alloys) materials. Constituent

particle of the silane molecule is 3-methacryloxy propyltrimetoksisilan. Silane molecule contains two different chemical structures including methacrylate and methoxy groups. While methacrylate group is connecting organic matrix of the resin structure, methoxy group forms a chemical bond with the ceramic structure.

Nano ceramics are composed of 80% ceramics and 20% resin materials. It is stated that, a high proportion of nanoparticles embeddedin resin matrix enables the material abrasion and fracture resistant. Nano-sized structureof the ceramics also strengthens chemicalbonds formed between inorganic ceramicsand organic resin matrix. The dimensionsof nanoparticles are ranged between 0.6-1micrometers. The modulus of elasticity is defined as the measure of elastic deformation of the material under stress. The elastic moduli of restorative materials used in dentistry have to be compatible with elastic modulus of tooth. This compatibility has a positive impact on the long-term success of the restorations.It is stated that, concordant elastic modulus value of tissues and nanoceramics prevents material from fractures and provides long term of success in high rates. The minimum thickness of the nanoceramic restorations has to be at least 1mm in order to exhibit sufficient fracture resistance against occlusal forces. However, hardness value of nanoceramics is compatible with tooth, for this reason, the amount of wear on the opposing teeth formed quite low. Additionally, ceramic material in the structure provides high colour stability when compared to the composite materials.
Simple surface finishing process and long-term survive of polished surfaces were reported as a major advantage of nanoceramic materials. Recent developments in the field of dental technology enable treatment of edentulous regions with dental implants. Dental implants have proper features like, giving any damage to adjacent tissues, increasing the chewing efficiency, fulfilling the esthetic and phonation. However, one of the most important disadvantages of the implants is inability to form periodontal ligament. Periodontal ligaments are located between the root surface and alveolar bone; and ligaments absorb chewing forces, and distribute them to the alveolar bone. Therefore, choosing force-absorbing featured restorative materials in the production of implant prosthesis is very important. It was stated that the force absorption capacity of the nanoceramics was higher than traditional ceramics used in the fabrication of implant prosthesis.
Lava Ultimate (3M ESPE, USA) is in the group of nanoceramics and used in conjunction with CAD/CAM systems. As a reason of the strong chemical bonds formed between nanoceramic structure and resin, the material has high fracture strength. Besides, flexural strength of the material is 200 MPa. Lauvahutanon and et al. reported the elastic moduli of Lava Ultimate as 29.8 GPa and stated that this value is very close to the dentin. For this reason, it was thought that force-absorbing property of the material is high enough and this allows fabrication of posterior nanoceramic restorations Inlay, onlay, laminate veneers and crown restorations can be manufactured with Lava Ultimate blocks. Adhesive bonding systems are recommended in the cementation of restorations that fabricated with this system. Incontrast to conventional adhesive cementationtechnique the inner surface of the restorationthat fabricated with this system does notrequire hydrochloric acid etching. Sandblasting technique is more proper to roughenthe inner surface of the restorations. Lava Ultimate has high translucent (HT) andlow translucent (LT) blocks, and each blockhas 8 different shades (A1, A2, A3, A3.5,B1, C2, D2 and Bleach). In order to produce larger restorations in 14 L-size blocks are alsoavailable.
Nano ceramics are recently introduced in prosthetic and restorative dentistry, and these materials have a potential success in clinical use.

References

1. Fasbinder, DJ. Restorative materials for chairside CAD/CAM restorations. Compend Cont Educ Dent 2010; 31(9):2-17.

2. Fasbinder DJ. Clinical performance of chairside CAD/CAM restorations. JADA 2006; 137:22S-31S.

3. Fasbinder DJ, Dennison JB, Heys D. Clinical Evaluation of CAD/CAM-Generated Composite Inlays: Ten-Year Report, AADR 2011, Abstract #379.

4. Kassem AS, Atta O, El-Mowafy O. Combined effects of thermocycling and load-cycling on microleakage of computer-aided

design/computer-assisted manufacture molar crowns. Int J Prosthodont 2011 Jul-Aug;24(4):376-8.

1st International Online Conference on Emerging Smart Materials in Applied Chemistry(ESMAC-2020)
10-12 August 2020

Paper ID: 13

Zn^{2+} and HPO_4 selective arrest and bail to a trimethylbenzene -naphthalene anchored schiff base as molecular switch

Jnana Ranjan Sahu[a], Tejaswini Sahoo [a], Rojalin Sahu[*a],Niraj Kumari[b*]

[a] *School of Applied Sciences, Kalinga Institute of Technology (KIIT) Deemed to be University, Bhubaneswar India*
[b] *Department of Chemistry, School of Physical Sciences, Guru Ghasidas Central University, Bilaspur, Chhatishgarh India*
[*]*Corresponding authors: rsahufch@kiit.ac.in, nirajchem@gmail.com*

Abstract- A trimethylbenzene-naphthalene anchored Schiff base (R1) showed Zn^{2+} selective conformational arrest by inhibition of its C=N isomerization leading to its fluorescent switching. The receptor is bailed by HPO_4^{2-} from Zn^{2+} arrest leading to its switching 'off'. This conformational arrest and bail of R1 is extremely explicit as no other ion pairs were able to show the same activity. The detection limit of the R1 for Zn^{2+} is 2,47 x10^{-7} M. while for HPO_4^{2-} is found to be 2.27 x 10^{-6}. The mechanistic facts for 'on-off' switching of R1 by the ion- pairs have been investigated through various spectroscopic studies .The 'on-off' switching of R1 by inputs Zn^{2+} and HPO_4^{2-} led it to imitate with INHIBIT logic gate.

***Keywords*—Schiff base, receptor, molecular switch, logic gate.**

Introduction

The design and synthesis of artificial new fluorescent receptors for the highly selective recognition of analyte is an eye-catching area for research in supramolecular chemistry because of their broad applications in environmental, chemical, biological, industrial and agricultural, process.[1] Zinc(II) is the second most abundant trace metal ion after iron in the human body. Biological processes, such as gene expression, apoptosis, metalloenzymes regulation and neurotransmission is significantly controlled by zinc(II) ion.[2] Severe neurological diseases, including Alzheimer's, ischemia and epilepsy are associated with the disorder of the Zn^{2+} metabolism. In addition, increased levels of Zn^{2+} ions in water escort to environmental problems, viz., suppressed soil microbial activity causing phytotoxic effects, creating water smelly and dirty.[3] Due to the low cost, faster response time, and low detection limit with high selectivity and sensitivity, fluorescent chemosensors has recently gained considerable interest. Therefore, the design and development of efficient fluorescent chemosensors selective to Zn^{2+} are of considerable interest. Herein, we report the synthesis and sensing behavior of R1 by using various spectroscopic tools. Moreover combination of Zn^{2+} and HPO_4^{2-} as inputs, receptor 1 obeys the truth table of INH logic function for output. Hence receptor 1 possesses the ability to work as a molecular switch for the simplistic sensing of Zn^{2+} and HPO_4^{2-} through changes in its fluorescence intensity. This sensing process is also exhibited in a human cervical cancer cell lines (SiHa cells).

Materials and methods

The reagents and solvents were obtained from commercial sources. Solvents were dried and distilled prior to their uses. Elemental analyses for C, H, and N were carried on a CE-440 Elemental

analyzer. Infrared and absorption spectra were recorded using a Varian 3300 FT-IR and Shimadzu UV-1601 spectrophotometers, respectively. ^{1}H (300 MHz) and ^{13}C (75.45 MHz) NMR spectra were obtained on a JEOL AL300 FT-NMR spectrometer using tetramethylsilane (TMS) as an internal reference. Fluorescence spectra were recorded on a Perkin Elmer Fluorescence spectrophotometer using acetonitrile water, (7:3) HEPES buffer, (pH 7.4) at room temperature. Electrospray ionization mass spectrometry (ESI-MS) was carried out on a AMAZONSL Max ion trap mass spectrometer.

Synthesis

2,4,6-Trimethylbenzene-1,3-diamine (0.189 g, 1 mmol) was dissolved in ethanol (10 ml) and added to the solution of 2-Hydroxy-6-nitro-1-naphthaldehyde (0.440 g, 2 mmol) in ethanol (10 ml). The solution was refluxed for3 h, and a yellow precipitate was obtained. The solvent was evaporated under vacuum and washed with hexane. yield 86%, m.p. 172–174 °C.^{1}H-NMR (300 MHz, $CDCl_3$, ppm) δ = 2.29 (s, 6H,-CH_3), 2.21 (s, 3H,-CH_3) 8.01-7.11 (m, 14H, Ar–H),9.13 (1H, –CH ═N–, imine),15.10 (1H, –OH),. ^{13}C NMR(75 MHz, $CDCl_3$, ppm) δ = 167.3, 161.94, 145.04, 135.98,133.10, 130.45, 128.08,121.25, 119.2, 119.0, 118.79, 108.49, 18.47, 14.43; ESI-MS: [(M $+H^+$) $C_{31}H_{26}N_2O_2$] 458.2; found459.2 IR (KBrpellets, cm^{-1}): 464 (w), 649 (w), 752 (s), 826 (m), 1033 (w), 1187 (w), 1387,(m),1475 (m), 1574 (s),1622 (vs), 2926 (w).

Results and discussion

A new receptor 1,1′-(1E,1′E)-(2,4,6-trimethyl-1,3-phenylene)bis-(azan-1-yl-1-ylidene)bis(methan-1-yl-1-ylidene) dinaphthalen 6- nitro-2-ol (R1) was synthesized by the reaction of 2,4,6-trimethylbenzene- 1,3-diamine with 2-hydroxy 6-nitro-1-naphthaldehyde (1 : 2) in ethanol under reflux conditions for 3 h . R1 has been characterized by elemental analysis, NMR and ESI-MS spectroscopic techniques.

Photopysical Behavior of R1

The absorption spectra of R1 in an ACN–H_2O mixture (7 : 3 v/v in 10 μM HEPES buffer at pH = 7.4) were dominated by two absorption peaks at approx λ_{max} 320 nm and 380 nm wavelength corresponding to the n–π* and π–π* transitions, respectively. Further, different metal ions like Cd^{2+}, Hg^{2+}, Mg^{2+}, Ca^{2+}, Ni^{2+}, Co^{2+}, Cu^{2+}, Zn^{2+}, Pb^{2+}, Fe^{2+}, Ag^{+}, Na^{+}, K^{+}, and Al^{3+} at varying concentrations were added to **R1** solution. The subsequent addition of Zn^{2+} results in a gradual decrease of absorption maxima at 380 nm..However, titration of **R1** with other metal ions shows no major change in the absorbance. In the case of emission studies of **R1** shows weak fluorescence at approx λ_{max} 450 nm which is attributed to the isomerization of the imine bond (−HC=N) and excited state intramolecular proton transfer (ESIPT) from the –OH group to the imine nitrogen at 370 nm excitation in the ACN–H_2O mixture (7 : 3 v/v in 10 μM HEPES buffer at pH = 7.4). The titration of **R1** with Zn^{2+} showed gradual fluorescence enhancement at 450 nm which may be due to the formation of a rigid system on binding with Zn^{2+} ions. Further, titration of **R1** with different metal like Cd^{2+}, Hg^{2+}, Mg^{2+}, Ca^{2+}, Ni^{2+}, Co^{2+}, Cu^{2+}, Pb^{2+}, Fe^{2+}, Ag^{+}, Na^{+}, K^{+}, and Al^{3+} was carried out and the resulting emission spectra show no enhancement of fluorescence intensity at 450 nm. However, on addition of Zn^{2+} the receptor showed fluorescence turn-ON with about 7 fold enhancement in fluorescence intensity. The possible reasons for the fluorescence turn-ON may be because of (i) the deprotonated form of **R1** by addition of Zn^{2+} ions, and (ii) the photoinduced electron transfer (PET) suppressed by Zn^{2+} coordination. Thus, the results obtained from absorption and emission studies authenticate the high sensing behavior of **R1** specific to Zn^{2+} ions. The binding constant of **R1** with Zn^{2+} has been calculated using the Benesi–Hildebrand equation[4] and found to be 1.13×10^5 M^{-1} by absorption.

Cell imaging studies

In order to explore the detection of Zn^{2+}ions in a living system, a solution of R1 was allowed to interact with SiHa cell lines (human cervical cancer cells). Its confocal images showed no fluorescence. But in the presence of an aqueous solution of $Zn(NO_3)_2$, it displayed an orange fluorescence. This fluorescence disappeared on the addition of an aqueous solution of HPO_4^{2-}ions. This process was repeated several times and it was found reversible. Thus, sequential detection of Zn^{2+}ions and $H_2PO_4^{2-}$ ions could also be demonstrated inside a cancerous cell lines.

Logic gate studies

The selective ‘on-off’ switching of **R1** with Zn^{2+} and $H_2PO_4^{2-}$motivated us to explore the complete sensing phenomenon as its budding application in the field of logic gates and molecular switches. The logic behavior of receptor **R1**is “A doesn't involve” in other words “true if Zn^{2+}, but not HPO_4^{2-}”. Thus the fluorescence turn ‘on’ (Readout ‘1’) occurs when Zn^{2+} is the only input. The introduction of $HPO_4^{2-}$to **R1** + Zn^{2+} ensemble bailed the receptor from Zn^{2+} arrest leading to turn ‘off’ fluorescence response. Therefore we expect this phenomenon to act as non-inference or more specifically inhibition (INH) logic gate. Thus Readout ‘1’ obtained only when the input is Zn^{2+} and in all other combinations of inputs the receptor remains in the

switched ‘off’ condition (Readout ‘0’) as shown in Fig 1.

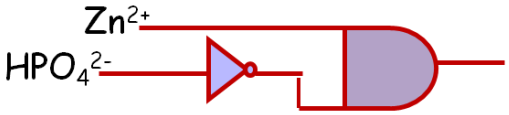

Inputs		Outputs
Zn^{2+}	HPO_4^{2-}	INHIBIT Logic Gate
0	0	0
0	1	0
1	0	1
1	1	0

FIG.1: Electronic equivalent circuitry of The “INHIBIT " logic gate.; and truth table of the INHIBIT gate.

Conclusion

A new receptor of a trimethylbenzene -naphthalene anchored Schiff base R1has been designed and synthesized. The receptor **R1** was utilized for metal sensing properties and found to be sensitive, selective and reversible in nature, which showed fluorescence turn-ON with Zn^{2+} ion among other metal ions. It also showed ‘on-off ’switching by Zn^{2+} and $H_2PO_4^{2-}$. This process is also demonstrated in vivo using a human cervical cancer cells (SiHa) lines. Moreover, appliance of receptor **R1** as potential logic gate and molecular switches adjoins further lustre to the same

References

[1] J. Y. Choi, D. Kim and J. Yoon, Dyes Pigm., 2013, 96, 176..

[2] S. C. Burdette and S. J. Lippard, Proc. Natl. Acad. Sci. U. S. A., 2003, 100, 3605.

[3] A. Voegelin, S. Poster, A. C. Scheinost, M. A. Marcus and R. Kretzsch-mar, Environ. Sci. Technol., 2005, 39, 6616.

[4]H. A. Benesi and J. H. Hildebrand, J. Am. Chem. Soc., 1949, 71, 207

[5] Y., Hu, Y. Liu, G. Kim, E. J. Jun, K. M. K. Swamy, Y. Kim, and J. Yoon, Dyes and Pigments, 2015, *113*, 372-377.

[6] H. G. Lee, J. H. Lee, S.P. Jang, I. H. Hwang, S. J. Kim, Y. Kim, and R. G. Harrison, *Inorganica Chimica Acta*, 2013, *394*, 542-551.

[7] J. H. Kim, J. Y. Noh, I. H. Hwang, J. Kang, J. Kim, and C. Kim, *Tetrahedron Letters*, 2013. *54*(19), 2415-2418.

[8] H. Y. Lin, P. Y. Cheng, C. F. Wan, and A. T. Wu, *Organic letters* 2012. *137*(19), 4415-4417.

1st International Online Conference on Emerging Smart Materials in Applied Chemistry(ESMAC-2020)
10-12 August 2020

Paper ID:14

Synthesis, characterization of 4′-(2-pyridyl)-2,2′:6′,2′′-terpyridine complexes of Zn(II) and Ag (I) having antibacterial activity against M. Smegmatis and S. Aureus

Jagannath Panda[a],Deepak Senapati[a], Jnana Ranjan Sahu[a], Jatin Kumar Sinha[a],Rojalin Sahu[a*]

[a] *School of Applied Sciences, Kalinga Institute of Technology (KIIT) Deemed to be University, Bhubaneswar India*
[*]*Corresponding author:* rojalinsahu.chem@gmail.com

Abstract- Zinc(II) and Silver (I) complexes were synthesized by using 4′-(2-pyridyl)-2,2′:6′,2′′-terpyridine (QPY) and Isoniazid (ISN) as ligand. The ligand is well characterized by NMR, IR and single crystal XRD. The complexes were characterized by UV-Vis, IR, NMR, and Mass spectroscopy. Antibacterial activity of the three complexes [$ZnNO_3$(QPY)], [AgNO3(QPY)], [ZnQPYISN] were tested against M. Smegmatis and S. Aureus. Among the four complexes, [$AgNO_3$(QPY)] is more active against M. Smegmatis and S. Aureus.

***Keywords*— Zinc (II); Silver(I); Isoniazid, Terpyridine, Antibacterial activity.**

Introduction

Infectious diseases are the major problem in developing countries like India and the most important concern is development of antimicrobial resistance among pathogens. Compared to developed countries, the incidence of drug resistance problems are more in economically disadvantaged person due to inappropriate and irrational use of antimicrobial agents. According to a recent report, the infectious disease burden in India is among the highest in the world [1]. First line drugs include isoniazid (INH), rifampicin (RIF), pyrazinamide (PZA), ethambutol (EMB) and streptomycin (STR); whereas second line drugs include aminoglycosides, fluoroquinolones, cycloserine and P-aminosalicylic acid. It has been emphasized that indiscriminate use of drugs led to development of multidrug resistant (MDR), extremely drug resistant (XDR) and totally drug resistant (TDR) Mtb strains. MDR-TB is resistant to isoniazid and rifampin, the major first line anti-TB drugs; XDR-TB is resistant to any fluoroquinolone, and at least one of three injectable second-line drugs (capreomycin, kanamycin, and amikacin), in addition to isoniazid and rifampin; line drugs tested, which makes it virtually untreatable. Clearly, there is an urgent need to improve treatment by either enhancing the potency of existing anti-TB or introducing new drugs. In this regard natural products and their semisynthetic derivatives can play crucial role of clearing tuberculosis infections. Recently plant polyphenols was studied against Mtb dihydrofolate reductase inhibitors which showed potential activity against Mtb H37Rv [2]. On the other hand many virulence proteins are involved in biosynthesis of mycolic acids and other components that are found uniquely in the cell envelope of Mycobacterium tuberculosis and are essential for survival and virulence of Mtb [3]. Importantly Mycobacterium contains very complex cell wall with specific mechanisms which help in removal of drug molecules by specific efflux pumps [4]. Taken together there is a growing need to develop novel therapeutic strategies against TB. One approach for combating drug resistant infections is to use composite molecules having synergistic activities with different mode of actions. For example, combination therapy regimens have long been used to treat cancer [5] and HIV infected patients [6]. Therefore in this study we used Terpyridine (QPY) as it has been used as ligand in coordination chemistry. Here we synthesized QPY and anti TB drug complexes as well as QPY complexes with different drug combinations.

Materials and methods

The complexes were synthesized by using 1:1 of metal and ligands in aqueous methanolic solution. The solid obtained was filtered, washed with methanol and then dried at room temperature for further characterizations.

Synthesis

[Zn(Qpy) (NO_3)$_2$] (1): Yield: ~81%. Anal. Calcd. for $C_{20}H_{14}N_5O3Zn$: ESI–MS in 5% aqueous methanol: *m/z* 436.04 [Zn–(NO3-)]. FT–IR data/ cm-1: 1682 s, 1613 s,

1471 vs, 1410 s, 1383 s, 1250 s,1156 m, 1013 s, 894 w, 780 w, 727 s, 735 m, 657 m, 637 m (vs, very strong; s, strong; m, medium; w, weak; sbr, strong broad). UV–visible in 5% aqueous DMF [cm-1max)]: 280 (71,200).

[Ag(Qpy) $(NO_3)_2$] (2): Yield: ~79%. Anal. Calcd. for $C_{20}H_{14}N_5O_3Ag$: ESI–MS in 5% aqueous methanol: *m/z* 479.01 [Ag–(NO3-)]. FT–IR data/ cm-1: 1679 s, 1570 s, 1466 vs, 1383 s, 1284 s,1164 m, 1032 s, 1006.81s, 893 w, 778 w, 750 s, 735 m, 656 m, 644 m (vs, very strong; s, strong; m, medium; w, weak; sbr, strong broad). UV–visible in 5% aqueous DMF [nm)]: 276nm.

[Zn(Qpy) $(NO_3)_2$]ISN (3): Yield: ~80%. Anal. Calcd. for $C_{26}H_{20}N_7OZn$: ESI–MS in 5% aqueous methanol: *m/z* 510.01[Zn–(NO3-)]. FT–IR data/ cm-1: 1685 s, 1511 s, 1471 vs, 1410 s, 1353 s, 1005 s,1024 m, 1051 s, 820 w, 755 w, 730 s, 697 m, 618 m (vs, very strong; s, strong; m, medium; w, weak; sbr, strong broad). UV–visible in 5% aqueous DMF [nm)]: 278nm.

M. smegmatis mc^2155 and *S. aureus* were grown in Middlebrook's 7H9 and LB broth medium. The mouse macrophage RAW 264.7 cells, peritoneal macrophages and dendritic cells were cultured in DMEM Dulbecco's modified Eagle's medium (DMEM; HiMedia, Mumbai, India) supplemented with 10% fetal bovine serum, 1% penicillin-streptomycin

Colony forming unit assay

***In vitro* killing assay**

To determine the antimycobacterial activity of drug complexes, 4-5 $X10^5$ bacteria were incubated with various concentrations of these complexes in 7H10 medium in 96-well round bottom plates in triplicates. Bacteria were harvested at the indicated time points and the number of colony forming units (CFUs) was assayed by plating suitably diluted cultures on 7H10 agar plates. All samples were plated in triplicate and values were averaged from three independent trials.

MTT assay

Cytotoxicity Assay

Peripheral blood monocyte cells (PBMCs) were isolated from human blood using 2.5% dextran T-500 as described previously [18] THP-1 and PBMCs ($1x10^5$cells/well) were grown in 24-well plates at 37 ^{0}C, 5% CO_2 for 24 h followed by treatment of cells with different concentrations of ZnO-NPs for another 24 h. Cell viability was determined by MTT assay as described previously [7].

Results and discussion

As shown in figure 1 A and B dose dependent inhibition of bacterial killing was observed in both 6 and 24h time points. In case of 6h time point in both M. smegmatis and S. aureus the Ag-QPY complex didn't exhibited killing efficiency but after 24 h of incubation period, the killing effect was significant (Figure 1 A, B).

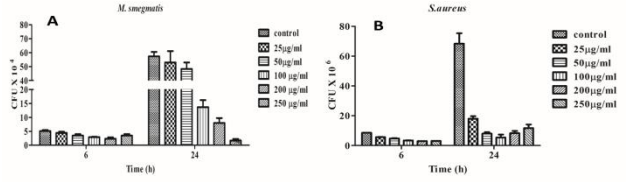

Figure 1: Dose dependent killing of bacteria by Ag-QPY complexes (A) Mycobacterium smegmatis (B) S. aureus.

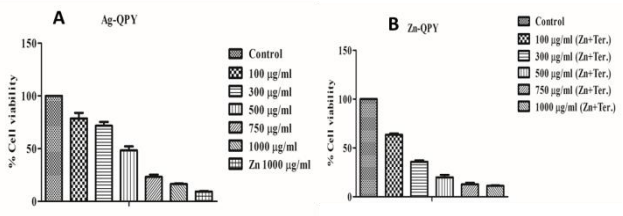

Figure 2: Cytotoxic activity of Ag-QPY complex (A) and Zn-QPY complex on **(B)** mouse macrophage cell lines.

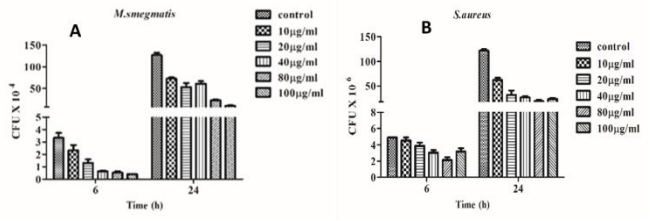

Figure 3: Dose dependent killing of bacteria by Zn-QPY complexes **(A)** *Mycobacterium smegmatis* **(B)** *S. aureus.*

As shown in figure 2, 500 μg/ml of Ag-Qpy complex reduced approximately 50% cell survival as compared to untreated control. Zn-QPY complex induced antibacterial activity against M. smegmatis and S. aureus in a dose dependent manner (Figure 3 A, B). To determine the cytotoxicity of Zn-QPY complex we performed MTT assay, where the tetrazolium dye to formazen crystals by viable cells. We observed that Zn-QPY complex induced a dose dependent reduction of macrophage cell viability (Figure 2B). As shown in the above figure, Zn-QPY-INZ showed enhance anti mycobacterial activity in comparison with only isoniazid in both the time points.

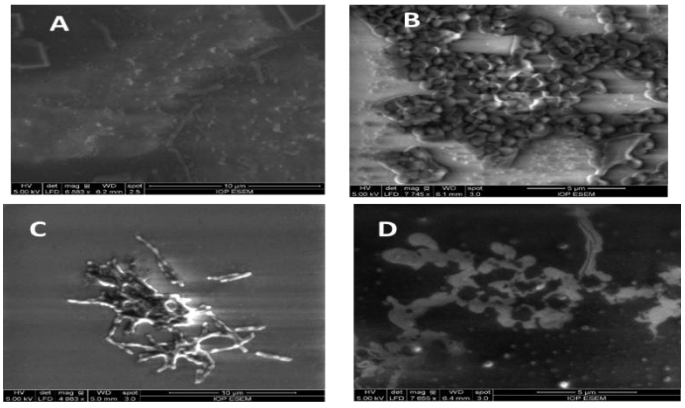

Figure 4: ESEM images of Control **(A)** *Mycobacterium smegmatis*, **(B)** *S. aureus*. **(C)** treated *Mycobacterium smegmatis*, and **(D)** treated *S. aureus*.

From the ESEM images, it has been observed that the complexes are having effective killing activity against the bacterial strains.

Conclusion

With this work we have synthesized and characterized Zinc (II) and Silver (I) complexes were synthesized by using 4′-(2-pyridyl)-2,2′:6′,2″-terpyridine (QPY) and Isoniazid (ISN) as complexes. Newly synthesized

compounds were examined for their antibacterial and cytotoxicity activity features. Zn-QPY-INZ complex was the most effective complex killing activity against the bacterial strains *Mycobacterium smegmatis* and *S. aureus*.

References

[1]. Kumar, S.G., Adithan. C., Harish, B.N., Sujatha, S., Roy, G., Malini, A. Antimicrobial resistance in India (2013). A review. *J Nat Sci Biol Med.* **4,** 286-91.

[2]. Raju, A., Degani, M.S., Khambete, M.P., Ray, M.K., Rajan, M.G. Antifolate Activity of Plant.Polyphenols against Mycobacterium tuberculosis (2015). *Phytother Res.* **29,** 1646-51.

[3]. Jamet, S., Quentin, Y., Coudray, C., Texier, P., Laval, F., Daffé et al. Evolution of Mycolic Acid Biosynthesis Genes and Their Regulation during Starvation in Mycobacterium tuberculosis (2015). *J Bacteriol.* **197,** 3797-811.

[4]. Szumowski, J.D., Adams, K.N., Edelstein, P.H., Ramakrishnan, L. Antimicrobial efflux pumps and Mycobacterium tuberculosis drug tolerance: evolutionary considerations (2013). *Curr Top Microbiol Immunol.* **374,** 81-108.

[5]. Peters B.M., Shirtliff M.E., Jabra-Rizk M.A.*PLoS Pathog*. 2010, 6.

[6]. Han Z., Pinkner J.S., Ford B., Chorell E., Crowley J.M., Cusumano C.K. *et al. J Med Chem*. 2012, 55:3945–59.

[7]. Pati, R., Mehta, R.K., Mohanty, S., Padhi, A., Sengupta, M., Vaseeharan, B. Goswami, C., Sonawane, A. Topical application of zinc oxide nanoparticles reduces bacterial skin infection in mice and exhibits antibacterial activity by inducing oxidative stress response and cell membrane disintegration in macrophages (2014). *Nanomedicine.* **10,** 1195-208.

1st International Online Conference on Emerging Smart Materials in Applied Chemistry(ESMAC-2020)
10-12 August 2020

Paper ID:15

A chemically stable nanoporous coordination polymer *via* Cu^{2+} cation exchange for selective C_2H_2/CO_2 separation

Nibedita Behera[a] and Jingui Duan[a]*

[a]*State Key Laboratory of Materials-Oriented Chemical Engineering, College of Chemical Engineering, Nanjing Tech University, Nanjing 211816, China*
E-mail: duanjingui@njtech.edu.cn

***Abstract*—Being explosive in nature and industrial utilization of acetylene (C_2H_2), safe capture and highly pure storage is a great challenge and also need to overcome the separation difficulties due to its nearly similar molecule size with carbon dioxide (CO_2). Here, a new nanoporous coordination polymer (PCP) adsorbent (NTU-66-Cu) with was prepared through post-synthetic approach *via* cation exchange from the parent Zn(II) PCP NTU-66, an anionic framework with new 3, 4, 6-c topology and two kinds of cages. The significant improve in C_2H_2/CO_2 selectivity of NTU-66-Cu is observed from 6 to 32 (*v/v*: 1/1) at low pressure under 298 K and enhanced C_2H_2 capacity (from 89.22 to 111.53 $cm^3 \cdot g^{-1}$). Importantly, host-guest interaction responsible for acetylene separation was validated by density functional theory (DFT) calculation. Further, from breakthrough experiments under continuous and dynamic conditions, this chemical stable adsorbent can achieve recycle C_2H_2/CO_2 separation without loss of C_2H_2 capacity.**

Keywords—Nanoporous Coordination Polymer, High Porosity, New Topology, Post-synthetic Approach, C_2H_2/CO_2 Separation

As reactive in nature, acetylene (C_2H_2) has been used for thesynthesis of various organic compounds [1]. The industrial methods of production of acetylene also include CO_2 as an impurity.Therefore, the purity of C_2H_2 is important, which may affectthe reaction process and even the product grade. However, similar kinetic parameters, molecularshape and physical propertyare the obstacles for the selective separation by traditional methods with high energy consumption, expensive, and high risks [2]. Hence, to achieve a reversible adsorption/desorptionprocess and greatly reduce energy consumption [3]porous coordination polymers (PCPs) emergeas a new class of porous materialopens up as promising platform for various separation applications [4–6] due toits inbuiltproperties; pore size, shape, functionality and flexibility, whichcan be exquisitely designed and controlled. Specifically, asynthetic approach of post-synthetic modification can tune the function of the PCPs [7–10]. Though, charged framework amongvarious PCPs, can induce the gas adsorption capacity and counterion existed in thenanospace can be exchanged to tune the interaction site in the pore surface for supporting the host-guest interaction [11,12]the challenging separation ofC_2H_2/CO_2 separation using post-modified PCPs still remainsin fancy.

Here, in this report, a three-dimensional (3D) framework of **djh**net topology with (3,4,6)-connection which incorporates two different cages named as **NTU-66**[13] was produced from solvothermal reaction of tetrazolate ligand and Zinc salt. The single crystal X-ray diffraction (SCXRD) data indicates, it contains a$(Me)_2H_2N^+$counterion and two types of pores, which inspired to use the PCP as a parent material for conversion into Cu(II) exchange PCP, characterized by PXRD pattern, matches well with that ofsimulated curve of **NTU-**

66, X-ray photoelectron spectra (XPS) study, inductively coupled plasma (ICP) and surface analysis by scanning electron microscopy mapping (SEM-mapping)and optical photograph, where uniform distribution of Cu^{2+}ions in **NTU-66-Cu** was observedand its ability for gas adsorption. As analysed from N_2 adsorption both **NTU-66** and **NTU-66-Cu** have similar BET surface area and pore volume and further single gas adsorptions experiments of C_2H_2 and CO_2reveal that in both C_2H_2 uptake volume is higher. Moreover, the uptake of C_2H_2

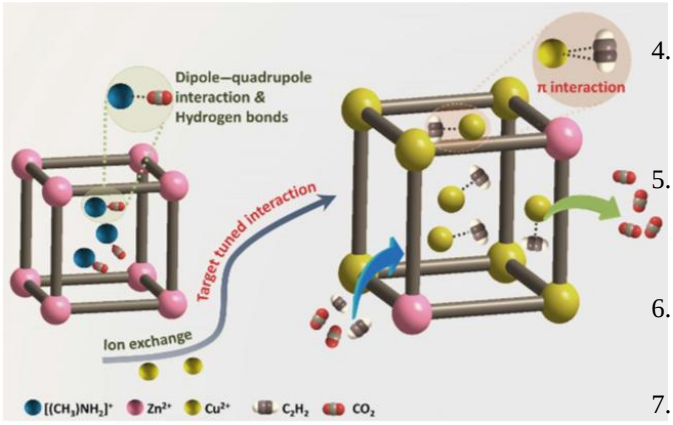

Scheme 1. Schematic view of tuned host–guest interaction*:* Post modificationallows the **NTU-66-Cu** to have fixed and free Cu^{2+} sites, which boostselective C_2H_2 capture through π interaction.

is111.53 $cm^3 \cdot g^{-1}$at 298 K for **NTU-66-Cu** is higher than that of **NTU-66**. These resultshave taken into a point that Cu^{2+} cation exchange may createadditional π interaction between Cu^{2+} and C_2H_2 molecule byreplacing the dipole–quadrupole and hydrogen bondinginteraction with CO_2 that originates from $[(Me)_2NH_2]^+$ moiety[14] having good selectivity of **NTU-66-Cu** showedthe value32 (1:1, *v*/*v*) and the Q_{st}values of C_2H_2 in**NTU-66-Cu** increases to 32.3 $kJ \cdot mol^{-1}$higher than that of parent PCP.The host–C_2H_2 and host–CO_2interactions in **NTU-66-Cu**, is also supported by DFT calculations where C_2H_2 interacts more preferable in **NTU-66-Cu**. For practical utility of PCP, separation behaviour of binaryC_2H_2/CO_2 mixtures under continuous and dynamic conditions,breakthrough experiments were performed on **NTU-66-Cu**at 298 K and alsoshows a nearly overlappingC_2H_2/CO_2 breakthrough curve in second round test where mild reactivation is required for reuse of PCP for further separation.

A new anionic PCP with two different kinds of cages was designed and synthesized and post-synthetic *via*Cu^{2+} exchange, shows a rare phenomenon that both C_2H_2 adsorption capacity and C_2H_2/CO_2 selectivity increase simultaneously at 298 K. The excellent chemical stability, even at wide range pH and high temperature, made this material for potential applications in feasible conditions. Therefore, this work reports not only a good adsorbent for highly efficient C_2H_2/CO_2 separation, but also an idea for future materials design.

References:

1. Stang, P. J.; Diederich, F. *Modern Acetylene Chemistry*; VCH: New York, 1995.
2. Lin, J. Y. S. Molecular sieves for gas separation. Science 2016, 353, 121–122.
3. Sholl, D. S.; Lively, R. P. Seven chemical separations to change the world. *Nature* **2016**, *532*, 435–437.
4. Wang, H.; Li, J. Microporous metal-organic frameworks for adsorptiveseparation of C5-C6 alkane isomers. *Acc. Chem. Res.* **2019**, *52*, 1968–1978.
5. Furukawa, H.; Cordova, K. E.; O'Keeffe, M.; Yaghi, O. M. The chemistry and applications of metal-organic frameworks. *Science***2013**, *341*, 1230444.
6. Walton, K. S. Metal-organic frameworks: Recognizing the unrecognizable. *Nat. Chem.* **2014**, *6*, 277–278.
7. Han, Y.; Li, J. R.; Xie, Y. B.; Guo, G. S. Substitution reactions in metal-organic frameworks and metal-organic polyhedra. *Chem. Soc. Rev*. **2014**, *43*, 5952–5981.
8. Sen, R.; Saha, D.; Koner, S.; Brandao, P.; Lin, Z. Single crystal to single crystal (SC-to-SC) transformation from a nonporous to porous metal-organic framework and its application potential in gas adsorption and Suzuki coupling reaction through postmodification. *Chem.—Eur. J*. **2015**, *21*, 5962–5971.
9. Li, L.; da Silva, I.; Kolokolov, D. I.; Han, X.; Li, J. N.; Smith, G.; Cheng, Y. Q.; Daemen, L. L.; Morris, C. G.; Godfrey, H. G. W. et al. Post-synthetic modulation of the charge distribution in a metalorganic framework for optimal binding of carbon dioxide and sulphur dioxide. *Chem. Sci*. **2019**, *10*, 1472–1482.
10. Fracaroli, A. M.; Siman, P.; Nagib, D. A.; Suzuki, M.; Furukawa, H.; Toste, F. D.; Yaghi, O. M. Seven post-synthetic covalent reactions in tandem leading to enzyme-like complexity within metal-organic framework crystals. *J. Am. Chem. Soc*. **2016**, *138*, 8352–8355.
11. Wang, X. J.; Li, P. Z.; Liu, L.; Zhang, Q.; Borah, P.; Wong, J. D.; Chan, X. X.; Rakesh, G.; Li, Y. X.; Zhao, Y. L. Significant gas uptake enhancement by post-exchange of zinc(II) with copper(II) within a metal-organic framework. *Chem. Commun*. **2012**, *48*, 10286–10288.

12. Patel, H. A.; Islamoglu, T.; Liu, Z. C.; Nalluri, S. K. M.; Samanta, A.; Anamimoghadam, O.; Malliakas, C. D.; Farha, O. K.; Stoddart, J. F. Noninvasive substitution of K^+ sites in cyclodextrin metal-organic frameworks by Li^+ ions. *J. Am. Chem. Soc*. **2017**, *139*, 11020–11023.
13. Chen, S.[§]; Behera, N.[§]; Yang, C.; Dong, Q.; Zheng, B.; Li, Y.; Tang, Q.; Wang, Z.; Wang, Y.; and Duan, J. A chemically stable nanoporous coordination polymer with fixed and free Cu^{2+} ions for boosted C_2H_2/CO_2 separation, *Nano Res.* 2020, DOI: 10.1007/s12274-020-2935-1. ([§]*Si Chen and NibeditaBehera contributed equally to this work*)
14. Zheng, B. S.; Bai, J. F.; Duan, J. G.; Wojtas, L.; Zaworotko, M. J. Enhanced CO_2 binding affinity of a high-uptake rht-type metal-organic framework decorated with acylamide groups. *J. Am. Chem. Soc*. **2011**, *133*, 748–751.

.

1st International Online Conference on Emerging Smart Materials in Applied Chemistry (ESMAC-2020)
10-12 August 2020

Paper ID:16

Volumetric properties of isoniazide in aqueous solutions of sodium citrate

Mamata Pradhan[1], Ranjan K. Pradhan[2], Prativa Kar[1], Braja B. Nanda[2*]

[1]Department of Chemistry, GIET University, Gunupur, Odisha, India
[2]P. G. Department of Chemistry, Vikram Deb Autonomous College, Jeypore-764001, Odisha
Corresponding author's e-mail: bbnanda.driems@gmail.com

***Abstract*—The volumetric properties of isoniazid in aqueous solutions of sodium citrate has been determined from the experimentally obtained density values of isoniazid at various temperatures and at atmospheric pressure. Apparent molar volume and limiting apparent molar volume obtained from Masson equation were used to study the inter molecular interactions. The apparent molar volume, limiting apparent molar volume and standard partial molar volume of transfer for isoniazid from water to aqueous sodium citrate have been calculated from density data.The values of partial molar expansivity and Helper constants were used to investigate the structure making and breaking capacity of isoniazid in the mixed solvents.**

Key words: Isoniazid; apparent molar volume; sodium citrate; ion-solvent interactions.

I. Introduction

Drugs are the chemicals which have low molecular mass of about 100-500amu and when it will interact with biomolecule initiate a physiological or biological response. In pharmacology, a drug is a chemical substance typically of known structure, which when administered to a living organism, produces a biological response. Drugs are also called medicines when they are therapeutic value. When drugs are taken in safe doses they are used as medicines which is taken for diagnosis, prevention and treatment of diseases.All drugs have active pharmaceutical ingredients (API) means the part of medicine which is used to target the disease, example paracetamol have only 0.01% API which target to lower the body temperature.Volumetric properties of drugs and their interactions with the citrate ions helps the drugs action in molecular levels. The drug macromolecular interactions are an important phenomenon in physiological media, which includes membranes, blood, intra and extracellular fluids [1–3]. The drug-solvent interactions are not easy to understand directly in biological systems, various co-solutes such as carbohydrates, salt, polymer, osmolytes, amino acids, peptide, protein and surfactants can alter these interactions [4]. The phenomenon like protein binding and drug transport can be understood in the term of their macromolecular interactions, whose mechanism is very complex to understand.Almost all biochemical reactions are taking place in presence of aqueous media. Therefore, the physicochemical properties like volumetric properties of drugs in aqueous solutions of various co-solutes, helps to understand the inter molecular interactions of drug molecules with the solvents and this information is found to be useful in the field of pharmacy and medicinal chemistry [5,6]. From the medical point of view, Sodium citrate is used to neutralize the excess acid in the blood. So, it acts as an alkalizing agent. It has been designated for the handling of metabolic acidosis. In this paper the intermolecular interactions of isoniazid with aqueous solution of sodium citrate at T= (298.15 to 303.15) K, have been studied by volumetric methods.

. ***REFERENCES***

[1] S. Mondal, S.S. Dhondge, L.J. Paliwal, V.M. Tangde, S.P. Jengathe, J. Chem. Thermodyn. 90 (2015) 147–157.
[2] P. Ament, J. Bertolino, J. Liszewski, Am. Fam. Physician 61 (2000) 1745–1754.
[3] S.S. Dhondge, S.P. Zodape, D.V. Parwate, J. Chem. Thermodyn. 48 (2012) 207– 212.
[4] S. Ryshetti, B.K. Chennuri, R. Noothi, S.J. Tangeda, R.L. Gardas, Thermochem. Acta 597 (2014) 71–77.
[5] T.S. Banipal, H. Singh, P.K. Banipal, J. Chem. Eng. Data 55 (2010) 3872–3881.
[6] M.J. Iqbal, M.A. Chaudhry, J. Chem. Thermodyn. 41 (2009) 221–226.

1st International Online Conference on Emerging Smart Materials in Applied Chemistry (ESMAC-2020)
10-12 August 2020

Paper ID:17

Removal of Basic Blue Dye from Aqueous Solution by Adsorption onto poly(Acrylic Acid/Acrylamide/SodiumHumate)

Singhal R.[a*], Singh T.[b]

[a]Department of Plastic Technology, Harcourt Butler Technological Institute, Kanpur (U.P.)-208002 India
E-mail-reena_singhal123@rediffmail.com

[b]Department of Chemistry, VSSD College, Kanpur (U.P.)-208002 India, E-mail-singh.tripss@gmail.com

***Abstract*—A series of hydrogels composed of poly(acrylic acid-acrylamide)/sodium humate poly(AAc/AM/SH) were synthesized and applied as an adsorbent to adsorb basic blue (BB) dye from the aqueous solutions. The swelling behaviors of the synthesized hydrogels were investigated. The factors affecting adsorption capacity of the poly(AAc/AM/SH) hydrogel such as temperature, contact time, SH content (wt%), initial concentration of the dye were also systematically investigated. The experimental data reveals that an appropriate addition of SH (2.4 wt%) increases the swelling as well as adsorption capacity of poly(AAc/AM/SH) hydrogel. The adsorption capacity was approximately to 164 mg/g for BB. The results also suggest that the adsorption equilibrium data fitted very well to the Langmuir isotherm. Thermodynamic parameters of adsorption were also calculated, and the negative value in ΔG^0 and ΔH^0 confirmed that the BB dye adsorption process was spontaneous and exothermic in nature.**

***Keywords*— Adsorption, Dye, Swelling behavior, Thermodynamic Parameter**

I. Introduction

In the last decade, a tremendous increase in the use of dyes contaminant volume has posed various serious environmental problems because they toxic to many life forms(1) and can not be destroyed by chemical or biological remediation processes (2). Adsorption process is generally recommended for the removal of dyes due to its easy handling, high efficiency, regenerability as well as availability of different adsorbents and cost effectiveness (3). AAc is cheap and can be easily polymerize to products having high molecular weight. Polyacrylamide and its copolymers have the capability to absorb water and capable of dye adsorption. Humic acid, a natural product, composed of large number of functional hydrophilic groups (such as carboxylates and phenolic hydroxyls) (4). Sodium humate form complexes with cationic dye due to presence of the carboxylate and phenolate groupsBasic Blue, well-known hazardous dye being used for various purposes: a biological stain, a veterinary medicine, an additive to poultry feed to inhibit propagation of mold, intestinal parasites as well as fungus etc. It is also used in textile, dying and paper printing industries. It is necessary to remove the dye from contaminated water before discharging to environment.

II. Materials and Methods

a. Reagents

Acrylic acid (AAc), acrylamide (AM), ammonium per sulphate (APS), sodium hydroxide (NaOH), N, N-methylene bisacrylamide (NMBA), were purchased from CDH New Delhi, India. Basic blue dye Qualigens Fine Chemicals, Mumbai, India), Methanol was purchased from Qualikems, New Delhi and Sodium humate (SH), (supplied

from Aldrich). Double distilled water was used throughout the experiment.

B. Synthesis of poly (AAc/AM/SH) hydrogels

AAc and AM were dissolved in distilled water. Then the NaOH solution was added to neutralize. 0.20 wt% NMBA and then SH was added and heated in a thermostat oil bath at 50ºC, and then APS (0.40 wt%), was introduced. The solution was stirred vigorously with heating at 50ºC. After polymerization product was washed with methanol and water, and then dried in an oven at 50ºC (Table 1).

C Measurement of BB dye molecules adsorption

The calculation of adsorption capacity was performed by the equation-

$$q_e = \frac{C_o - C_e}{m} \times V$$

Where C_o is the initial concentration of BB dye molecules, C_e is the equilibrium concentration; V is the volume of the BB dye solution; and m is the mass of hydrogel sample.

D. Desorption/regeneration of adsorbent

Recovery of the BB dye molecule sadsorbed(mg/g) were carried out in distilled water.

$$\text{Desorption ratio} = \frac{\text{Amount of } Cu^{2+}\text{ion/MB dye desorbed to the elution medium}}{\text{Amount of } Cu^{2+}\text{ion/MB dye adsorbed on the superabsor bent hydrogel}} \times 100$$

III. Results and Discussion

a. Effect of Sodium Humate concentration on water absorbency

The relationship between equilibrium swelling and SH concentration variation is shown in figure (1).

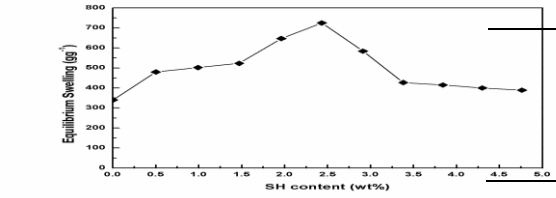

Figure-1: Effect of SH concentration (wt %) on the equilibrium swelling of the synthesized poly(AAc-AM-SH) SAHs at 0.04 wt% APS, 0.20 wt% NMBA

It can be observed from the figure (1) that the hydrogel with SH concentration 2.40wt% shows maximum water absorbency of 724gg^{-1} as, SH is a complex organic macromolecule, contains free and bound phenolic –OH groups, nitrogen and oxygen as bridge unit, quinine structure, , -COOH and –NH_2 groups variously placed on aromatic ring. When the SH content increases above 2.40 wt%, the apparent decrease of water absorbency due to excessive SH only act as a filler.

B. Effect of SH concentration on adsorption of BB Dye

Effect of SH content on adsorption capacity of poly(AAc-AM-SH) SAHs for BB dye has been shown in figure (2). It can be observed from the figure that adsorption capacity of poly(AAc-AM-SH) SAHs increases from 110 to 164 mg/g when the SH content was less than 2.40 wt %. As SH has many functional groups to react with AAc and AM and improve the polymeric network, so enhanced the adsorption ability to a certain extent. However, on further increasing the SH content above 2.40 wt%, resulted in a decrease of adsorption capacity.

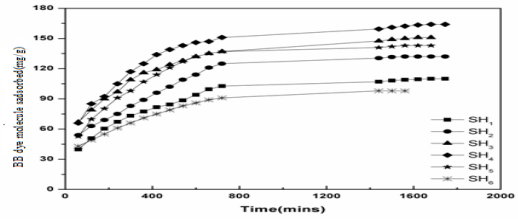

Figure-2: Effect of SH concentration on the adsorption capacity for BB dye of (AAc-AM-SH)SAHs

E. Adsorption Isotherms

The most widely used isotherm for modeling of the adsorption is the Langmuir adsorption isotherm. The Langmuir adsorption isotherm equation described as (Langmuir I. J.)

$$\frac{C_e}{q_e} = \frac{1}{K_e q_{max}} + \frac{C_e}{q_{max}}$$

The Langmuir constants were calculated from the linear plots of C_e/q_e vs C_e. The q_{max} values of the superabsorbent hydrogels obtained by Langmuir equation were quite consistent with the experimental one (Table 2).

Sample designation	Langmuir model			
	q_e (mg/g)	q_{max} (mg/g)	$K_e x 10^3$ (L/mg)	R^2
SH_1	110.0	126.5	10.0	0.99
SH_2	132.0	151.5	9.63	0.99
SH_3	151.0	172.4	9.37	0.99
SH_4	164.0	181.8	7.75	0.99
SH_5	143.0	158.3	7.84	0.99
SH_6	98.0	123.7	9.98	0.99

IV. Conclusion

Experimental results show that swelling behavior of SAHs poly(AAc-AM-SH) was dependent on the sodium humate in a nonlinear fashion with equilibrium swelling ratio of 724 gg^{-1} The results revealed that the maximum adsorption capacity was obtained when 2.44 wt % SH was used as 164 mg/g. The adsorption isotherms agree well with the Langmuir model. The results of five time consecutive adsorption-desorption cycle show that the poly(AAc-AM-SH) SAHs have high adsorption and desorption efficiency, which indicates that it can be used as effective solid adsorbent for the removal of metal ions from waste water and aqueous effluents.

References

[1] A. Kara, ; L. Uzun,; N. Besirli,; A. Denizli, *J. Hazard Mater* **2004**, B106,

[2] A. Demirbas, *J Hazard Mater*, 157, 220, **2008**.

[3]H. A.Essawy, H. S. Ibrahim, *React Funct Polym*, 61,421, **2004**.

[4.] W. Wang,; A. Wang, *J. Appl Polym Sci*, 112, 2102, **2009**.

Sample designation	AAc	AM	SH	Adsorption capacity		Desorption capacity	
	(wt%)	(wt%)	(wt%)	A_1	A_5	D_1	D_5
SH_1	50.00	50.00	0.00	110.00	109.30	93.20	93.40
SH_2	49.62	49.62	0.74	132.00	130.10	93.60	92.90
SH_3	49.34	49.38	1.23	151.00	149.81	94.10	94.76
SH_4	48.78	48.78	2.44	164.00	163.47	91.80	91.90
SH_5	48.09	48.19	3.61	143.00	141.70	89.40	89.40
SH_6	46.50	46.51	6.98	98.00	96.29	87.40	85.70

Table 1. The feed compositions for synthesis of various poly(AAc-AM-SH) SAHs and their adsorption and desorption capacity Other conditions: NMBA, 0.20 wt%; APS, 0.40 wt%; distilled water, 30 ml; temperature 60^{o}C. A_1-and A_5 adsorption amount in first and fifth cycle (mg/g) respectively, D_1-and D_5- desorption(%) in first and fifth cycle respectively

1st International Online Conference on Emerging Smart Materials in Applied Chemistry(ESMAC-2020)
10-12 August 2020

Paper ID:18

Photocatalytic Degradationof Methylene Blue byFerric Oxide-supported Ag NanoparticlesUnder Visible Light Irradiation

Niladri Maity[a*], Sonali Samal[a] *and* Binod Bihari Panda[a]

[a]Department of Chemistry, Indira Gandhi Institute of Technology, Sarang, Odisha, India, E-mail: niladriiitb@gmail.com

Abstract: **Ferric oxide (Fe_2O_3) supported Ag nanoparticles (Fe_2O_3-Ag) was prepared by reducing Ag(I) salts onto the dispersed solid supportin aqueous medium. The photocatalytic efficiency of Fe_2O_3-Ag was investigated by conducting degradation of methylene blue (MB) under visible light irradiationat an ambient condition.TheFe_2O_3-supported Ag nanoparticles exhibit an efficientcatalytic degradation of MB following a pseudo-first-order reaction kinetics (k_{Ag} = 0.243h^{-1}).**

***Keywords*:Dye degradation, Methylene blue, Ferric oxide, Silver nanoparticles, Visible light**

Introduction

Organic dyes is one of the major groups of pollutants widely used in textile, plastic, medicine and many other industries. These industries exhausted large quantity of high content color effluents, which are generally more toxic and resistant to destruction by conventional methods. The superiority of photocatalytic degradation by nanoparticles in wastewater treatment is due to its advantages over the conventional methods, such as quick oxidation, no formation of polycyclic products and oxidation of pollutants. It is an effective and rapid technique in the removal of pollutants from wastewater.Nano sized semiconductors, such as TiO_2, ZnO, ZnS, WO_3 and Fe_2O_3 are often used as catalytic agents because of their high catalytic efficiency.[1] Among themFe_2O_3 nanomaterials exhibit promising photocatalytic activities due to its environmental friendly behavior, low cost, high stability, high surface area, high crystallinity and band gap of ~2.2 eV for absorbing visible light irradiation.[2-4] However, the photocatalytic activity of the iron oxide is dependent on the particle size. It is difficult to synthesize nano-sized iron oxide by conventional due to the agglomeration of nano-particles in the aqueous solution, which causes the reduction of photocatalytic efficiency.[5] One way to overcome this drawback is to apply new synthetic method for iron oxide nanoparticles and can be well mixed with different metal/metaloxide nanoparticlesto improve the photocatalytic activity.[6] Silver nanoparticles are particularly suitable for medical diagnosis, drug delivery, water purification, with minimal risk of toxicity.[1,2]

In this article we report the photocatalytic activity of Fe_2O_3-supported Ag nanoparticles on degradation of methylene blue under visible light irradiation at an ambient condition.

Materials and Methods

A. Reagents

The chemicals were purchased from commercial sources and used as received.The glassware werecleaned with aquaregia and thoroughly rinsed with a copious amount of distilledwater. All

aqueous solutions were prepared by double-distilled water.

B. Preparation of Iron(II) oxalate

15 gm (38.25 mMol) of Ferous ammonium sulphate were dissolved in 50 cm3 of warm water which has been acidified with 5-6 drops of HCl. 75 cm3 of 10% oxalic acid solution was added with the ferrous ammonium sulphate solution with rapid stirring. The mixture was heated gently to the boiling point and the yellow precipitate of ferrous oxalate was allowed to settle. The precipitate was removed by filtration by using a buncher funnel. After filtration the precipitate was washed thoroughly with distilled water and acetone. After that the product was allowed to dry by using a micro oven at 50˚C for 3-4 hours. The amount of iron oxalate obtained is 6.52 g. Yield of the product was found to be 95%.

C. Preparation of Iron(III) oxide

The iron oxalate dihydrate prepared in the earlier step was used as a precursor for the preparation of iron oxide. Before thermal treatment, the precursor compound was finely grinded by using a mortar and pestle. Then 1g of powdered precursor was taken in a crucible and calcined at 175 ^{o}C inside an oven under the air for 6 h. After the calcination brown Fe_2O_3powder was collected.

D. Preparation of Fe_2O_3-supported Ag nanoparticles

A 0.495 g of Fe_2O_3 along with 6 ml of water was taken in a round bottom flask and stirred for 30 mins by utilizing a magnetic stirrer.A freshly prepared $AgNO_3$ solution containing 0.008g of $AgNO_3$ and 10 ml of water was added to the dispersion of Fe_2O_3under stirring. The mixture was continued to stir for 30 min in the absence of light. Next, $NaBH_4$ solution (17 mg of $NaBH_4$ in 3 ml of water) was added to above mixture and stirred for another 30 min. After the reaction, the solvent was filtered out and washing several times with distilled water and then with acetone.

E. Catalytic degradation of methylene blue by Fe_2O_3-supported Ag nanoparticles and determination of reaction kinetics

10 mg of methylene blue dye was dissolved into 100 ml of distilled water and used as stock solution. The experiment was conducted by adding 2 mg of Fe_2O_3-Ag catalyst to 50 ml solution of MB in a round bottom flask at room temperature. The reaction mixture (at 25 ^{o}C) was stirred using a magnetic stirrer. A 100 watt light source 22 cm away from the reaction mixture was provided for photochemical reaction. Degradation of methylene blue was monitored by measuring the change in intensity of the absorption band at 665 nm. The UV-vis spectra were recorded at different time intervals to study reaction kinetics. Identical reaction conditions were employed for conducting the reduction using Fe_2O_3.

The rate of the reaction can be represented by the equation $-(dC/dt) = kC$ or $\ln(C/C_0) = -kt$ (C and C_0 are the methylene blue concentrations at time t and 0, respectively). The ratio C/Co can directly be given by the ratio of A/A_0 (absorbance values of methylene blue at time t and 0, respectively), obtained from the UV-vis spectra of the kinetic study. The rate constant (k) can be obtained from the slope of a straight line by plotting $\ln(C/C_0)$ with respect to time (t). Efficiency of degradation (%) $=100((A_0-A_t)/A_0)$

Results and Discussion

The photocatalytic activity of Fe_2O_3-Ag was evaluated by the degradation of MB dye in aqueous solution with the help of UV–Vis spectrophotometer. The decolourization of MB dye was examined under two different conditions, visible light irradiation (i) in the absence of any catalyst and (ii) in the presence of Fe_2O_3-Ag, respectively.

In order to evaluate photocatalytic activity in black condition the time monitored absorption spectrum was plotted (Figure 1). The % conversion vs time plot (Figure 2) represents that a non-significant amount (~16%) of dye was degraded in the absence of catalyst after irradiating for 6 h.

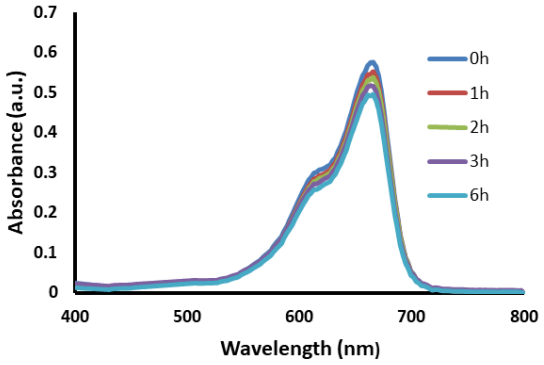

Figure 1: Absorption spectra of photo degradation of MB (λ_{max} = 665 nm) without catalyst.

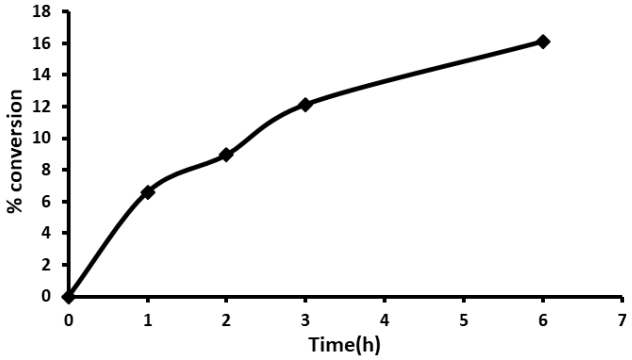

Figure 2: Plots of conversion of MB dye as function of time under visible light irradiations in blank solution (without catalyst).

However, significantly when the dye solution was exposed to visible light irradiation for 7h in the presence of Fe_2O_3-Ag ~81% of the MB dye was degraded. The absorption spectra of MB with Fe_2O_3 supported Ag nanocatalyst is shown in (Figure 3) and the corresponding plots of percentage degradation of MB dye as function of time under visible irradiation are shown in Figure 4).

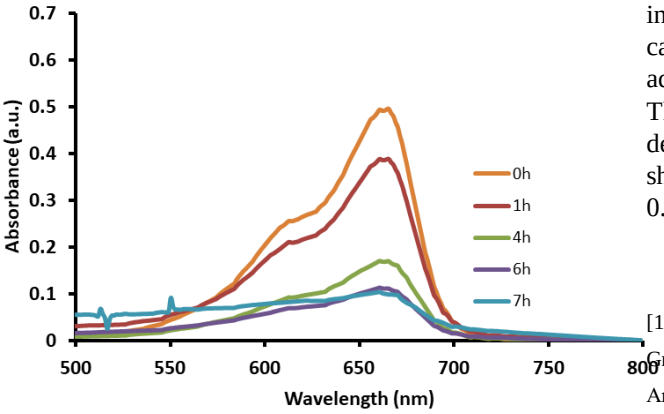

Figure 3: Absorption spectra of MB with Fe_2O_3–Ag nanocatalyst.

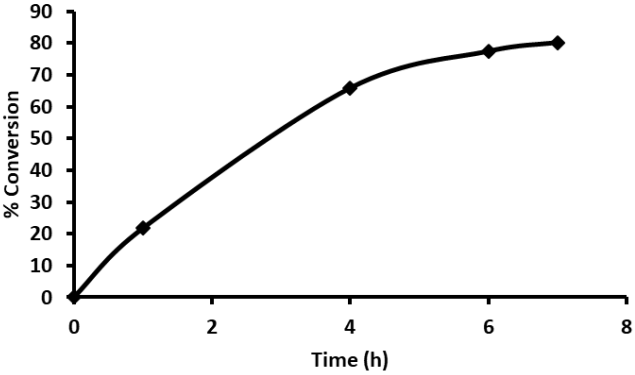

Figure 4: Plots of percentage degradation of MB dye as function of time with Fe_2O_3–Agnanocatalyst.

Analysis of the kinetic data of degradation reactions reveals pseudo-first order reaction kinetics. The linear plot (Figure 5) of ln [C/Co] versus time supports the kinetic theory, where the k value obtained was 0.243 h^{-1}.

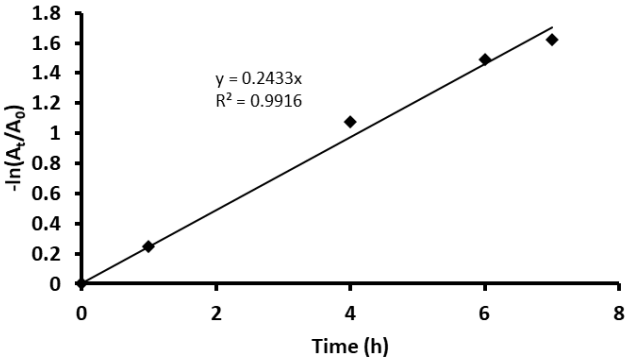

Figure 5: Kinetic studies of MB degradation process catalyzed by Fe_2O_3-Ag.

Conclusion

Present study reports the preparation of Fe_2O_3 nanoparticles via thermal decomposition of $Fe(C_2O_4).2H_2O$ and subsequent deposition of Ag nanoparticles through reduction of Ag(I) complex in aqueous medium. The Fe_2O_3–Agwas utilized as catalyst for degradation of methylene blue in aqueous medium under visible light irradiation. The photocatalysis result reveals that 81% degradation of MB occurs in 7h. The catalyst shows a pseudo-first-order reaction kinetics (k_{Ag} = 0.243 h^{-1}).

References

[1] M. Vanaja, K. Paulkumar, M. Baburaja, S. Rajeshkumar, G. Gnanajobitha, C. Malaraodi, M. Sivakavinesan and G. Annadurai. 'Degradation of Methylene Blue using biological synthesized silver nanoparticles'. Bioinorganic Chemistry and Applications. Vol. 2014, Article ID 742346, pp.1-8.

[2] Y. Chung, S. K. Lim, C. K. Kim, Y.-H. Kim and C. S. Yoon, Journal of Magnetism and Magnetic Materials, 272–276, pp. 1167–1168, 2004.

[3] J. W. Verhoeven, "Glossary of Terms Used in Photochemistry," Pure and Applied Chemistry, vol. 68, pp. 2223-2286, 1996.

[4] B. C. Faust, M.R. Hoffmann and D. W. Bahnemann, "Photocatalytic oxidation of sulfur dioxide in aqueous suspensions of α-Fe_2O_3". The Journal of Physical Chemistry, vol. 93, pp. 6371-6381, 1989.

[5] W. Z. Tang, H. An, "UV/TiO_2 photocatalytic oxidation of commercial dyes in aqueous solutions", Chemosphere, vol. 31, pp. 4157–4170, 1995.

[6] G. Mascolo, R. Comparelli, M. Curri, G. Lovecchio, A. Lopez and A. Agostiano, "Photocatalytic degradation of methyl red by TiO2: comparison of the efficiency of immobilized

nanoparticles versus conventional suspended catalyst", Journal of Hazardous Material, vol. 142, pp. 130-137, 2007.

1st International Online Conference on Emerging Smart Materials in Applied Chemistry(ESMAC-2020)
10-12 August 2020

Paper ID:19

Carbon-based Nanomaterials for Water Purification and Energy Applications

Trung Viet Huynh[a], Tzu-HengWang[b], *and* Ruey-an Doong[a,c*]

[c]Institute of Analytical and Environmental Sciences, National Tsing Hua University, Hsinchu 30013, Taiwan

[b]Department of Biomedical Engineering and Environmental Sciences, National Tsing Hua University, Hsinchu 30013, Taiwan

[c]Center for Energy and Environmental Research, National Tsing Hua University, Hsinchu 30013, Taiwan

***Abstract*—In this study, we report the facile synthesis of mesoporous carbon nitride with ordered, uniform channel morphology and their use as a photocatalyst to decompose pharmaceuticals as well as a support for ultrafine metal nanoparticles to catalytically reduce nitroarenes and other emerging pollutants. Results show that the C_3N_4 based nanomaterial has a tunable band gap and can effectively photodegrade > 99% of environmental pollutants such as sulfamethoxazole and diclofenac under visible light irradiation. In addition, C_3N_4 provides high surface area to well-disperse Au nanoparticles for the rapidly catalytic reduction of nitroarenes.The pseudo-first-order rate constant for 4-nitrophenol reduction over Au@C_3N_4can be up to 3.56 min^{-1} in the presence of $NaBH_4$.These results clearly indicate that structured nanomaterial is a promising green catalyst of great application potential in water and wastewater treatment as well as in energy storage.**

***Keywords*—graphitic carbon nitride, micropopllutants, nitroarenes, energy storage.**

I. Introduction

Nanomaterials are novel materials which can not only serve as a photoelectrochhemical catalyst but also as an electrode material because of their suitable band gap, high surface area. Two-dimensional (2D) materials such as graphene family and mesoporous carbon nitride (C_3N_4) have recently attracted considerable interest because of high surface area, appropriate chemical anchoring sites, large pore size/volume, good electrical conductivity, and thermal stability. Among these materials, graphitic carbon nitride (g-C_3N_4), an organic polymeric semiconductor mainly consisting of carbon and nitrogen with a band gap of 2.7 eV, exhibits high thermal and chemical stability, excellent electron transfer ability, and easy recycling, and has been commonly used as a photocatalyst for the effective decomposition of various hazardous chemicals. Furthermore, g-C_3N_4 has been successfully utilized as a support to disperse and stabilize metal nanoparticles such as Pd, Pt, Cu, and Co. Basically, g-C3N4¬ is formed by the linkage of N bridged tri-s-triazine repeating unit, which is generated by two-dimensional conjugated planes packed together via van der Waals interactions. In view of its unique structure and preponderance, g-C_3N_4 has been widely employed in a wide variety of fields such as oxygen reduction reaction, photocatalysis, photoelectrochemical reaction, and sensor.

For heterogeneous (photo)catalytic processes, organic compounds and metal derivatives could bind or intercalate into the matrix of g-C_3N_4through the surface anchoring sites to improve the (photo)catalytic reaction rate, and thus broaden the (photoelectro)catalytic application of g-C_3N_4 toward organic decomposition. The unique architecture of g-C_3N_4 and the outstanding (photo)catalytic performance of metal and metal oxide nanoparticles such as Au, CeO_2, and graphene quantum dots (GQDs) provide a great impetus to use g-C_3N_4 as a promising support to judiciously decorate metal/metal oxide for the formation of highly active and green heterogeneous (photo)catalyst. Herein, we report the facile synthesis of mesoporous carbon nitride with ordered, uniform channel morphology and their use as a photocatalyst to decompose pharmaceuticals as well as a support for metal/metal oxide nanoparticles to catalytically reduce nitroarenes as well as for energy storage.

II. Reduction of nitroarene

The g-C_3N_4nanosheet is an excellent support to homogeneously disperse Au NPs that constrains the growth of Au NPs, and the Au@g-C_3N_4 can be prepared using thermal exfoliation with reduction method. After loading 2 wt% of Au NPs, the Au@g-C_3N_4 exhibits superior reduction capability toward nitroarene reduction. Addition of Au NPs significantly enhances the reduction efficiency and rate of 4-NP over Au@g-C_3N_4 in the presence of $NaBH_4$. The reduction of 4-NP to 4-amnophenol increases from 66 to > 99% when the Au loading increases from 0.5 to 2 wt%, and then slightly decreases to 96% at 3 wt% after 10 min of reaction. The pseudo-first-order rate constant (k_{obs}) for 4-nitrophenol reduction is 1.83×10^{-3} ($r^2 = 0.998$), 3.07×10^{-3} ($r^2 = 0.995$), 1.50×10^{-2} ($r^2 = 0.983$), and 5.33×10^{-3} sec^{-1} ($r^2 = 0.997$), respectively, over the 0.5-, 1-, 2- and 3-wt% Au@g-C_3N_4. When normalized to the specific surface area of Au@g-C_3N_4, the normalized surface rate constant (k_m) for 4-NP reduction increases from 3.24 to 20.25 min^{-1} m^{-2} at 0.5 – 2-wt% Au@g-C_3N_4 and then decreases to 6.78 min^{1} m^{-2} at 3-wt% Au@g-C_3N_4, indicating that 2-wt% Au@g-C_3N_4 provides optimal active sites for both $NaBH_4$ and 4-NP to exhibit the best catalytic activity in comparison with other Au loadings of Au@g-C_3N_4.

To further understand the applicability of Au@g-C_3N_4 nanocomposite to catalyze the reduction of nitrophenol, several nitroaromatics including 2-NP, 3-NP, 4-NP, 2,4-DNP and 2,4,6-TNP are selected as the target compounds. The Au@g-C_3N_4nanocomposite exhibits remarkable catalytic activity toward nitrophenol reduction by $NaBH_4$. Both the k_{obs} and normalized surface rate constants of nitrophenol reduction follow the order: 4-NP >2-NP >3-NP > 2,4-DNP > 2,4,6-TNP, indicating 4-NP reduction the most favorable over Au@g-C_3N_4nanocatalyst. The rate constant of nitrophenol reduction decreases with the increase in number of nitro-substituent, which is mainly attributed to the molecular hindrance and steric effectof nitroaromatics to penetrate into the catalyst network.

III. Photodegradation of micro pollutant

Not just only shows the superior catalytic capabilitytoward nitroarenes reduction, g-C_3N_4 also exhibit the excellent photocatalytic activity toward pharmaceuticals degradation. We have proposed a simple method to fabricate visible-light responsive iodine- and potassium-codoped for sulfamethoxazole (SMX) photodegradation. The SMX photodegradation were computed at 0.027, 0.035 and 0.106 min^{-1} at doping temperature of 450, 500 and 530 °C, respectively. The k_{obs} for SMX photodegradation by IK-C_3N_4 at 530 °C was 4 times higher than that at 450 °C. The increased reaction rate at high doping temperature is mainly attributed to the enhanced exfoliation and doping efficiency, resulting in the acceleration of photocatalytic performance towards SMX removal.

Cerium oxide (CeO_2), an abundant rare-earth oxide, is a n-type photocatalyst with band gap of around 2.8 - 2.92 eV, which makes it highly capable of absorbing light in the visible spectrum. The combination of CeO_2 and IK-C_3N_4 can form direct Z-scheme n-n heterjunction for enhanced photodegradation. The adsorption and photodegradation of acetaminophen (ACT) over various amount of CeO_2/IK-C_3N_4 shows thatonly 12% and 15% ACT removal by pure g-C_3N_4 and 15% CeO_2/ IK-C_3N_4 nanocomposite in 90 min of continuous mixing. Moreover, the enhanced ACT removal was observed immediately after visible light irradiation, which confirms that the ACT elimination is mainly due to the photocatalysis. Different CeO_2 loading over g-C_3N_4 were optimized for enhanced photocatalytic degradation of ACT. The 10% weight of CeO_2 was recorded with only 60% ACT degradation, 1.56 times higher than that of g-C_3N_4. The 15% CeO_2/ IK-C_3N_4 nanocomposite was found to be the optimal ratio wherein highest photocatalytic performance was observed. After 90 min of visible light irradiation, 98% of ACT was eliminated. This boost in performance is mainly caused by the balance of lattice defects introduced while suppresses the recombination of excitants from increased in area for surface charge. Meanwhile, further increase produces a surplus CeO_2 that competes for reactive sites, blocks available light energy and produces more defects that causes the decrease in performance. The 20% and 25% CeO_2 immobilization show only 91% and 94% removal efficiency, respectively in 90 min of reaction time. The ACT degradation rate is modelled by a pseudo-first-order reaction and the k_{obs} values are 0.010, 0.039, 0.0319, 0.027 and 0.005 min^{-1} for 10%, 15%, 20%, 25% CeO_2/IK-C_3N_4 and bare g-C_3N_4, respectively.

References

[1] Nguyen, T. B.; Huang, C. P.; Doong, R. A. (2019). Appl. Catal. B Environ. 240, 337-347.

[2] De Luna, M. D. G.; Paragasb, L. K. B.; Doong, R. A. (2019) Sci. Total Environ. 669, 1053-1061.

[3] Paragas, L. K. B.; De Luna, M. D. G.; Doong R. A. (2018). Chemosphere, 210, 1099-1107.

[4] Saha, R. S.; Lee, D. L.; Doong, R. A. (2018) Chem. Eng. J. 334, 30-40.

1st International Online Conference on Emerging Smart Materials in Applied Chemistry(ESMAC-2020)
10-12 August 2020

Paper ID: 20

PHYTOCHEMICAL SCREENING AND ANTIBACTERIAL ACTIVITY OF POTENTIAL MANGROVES OF SARTHA ESTUARY

Sujit Kumar Nayak [a*] and Ranindra Kumar Nayak[b]

[a*]*Department of Environmental Science, Fakir Mohan University, Balasore-756089,India*

E-mail: contactsujit98@gmail.com

[b]*Department of Environmental Science, Fakir Mohan University, Balasore-756089,India*

E-mail: ranindra1968@gmail.com

***Abstract*—This study was carried out with an objective to investigate the qualitative phytochemical screening of different compounds such as alkaloids, flavonoids, glycosides, phenols, tannins, saponins and antimicrobial potentials of leaves of some potential mangroves of Sartha estuary in the Balasore district of Odisha coast. These species are *S. caseolaris* (L.) Engl.,*A. ilicifolius* L., *A. alba* Blume, *A. marina* (Forssk.) Vierh.and*R. apiculata* Blume.The results reveal the presence of alkaloids in *S. caseolaris, A. alba and A. marina*, flavonoids in *S. caseolaris, A. ilicifolius and A. alba*, glycosides in *A. alba*and *R. apiculata*, phenols in *S. caseolaris and A. marina*, tannins in *S. caseolaris, A. alba, A. marina and R. apiculata* and saponins are found to be present in all the above mentioned species. The antimicrobial activity was determined in the ethanolic extracts using agar disc diffusion method. The antibacterial activities of all these mangrove plants species were tested against Gram-positive *Brevibacillus sp*. and Gram-negative *Escherichia coli* bacteria. The results showed that remarkable inhibition of the Gram-positive bacterial growth was shown by *A. marina* (Forssk.) Vierh.and inhibition of the Gram-negative bacterial growth was shown by *S. caseolaris* (L.) Eng l. respectively.**

***Keywords*—Phytochemical screening, antibacterial activity, mangroves, Sartha estuary**

I. Introduction

Plants consist of several natural bioactive compounds known as Phytochemicals. In association with the nutrients and fibers, these Phytochemicals form an integrated part of defense system against various epidemic diseases and stress conditions. Mangrove plants are used as the potential sources of biologically active chemicals which have commercial applications in the field of ethno- pharmaceutical sector (Bandaranayake, 1998; 2002). Mangroves are highly resistant to salinity and tidal fluctuations and they are known to be a source of several bioactive compounds and secondary metabolites like alkaloids, phenols, tannins, flavonoids, steroids and terpenoids with toxicological, pharmacological and ecological importance (Selva, 2013).

In this study, attempt have been made to demonstrate the ethanolic extract of five different mangrove species, growing at Sartha Estuary of Balasore district of Odisha coast in India to establish its effectiveness against killing or inhibiting the growth of bacterium *Escherichia coli*, and *Brevibacillus sp*. which can cause illness in different circumstances.

II. Materials and Methods

The present investigation has been undertaken to carry out the study of qualitative phytochemical analysis, antimicrobial activity of some mangrove plants of Sartha estuary.

A. Plant Collection

The selected mangrove species were collected from the Sartha estuary located in Balasore districtof Odisha coast in India.

B. Extraction of test sample for phytochemical screening

From the selected species test sample was prepared for various qualitative phytochemical screening.

C. Qualitative Phytochemical Analysis

Phytochemical constituents from the mangrove sample extracts were determined qualitatively. Crude extracts of the plants under study were screened for the presence of

alkaloids, flavonoids, glycosides, phenols, tannins, saponins using the following laboratory procedures.

D. Extraction of test sample for Antibacterial assay

Five grams of each sample powder were weighed and dissolved in 50 ml of solvents in a conical flask. After 24 hour solvent extract was collected in sterile test tubes wrapped with aluminium foil.

E. Antibacterial assay

All of the phytochemical extracts were individually tested against a panel of bacteria including Gram negative *Escherichia coli* and Gram positive *Brevibacillus species*. The strains of bacteria were maintained on broth culture in orbital shaker overnight and a subculture stored in broth culture at 4°c.

The pure cultures of bacteria maintained in the Laboratory were used for the microbiological work. The test organisms were maintained on Nutrient broth culture. The test organisms used for work are *E. coli* and *Brevibacillus* sp.. Disc diffusion method (Bauer et al., 1966) was used to test antimicrobial activity of the extracts against the bacteria.

III. Results and Discussion

During the present investigation, phytochemical analysis and antimicrobial activity of mangrove plants have been carried out which have been collected from the Sartha Estuary of Balasore district.

Phytochemical analysis of some plants has done by following standard methods. The qualitative phytochemical screening of plant leaves such as alkaloids, flavonoids, glycosides, phenols, tannins and saponins were carried out for ethanolic extracts which gives evidence on the medicinal properties of these plants(Table-1,Fig-1).

Results of the antimicrobial activity of some selected mangrove plants collected from the Sartha Estuary of Balasore district viz. *Sonneratia caseolaris* (L.) Engl.,*Acanthus ilicifolius* L., *Avicennia alba* Blume, *Avicennia marina* (Forssk.) Vierh.,*Rhizophora apiculata* Blume shows that the plants have inhibitory effects on the growth of the bacterium *E. coli* and *Brevibacillus sp*.It gives an idea that medicines prepared from leaves of these plants will be much effective for the treatment of various diseases.

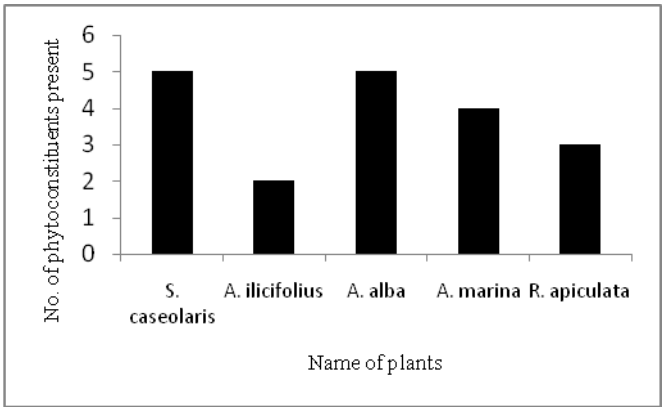

Fig. 1: Number of phytochemical constituents present in the selected mangrove plants species.

IV . Conclusion

From this investigation it is found that the mangrove plants contain several types of phytoconstituents which can be utilized in a proper way for the preparation of the medicines for the treatment of various diseases as these bioactive compounds show significant antimicrobial effects.During the qualitative analysis of phytochemicals it has been observed that there is presence of various chemicals such as alkaloids, flavonoids, glycosides, phenols, tannins and saponins in leaf of tested mangrove plant samples which have much medicinal value. Quantitative estimation of these phytochemicals will be much useful for the preparation of new drugs in the herbal drug industry.

Results of the antimicrobial activity of five different mangrove plants species shows that leaves of all these species have inhibitory effects not only on the growth of the gram positive bacterium (*Brevibacillus sp.*) but also on the growth of the gram negative bacterium (*E. coli*). Among all the collected leaf sample of mangrove plants *Sonneratia caseolaris* (L.) Engl. has maximum inhibitory effect on the growth of the gram negative bacterium (*E. coli*) whereas *Avicennia marina* (Forssk.) Vierh.has maximum inhibitory effect on the growth the gram positive bacterium (*Brevibacillus sp*.). It gives an idea that medicines can be prepared from leaves of these plants which will be much effective for the treatment of various disease causes by the infection of various microorganisms.

Botanical Name Family	Plant Parts	Alk	Fla	Gly	Phe	Tan	Sap
Sonneratia caseolaris (L.) Engl. (Lythraceae)	Leaf	+	+	-	+	+	+
Acanthus ilicifolius L. (Acanthaceae)	Leaf	-	+	-	-	-	+
Avicennia alba Blume (Acanthaceae)	Leaf	+	+	+	-	+	+
Avicennia marina (Forssk.) Vierh. (Verbenas)	Leaf	+	-	-	+	+	+
Rhizophora apiculata Blume (Rhizophoraceae)	Leaf	-	-	+	-	+	+

Table 1: Phytochemical analysis of mangrove plants of Sartha Estuary (N.B: Alk- Alkaloids Fla- Flavonoids
Gly- GlycosidesPhe- Phenols
Tan - Tannins Sap - Saponins
+ **:** presence of a particular phytochemical
- **:** absence of a particular phytochemical)

References

Balandrin, M.F., A.J. Kjocke and E. Wurtele, 1985. Natural plant chemicals: *sources of industrial and mechanical materials. Science*, 228: 1154-1160.

Bandaranayake W.M. Traditional medicinal uses of mangroves; mangrove and salt marshes.*WetlEcol and Manage*. 1998,2, 133–48.

Bandaranayake, W.M., 2002. Bioactivities: Bioactive compounds and chemical constituents of mangrove plants.*WetEcol Manage*, 61(10): 421-52.
Selva Kumar S, SenPrajeet, Anbuselvi S. Preliminary phytochemical analysis of *Excoecaria agallocha* and *Avicennia*, *Bio Med Rx*. 2013; 1(4):371-373.

1st International Online Conference on Emerging Smart Materials in Applied Chemistry(ESMAC-2020)
10-12 August 2020

Paper ID:21

Synthesis and characterization of *p*-phenylenediamine Schiff base ligands and their macrocyclic complexs

Kanyanjali Samal[a], Manini Nayak[a], Anita Pati[a*]

[a] Department of Chemistry, School of Applied Sciences, KIIT Deemed to be University, Bubaneswar, Odisha, India
E-mail: anitapatifch@kiit.ac.in

***Abstract*—** Schiff bases compounds are generally bi, tri, or tetra-dentate chelate ligands and form very stable complexes with different metal ions. Schiff base ligands and their metal complexes have been extensively studied due to their wide range of applications. Schiff base ligands are potent anti-cancer, anti viral, anti bacterial agents and this activity tends to increase in metal (II) Schiff base complexes. Over the past few decades, Schiff base acyclic complexes with *p*-phenylenediamine have gained importance, due to their potential in medicinal inorganic chemistry and application with physicochemical and chemotherapeutic properties. Synthesis, characterization and application with different metals are well depicted in the literature. However complexation with Pd(II) metal and its application is yet be explored properly. Thus the present work is more focused on the synthesis of *p*-phenylenediamine based Schiff base ligands and their complexation ability with Pd(II) metal. *p*-phenylenediamine Schiff base ligands were prepared by the condensation of 4-hydroxyphenyl and 2-pyridine aldehydes. Two different type of metal complexes were prepared by the addition of *p*-phenylenediamine Schiff base ligands and $[Pd(II)(bpy)(NO_3)_2]$ in different stoichiometry. All the compounds were characterized by their IR and NMR spectral data.

***Keywords*— Schiff Base, phenylenediamine, Pd (II) complexes,** macrocyclic complexs

Introduction

Schiff base compounds and their metal complexes[1] have been extensively studied due to their wide range of applications like catalysts, medicine, crystal engineering, anti-corrosion agent, synthetic flexibility, selectivity and sensitivity towards the central metal atom. Schiff base ligands form very stable complexes with different metal ions. They have been extensively studied due to their wide range of applications in many fields including biological applications in inorganic, industrial and analytical chemistry. Schiff base ligands are potent anti-cancer, anti viral, anti bacterial agents and this activity tends to increase in metal (II) Schiff base complexes. Over the past few decades, Schiff base acyclic complexes with *p*-phenylenediamine have gained importance, due to their potential in medicinal inorganic chemistry and application with physicochemical and chemotherapeutic properties. Synthesis,

characterization and application with different metals are well depicted in the literature.[2,3,4] Schiff base Ligands using thiourea, thiosemicarbazide and thiocarbohydrazide and their metal complexes with Zn (II), Cd(II), Hg(II), Fe(II), Co(II), Ni(II), Cu(II), and Pd(II) are well reported.[3] Whereas *p*-phenylenediamine based Schiff base ligands are yet to be explored properly. Thus the present work is more focused on the synthesis of *p*-phenylenediamine based Schiff base ligands and their complexation ability with Pd(II) metal.

Materials and Methods

Preparation of Schiff base -2 (N1, N4-Bis (pyridin-2-ylmethylene) benzene-1,4-diamine):

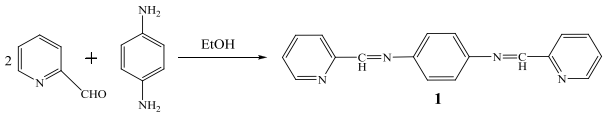

Hydrazone derivative of *p*-phenylenediamine was prepared by refluxing p-phenylenediamine (1mol) and 2-pyridinecarboxaldehyde (2mol) in EtOH (4hr). It was left at room temperature for 12 hours. Fine yellow colored crystals were formed which was washed with ethanol and dried under high vacuum to get pure crystalline product. Product was characterized by its IR and NMR data. (Yield: 90%, M.P. = 166 °C)

Preparation of Schiff base -3 (N1, N4-bis(pyridin-2-ylmethyl)benzene-1,4-diamine):

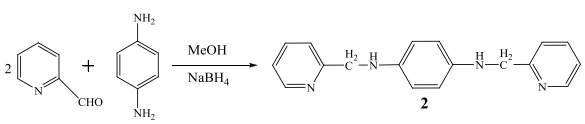

To a solution of pyridine-2-carboxaldehyde (2mmol) in 2 ml methanol was added *p*-phenylenediamine (1mmol). The solution was refluxed for 2hr. The resulting greenish-yellow solution was then reduced by $NaBH_4$ (4mmol). On addition, yellow color precipitate was formed which was stirred over night at room temp. It was filtered, washed with water and dried under high vacuum to get the ligand in pure form. Product was characterized by its IR and NMR data. (Yield: 80%)

Preparation of metal complex-1:

Complex-1 was synthesized by the addition of aqueous solution of metal (II) salt to the homogeneous solution of the Schiff base ligand (**2**) in the acetonitrile. The mixture was stirred for 24 hrs. The product formed was centrifuged and the clear part thus obtained was evaporated, dried under high vacuum to get the metal complex. The metal to ligand ratio used is 1:1 {$[Pd(bpy)(NO_3)_2]$ (0.04mmol) and Schiff base ligand **2** (0.04mmol), Yield-85%, M.P >300 °C}

Preparation of metal complex-2:

Complex-2 was synthesized by using the same procedure but with the metal to ligand ratio 2:1 {$[PdCl_2]$ (0.04mmol) and Schiff base ligand **3** (0.08mmol), Yield-90%, M.P >300 °C}.

Results and Discussion

In view the wide spread structural and biological importance of the metal complexes of *p*-phenylenediamine Schiff base ligands the present work is undertaken which includes the synthesis and characterization of some of the *p*-phenylenediamine Schiff base ligands and study their complexation behavior towards Pd(II) metal.

p-phenylenediamine Schiff base ligands (**1 & 2**) were prepared by the condensation of 4-hydroxyphenyl and 2-pyridine aldehydes. The metal complex-**1** was synthesized by using an equimolar ratio of *p*-Phenylenediamine Schiff-base ligand (**3**) and cis protected Pd(II) metal unit i.e. $[Pd(II)(bpy)(NO_3)_2]$ in acetonitrile : water (1:1) solvent system (Scheme-1). Similarly metal complex-**2** was produced by using 2:1 (Ligand:

Metal) ratio of p-Phenylenediamine Schiff-base ligand (**3**) and $PdCl_2$ in acetonitrile: water (1:1) solvent system (Scheme-1). Difference in the melting point, colour and solubility of the products formed than that of the p-Phenylenediamine Schiff-base ligand (**2**) indicates the formation of the metal complexes. Further the compounds were characterized by their IR and NMR spectral data.

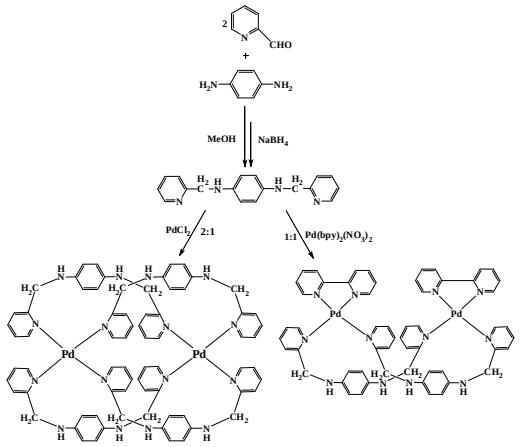

SCHEME-1

Conclusion:

A novel *p*-phenylenediamine based Schiff base ligand was prepared. Further it was utilized for the preparation of two different metal complexes using Pd(II) $[Pd(II)(bpy)(NO_3)_2]$ in different stoichiometry.

References

[1] Kumar, G.; Kumar, D.; Singh, C. P.; Kumar, A. and Rana, V. B. *J. Serb. Chem, Soc*., **2010**, *75*(5), 629-637.

[2] Agarwal, R.; Khan, M. A. and Ahmad, S. *Journal of Chemical and Pharmaceutical Research*, **2013**, *5*(10), 240-245.

[3] Burns, G. R. *Inorganic Chemistry*, **1968**, *7(2)*, 277-283.

[4] Tiwari, A. D.; Mishra, A. K.; Mishra, S. B.; Mamba, B. B.; Maji, B.; Bhattacharya, S. *Spectrochimica Acta Part A*,**2011,***79*,1050–1056.

1st International Online Conference on Emerging Smart Materials in Applied Chemistry(ESMAC-2020)
10-12 August 2020

Paper ID: 22

Plasmonics of HybridNanostructures

Hira Joshi

Physics department of Gargi College, University of Delhi, India, hirajoshi123@gmail.com

***Abstract*—** Metal nanoparticles that show localized surface plasmon resonance (LSPR) are extremely interesting as having applications in various fields as photonics, electronics, optical imaging, sensing , optical filtering optoelectronics devices and information storage. The characteristics of the SPR depend on the dielectric constant of the host medium and on size, shape and composition of the nanoparticles(NPs)[1-3]. Hybrid nanostructures (HNs) are combination of different material to attain unique property unattainable in their individual components. These hybrid structures are widely used in plasmonics which is a research field dealing with light at nanoscale. Hybrid nanostructures composed of semiconductor and plasmonic metal display extraordinary optical characteristics because of interactions between two components. The optical properties of such hybrids can be tuned by interaction between plasmons and excitons which help in designing active plasmonic devices and have potential applications in photocatalysis, Plasmon-enhanced spectroscopy[4], biotechnology and solar cells. In these HNS, LSPR of metals and excitonic effect of semiconductors are utilized to improve photo-conversion efficiency.

Keywords— Hybrid, LSPR, Extinction, NPS,

LSPR is a resonant phenomenon in which conduction electrons of metals are oscillating coherently when light is interacting at nanoscale. Resonant wavelength can be tuned by changing size, shape, composition and external matrix[5]. LSPRs result in in large absorption and scattering cross sections and hence enhancement of the electric field in the local environment ofthe plasmonic particles. Here we have investigated optical constants of noble metal hybrid nanostructures using Mie's theory in static regime for metallic spheres, valid for small particles of sizes compared to the incident wavelength of the electromagnetic wave, embedded in an isotropic dielectric medium. Hybrid nanostructures of noble metals such as Au and Ag with semiconductors (ZnO, Al_2O_3)are used to study absorption spectra of nanoparticles of different sizes and when placed in different external matrix. Extinction cross section which is sum of absorption and scattering cross sections is studied for various hybrid nanostructures and it is found that resonant wavelength is independent of size of nanoparticle but depends on external matrix. As external matrix dielectric constant increases resonant wavelength is found to be redshifted.

References

[1] U.Kreibig and M.Vollmer Optical Properties of Metal Clusters ,Berlin, Springer,1995

[2] C. F. Bohren and R. Hufman Absorption and scattering of light by small particles. Research supported by the University of Arizona and Institute of Occupational and Environmental Health, New York ,Wiley Interscience,1983 pp 530- 541

[3] S. Maier Plasmonics : Fundamentals and Applications ,Springer,2007.

[4] M. Merker " Founding fathers of light scattering and surface-enhanced Raman scattering". Appl. Opt. vol.30 pp 4699-4705, 1991.

[5] K. L .Kelly, E. Coronado, L. Zhalo , G.C. Schatz " The optical properties of metal nanoparticles the influence of size, shape, and dielectric environment". J. Phys. Chem. B vol.107 pp 668–77, 2003.

1st International Online Conference on Emerging Smart Materials in Applied Chemistry(ESMAC-2020)
10-12 August 2020

Paper ID:23

Fabrication of graphene oxide reinforced bio-nanocomposite films: Assessment of antibacterial potential

Mamata Das[a], Lipsa Ray[a], Chanakya Nath Kundu[b], Jasaswini Tripathy[a]*

[a] School of Applied Sciences (Chemistry), KIIT Deemed to be University, Bhubaneswar- 751024, India, jtripathyfch@kiit.ac.in

[b] School of Biotechnology, KIIT Deemed to be University Campus-11, Patia, Bhubaneswar, Odisha 751024, India

***Abstract*— In this study, we report graphene oxide GO) reinforced sodium carboxymethyl cellulose (CMC) and Poly (vinyl alcohol) (PVP) blend nanocomposite films by solution casting method. The graphene oxide was synthesized by modified Hummer's method. The formation of graphene oxide was confirmed by Raman spectroscopy. The films were characterized by Fourier transform infrared spectroscopy (FT-IR), scanning electron microscopy (SEM) and transmission electron microscopy (TEM).Thermogravimetric ananlysis (TGA) was performed to evaluate the thermal stability of films. FT-IR confirmed the formation of intermolecular hydrogen bonds between GO and polymers. The results revealed uniform dispersion of GO sheets in polymeric matrix. The thermogravimetric analysis showed higher thermal stability of CMC/PVP/GO films as compared to CMC/ PVP blend. In addition, CMC/PVP/GO nanocomposite films exhibited higher mechanical strength as compared to CMC/ PVP blend films. Further, the antibacterial studies revealed bactericidal capacity of CMC/PVP/GO films against gram-positive Staphylococcus aureus and gram-negative Escherichia coli bacterial strains.**

***Keywords*— Graphene oxide, Bio-nanocomposite, Antibacterial activity, Carboxymethyl cellulose**

IV. Introduction

In recent years, development of antimicrobial materials has received widespread attention due to the increased demand of these materials. The synthesis of antimicrobial agents is highly relevant for applications in food, textiles, packaging, health care etc. Further, there is an urgent need for new innovative solutions in the field of biomedicine, since non-healing wounds remain a major clinical issue and are a significant burden to the medical system [1]. In this regard, polymeric bio-nanocomposites have drawn widespread attention due to their environmental friendly, non-toxic and biocompatible nature. They are widely used in many fields such as drug delivery [1], tissue engineering [2], and different biomedical applications [3].

Carboxymethyl cellulose (CMC) is a water-soluble linear polymer, produced by partial substitution of the 2, 3, and 6 hydroxymethyl groups of cellulose by hydrophobic carboxymethyl groups. It has been used in numerous applications in a variety of fields, including the paper, textile, food, and pharmaceutical industries [4]. CMC based films find applications in food industry due transparency, water binding, and viscosity properties. Cellulose derivatives exhibit good barrier against gases with intermediate to good mechanical properties but are vulnerable to moisture [5]. Thus, the properties of CMC can be enhanced by blending with another polymer. PVP is a biodegradable polymer with excellent chemical and physical properties.

Graphene is a two-dimensional sheet of hexagonally arranged carbon with interesting physical properties. It has sparked great excitement in research field due to applications ranging from optoelectronics, to biomedicine [6]. In the last few years, it was reported that graphene oxide (GO) nanowalls exhibited strong antibacterial activity. Owing to these excellent antibacterial properties GO, it has been exploited for biomedical and environmental management applications.

The objective of current study was to fabricate GO reinforced CMC/PVP films with improved mechanical strength. The bactericidal efficiency of developed nanocomposite film was tested against S.aureus (Gram positive) and E. coli (Gram negative) by using the agar disk diffusion method.

MATERIALS AND METHODS

A. Materials

Sodium-carboxymethyl cellulose CMC (Mw = 70 kDa), Polyvinylpyrrolidone (PVP) and graphite powder were obtained from Sigma-Aldrich. Nutrient agar and mineral salt broth were procured from Himedia chemicals. All the reagents received were of analytical grade. Milli-Q ultra-pure water (Millipore, USA) was utilized in this work.

.

B. Preparation of films

The CMC/PVP film was prepared by solution casting method. Briefly, CMC and PVP were dissolved in 3:1 ratio in 50 mL of water under magnetic stirring. GO was prepared by modified hummers method as reported elsewhere. CMC/PVP/GO nanocomposite film was prepared by adding 2 wt% of GO in CMC/PVP solution (Fig.1) followed by magnetic stirring for 1 hour at 80 ^{o}C temperature. The films were obtained by casting and drying at room temperature.

C. Characterizations

FT-IR spectroscopy was conducted by Thermoscientific iS5. Morphological nature of blend and nanocomposite films were analysed by FEI SERION scanning electron microscope. The thermal stability of prepared films was evaluated by STA7200 Hitachi under nitrogen atmosphere. Transmission electron microscope (TEM) images obtained using instrument JEM 2100F. The mechanical testing was performed by Universal mechanical tester (Instron, Model 3382, USA)

D. Antibacterial Studies

The antibacterial action of the nanocomposite film was evaluated through the disk diffusion method using the Muller Hinton Agar (MHA) media for the bacterial cell growth. The antibacterial activity of the blend and nanocomposite film was tested against E.coli and S. aureus. The results were evaluated from zone of inhibition (diameter).

V. Results and Discussion

The formation of graphene oxide was confirmed by Raman spectroscopy. The FT-IR spectra of CMC/PVP (Fig. 2), exhibited a broad absorption band at 3291 cm^{-1} due to –OH stretching vibration of CMC, whereas a low-intensity band centered around 2918 cm $^{-1}$ represents the C–H asymmetric stretching vibrational mode of both the CMC and PVP chains. The presence of GO in the CMC/PVP/GO is confirmed by the peaks at 1406.49 cm^{-1} and 1730.51 cm^{-1} attributed to –COOH and -C=O groups. The shifting of O–H peak to 3339.16 cm^{-1} confirms formation of hydrogen bonding between GO and CMC/PVP.

SEM indicated good dispersion of GO in polymeric matrix which was further confirmed by TEM image which showed complete exfoliation of GO without any signs of aggregation of nanofiller. The CMC/PVP/GO nanocomposites exhibited improved mechanical strength and thermal stability as compared to CMC/PVP blend. The PVP/CMC blend exbited no zone of inhibition for against both the bacterial strains. However, PVP/CMC/GO showed significant zones of inhibition for both Gram +ve and Gram –ve strains. Its zone of inhibition was in the range of 11-14mm. Thus, the fabricated bio-nanocomposite may be considered as a potential antibacterial material.

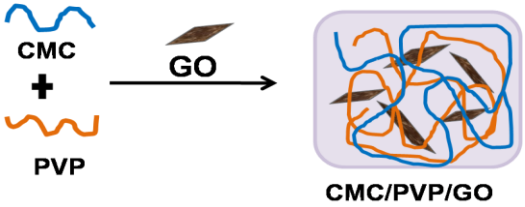

Fig. 1: Schematic of preparation of CMC/PVP/GO

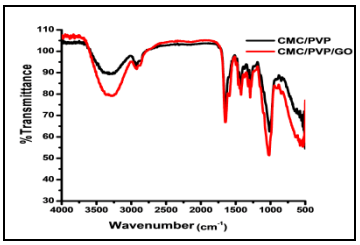

Fig. 2: FT-IR of films

VI. Conclusion

The CMC/PVP/GO nanocomposite films were fabricated by solution casting method and characterized by SEM,TEM, FT-IR, TGA. The graphene oxide reinforced nanocomposite films expressed good antibacterial activity against two bacterial strains. The nannocomposite films exhibited higher mechanical strength as comparedd to blend films. These films can potentially find applications in wound dressing and antimicrobial packaging materials.

REFERENCES

.

[1] J. H. Park, M. Ye and K. Park, “Biodegradable Polymers for Microencapsulation of Drugs”, Molecules, 10, 146, 2005.

[2] Armentano, M. Dottori, E. Fortunati, S. Mattioli and J. M. Kenny, “ Biodegradable Polymer matrix nanocomposites for tissue engineering-A review”, Polym. Degrad. Stab., 95, 2126, 2010.

[3] B. Guo, L. Glavas and A. C. Albertsson, “Biodegradable and electrically conducting polymer for biomedical application”, Prog. Polym. Sci., vol.38, 1263, 2013

[4] Song, Y., Zhou, J., Li, O., Guo, Y., & Zhang, L.. ,“Preparation and characterization of novel quaternized cellulose nanoparticles as protein carriers”, Macromolecular Bioscience, 9, 857–863, 2009.

[5] Mohammad Hossein Azizi, Mehrdad Mohammadi, and Alaleh Zoghi, “Antimicrobial activity of carboxymethyl cellulose–gelatin film containing *Dianthus barbatus* essential oil against aflatoxin”, producing molds, Volume8, Issue2, 1244-1253, 2020.

[6] F. Xia, T. Mueller, R. Golizadeh-Mojarad, M. Freitag, Y.-m. Lin, J. Tsang, V. Perebeinos and P. Avouris, “Photocurrent imaging and efficient photon detection in a graphene transistor”, Nano Lett., 9, 1039–1044, 2009.

1st International Online Conference on Emerging Smart Materials in Applied Chemistry(ESMAC-2020)
10-12 August 2020

Paper ID: 24

Liposomes as smart nanoplatform in carrying the antioxidant plant flavonoids Fisetin and 3-Hydroxyflavone

Monalisa Mohapatra *

School of Chemistry, Gangadhar Meher University, Amruta Vihar, Odisha 768004, India

E-mail: mmohapatra@gmuniversity.ac.in

***Abstract*—The antioxidant activity of antioxidants in smart carriers' like liposomes is significantly influenced by their location in the membrane and the site of generating free radicals. Depending on the extent of hydrophobicity, antioxidants are known to be located either at the membrane core region or in the interfacial head group region. The flavonoids which are known to be located in the polar surface region of the lipid bilayer can easily trap aqueous peroxyl radicals. Therefore, they are better accessible to chain-initiating radicals than the more hydrophobic antioxidants located within the membrane. The location of different prototropic forms of biologically important antioxidant excited state intramolecular proton transfer (ESIPT) molecules like 3-hydroxyflavone and fisetin, in the lipid bilayer membrane of liposomes has been studied from their different fluorescent parameters in several controlled experiments. Depending on the surrounding microenvironment these molecules exits in different prototropic forms.**

***Keywords*—Liposome, Flavonoid, ESIPT, Fluorescence, Fisetin, 3-Hydroxyflavone**

Flavonoids are important polyphenolic compounds with therapeutic activities such as antihemolysis, antiallergic, anticancer, anti-AIDS and anti-inflammatory [1-6]. In addition, they are also essential for potent antioxidant activity against a broad array of free radical mediated diseases. Flavonoids exhibit photoinduced excited state intramolecular proton transfer (ESIPT) processes which are photophysically interesting [6-11]. 3-Hydroxyflavone (3-HF) (Fig.1) is the basic structural skeleton of the naturally available flavonoids like fisetin, quercetin, robinetin etc.The location of sites for free radical generation in a lipid bilayer membrane and the availability of antioxidants in this neighborhood are crucial aspects in any study on antioxidant activity of flavonoids [12].

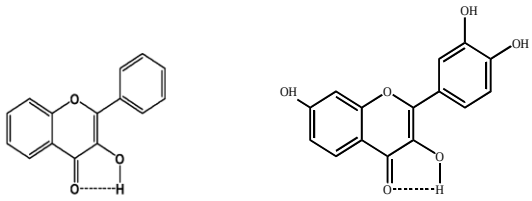

Fig. 1: Structure of 3-hydroxyflavone (3-HF) and fisetin.

Flavonoids near the interfacial region of the lipid bilayer membrane can trap the aqueous peroxyl radicals easily as compared to the flavonoids that are situated at the core region. Hence, less hydrophobic flavonoids are better available to the chain-initiating radicals than the more hydrophobic ones [13]. This paper presents a discussion on the preferential location of different prototropic forms of biologically important excited state intramolecular proton transfer (ESIPT) molecules like 3-hydroxyflavone and fisetin in liposome made of dimyristoylphosphatidylcholine (DMPC) phospholipid.

The ESIPT of 3-HF and its analogues leads to formation of phototautomer (PT) form in the excited state, whose fluorescence is red shifted compared to that of the fluorescence of the neutral form. In DMPC and egg yolk phosphatidylcholine

(EYPC) liposome membrane the existence of ground state anion (A^-) form of 3-HF has also been observed [14, 15]. The location of these prototropic forms of 3-HF is having significance to their antioxidant nature. Fluorescence studies on 3-HF in synthetic lipid membranes of DMPC and DPPC suggest that the phototautomer emission arises from the 3-HF molecules deeply buried in the hydrophobic acyl chain region of the bilayer where external H-bonding perturbation effects on the intramolecular ESPT processes are minimized [16,17].Subsequently a clear confirmation about the locations of these two species; PT and A^- has been obtained from fluorescence quenching studies using Ag^+ ion as a quencher [18]. Being hydrophilic in nature, Ag^+ ion stays near the water-accessible interfacial region of the lipid bilayer membrane, hence it should quench the form of 3-HF which stays near the interfacial region. Figure 2A shows the plot of fluorescence intensity of PT (λ_{ex} = 345 nm, λ_{em} = 535 nm) and A^-(λ_{ex} = 417 nm, λ_{em}= 490 nm) forms of 3-HF in DMPC liposomes verses Ag^+ concentration (0 M to 0.01 M). The Figure clearly shows a significant quenching in the fluorescence intensity of A^- form even at 0.002 M of Ag^+, however, the fluorescence intensity of PT form shows almost no change even at 0.01 M of Ag^+. Thus, the quenching study suggests that the preferential location of the phototautomer form of 3-HF is near the region which is not accessible to the hydrophilic Ag^+ quencher i.e near hydrophobic core, and the ground state anion locates itself at the water-accessible interfacial region of the lipid bilayer membrane [18]. This has been represented through the cartoon showing the probable location of the PT and A^- in lipid bilayer membrane (Fig. 2A).

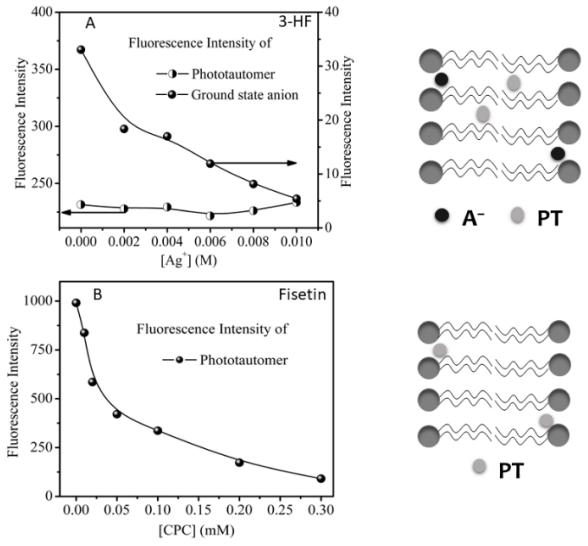

Fig. 2. (A)Plot of variation of fluorescence intensity of the PT (λ_{ex} = 345 nm) and A^-(λ_{ex} = 417 nm) forms of 3-HF in DMPC liposomes with Ag^+ concentration (0 M to 0.01 M). (B) Plot of variation of fluorescence intensity of the phototautomer form of fisetin (λ_{ex} = 370 nm) in DMPC liposomes with varying concentration of CPC (0 to 0.5 mM). Cartoon shows the probable location of the PT, A^- of 3-HF and fisetin in lipid bilayer membrane.

The intrinsic fluorescence behavior of fisetin has been used to look at its binding site (s) in egg lecithin lipid bilayer membranes [19]. As revealed by fluorescence studies, the antioxidant and antihemolytic behaviors are found to be significantly dependent on the locations of the flavonoids in the lipid bilayer membrane.The exact location of the phototautomer form of fisetin in the lipid bilayer membrane has been well understood from a fluorescence quenching study with cetylpyridinium chloride (CPC) as a quencher [20].Figure 2B represents the plot of variation of fluorescence intensity of the phototautomer form of fisetin in DMPC unilamellar vesicles with varying concentrations of CPC. The Figure shows a progressive decrease in PT fluorescence intensity with the increase in concentration of CPC [20]. The effective quenching of PT fluorescence intensity in presence of CPC suggests that the fisetin molecules are located near the water-accessible interfacial region of the lipid bilayer membrane. The location of phototautomer form of fisetin in the lipid bilayer membrane has been represented in the cartoon (Fig. 2B).

In summary, in lipid bilayer membrane of DMPC liposome, the phototautomer form (λ_{ex} = 370 nm, λ_{em} = 545 nm) of fisetin and 3-hydroxyflavone (λ_{ex}= 345 nm, λ_{em}= 535), and ground state anion (λ_{ex}= 417 nm, λ_{em}= 490 nm) of 3-hydroxyflavone are the primary emitting species.In case of 3-hydroxyflavone, the quenching study using a hydrophilic quencher Ag^+ provides strong evidence that the preferential location of its phototautomer and ground state anionform is at the hydrocarbon core and the bilayer interface regions, respectively. In case of fisetin, a fluorescence quenching study using cetylpyridinium chloride as a quencher suggests that its phototautomer form is evidently located near the bilayer interface of the liposome. The location of fisetin at the interfacial region of liposome would have some correlation with its antioxidant activity and can trap the aqueous peroxyl radicals easily.

References

1. Middleton, M. D. E., Jr. *Pharm. Biol.* 1996, 34, 344–348.
2. Cook, N. C.; Samman, S. *J. Nutr. Biochem.* 1996, 7, 66–76.
3. Gordon, M. H.; Roedig-Penman, A. *Chem. Phys. Lipids* 1998, 97, 79–85.
4. Benavente-García, O.; Castillo, J. *J. Agric. Food Chem.* 2008, 56, 6185–6205.
5. Wang, L.; Tu, Y.-C.; Lian, T.-W.; Hung, J.-T.; Yen, J.-H.; Wu, M.-J. *J. Agric. Food Chem.* 2006, 54, 9798–9804.

6. Chaudhuri, S.; Banerjee, A.; Basu, K.; Sengupta, B.; Sengupta, P. K. *Int. J. Biol. Macromol.* 2007, 41, 42–48.
7. Sengupta, P. K.; Kasha, M. *Chem. Phys. Lett.* 1979, 68, 382–385.
8. Zhu, A.; Wang, B.; White, J. O.; Drickamer, H. G. *J. Phys. Chem. B* 2004, 108, 891–894.
9. Demchenko, A. P.; Ercelen, S.; Roshal, A. D.; Klymchenko, A. S. *Pol. J. Chem*. 2002, 76, 1287–1299.
10. Parthenopoulos, D. A.; McMorrow, D.; Kasha, M. *J. Phys. Chem.* 1991, 95, 2668–2674.
11. Falkovskaia, E.; Sengupta, P. K.; Kasha, M. *Chem. Phys. Lett.* 1998, 297, 109–114.
12. Terao, J.; Piskula, M.; Yao, Q. *Arch. Biochem. Biophys.* 1994, 308, 278–284.
13. Ratty, A. K.; Sunamoto, J.; Das, N. P. *Biochem. Pharmacol.* 1988, 37, 989–995.
14. Shyamala, T.; Mishra, A. K. Photochem. Photobiol. 2004, 80, 309–315.
15. Chaudhuri, S.; Basu, K.; Sengupta, B.; Banerjee, A.; Sengupta, P. K. *Luminescence* 2008, 23, 397–403.
16. Denninson, S. M.; Guharay, J.; Sengupta, P. K. *Spectrochim. Acta Part A* 1999, 55, 1127–1132
17. Guharay, J.; Chaudhri, R.; Chakrabarti, A.; Sengupta, P. K. *Spectrochim. Acta Part A*, 1997, 53, 457–462.
18. Mohapatra, M.; Subuddhi, U.; Mishra, A. K. *Photochem. Photobiol. Sci.* 2009, 8, 373–378.
19. Sengupta, B.; Banerjee, A.; Sengupta, P. K. *FEBS Lett.* 2004, 570, 77–81.
20. Mohapatra, M.; Mishra, A. K. *J. Phys. Chem. B* 2011, 115, 9962–9970.

1st International Online Conference on Emerging Smart Materials in Applied Chemistry(ESMAC-2020)
10-12 August 2020

Paper ID:25

Synthesis and Characterization of $CaCu_3Ti_4O_{12}$ - $BaTiO_3$ – Epoxy Composite for Electronic Applications

Swagatika Mishra[1a*] and Punyapriya Mishra[2b]

[a]Department of Mechanical Engineering, Veer SurendraSai University of Technology, Burla, Odisha, India, E-mail: swagatika.mishra08523@gmail.com
[b]Department of Mechanical Engineering, Veer SurendraSai University of Technology, Burla, Odisha, India, E-mail: priya.punya@gmail.com

Abstact: Calcium Copper Titanate, $CaCu_3Ti_4O_{12}$ (CCTO) - Barium Titanate, $BaTiO_3$ (BTO) - Epoxy based polymer-ceramic composites are fabricated and characterized for electronic applications. CCTO is well-known for its high dielectric constant value. At the mean while, it shows a very high dielectric loss. In order to suppress the dielectric loss in CCTO, BTO has been incorporated with it, as it possesses high dielectric constant with a low dielectric loss. The CCTO-BTO-Epoxy based hybrid composites has been fabricated by varying the weight % ratios of CCTO and BTO ceramic materials under a constant weight % of epoxy matrix phase. Later on, the effect of frequency on the dielectric property of the fabricated hybrid composites at room temperature has been studied by taking frequency variation from 100 Hz to 1 MHz range. Eventually, the effect of hybrid filler on the dielectric property, electrical conductivity, and XRD of composite has been studied. The experimental data indicates a positive hybrid effect on dielectric property. In addition, there is a decrease in dielectric constant and dielectric loss has been obtained with increase in frequency for a fixed ceramic composition. In future, there is scope in study of surface morphology along with property evaluation under different surface modification.

Keywords—polymer-ceramic composite, Calcium Copper Titanate, Barium Titanate, dielectric property, ceramic

Miniaturization of electrical and electronic devices has raised its demandforhigh-performance light-weight materials for its design and manufacturing. Energy storage devicessuch as a capacitor, batteries, etc. play an important rolein electronic industries as it stores electric energy. Dielectrics are mainly used in capacitors to acquire the same electric charge with low voltage when placed

between two conducting plates. So, it raised a serious challenge to develop a dielectric material for capacitors with high dielectric constant and low dielectric loss. So far, four kinds of materials, namely anti-ferroelectrics, dielectric glass-ceramics, relaxor ferroelectric, and polymer-based ceramics are thought to be more likely used in next-generation capacitors and have been widely studied [1].Electro-ceramicsare well known for their outstanding electrical, thermal properties, and high-temperature stability. However, lacking of flexibility restricts its applicability. Hence polymer is used as an alternative solution to overcome that limitation.By combining these two materials, one may be able to develop a polymer ceramic composite which possesses properties high dielectric constant, high breakdown field, low processing temperature with good processability, flexibility, and low cost [2-3].

There are several electro-ceramicshave been widely used as dielectric materials due to their high dielectric constant. However, considering the environmental factors, lead-free ceramics are more preferred in contrast to other electro ceramic materials. Improving the synthetic technology and dielectric properties of these lead-free electro-ceramic materials is a current focus of research and development in the area of materials chemistry. The lead-free high dielectric constant calcium copper titanate, $CaCu_3Ti_4O_{12}$ (CCTO), and its isomorphs have attracted much attention for the development of promising capacitor materials for electronic industries [4-9]. Insulating polymers like

polyethylene, polyimide, silicone, epoxy resin, etc. has been widely used as packaging materials because of their superior electric performance and low-temperature processability with other materials [10-11].Recently, several researchers have adopted hybrid composites in which two or more than two fillers can use as areinforcement which enhances the properties and performance of the composites as compared to single filler [12-13].

The present study develops and investigates the dielectric properties of Calcium copper titanate ($CaCu_3Ti_4O_{12}$, CCTO) and Barium titanate ($BaTiO_3$, BT) hybrid filler reinforced epoxy composites for capacitors. Despite the high dielectric strength of CCTO, it also possesses high dielectric loss, which limits its potential application in the electronic industry. To compensate for this high dielectric loss of CCTO, BT is used as a secondary filler material, which also hasa high dielectric constant but not as compared to CCTO [13]. Five different compositions for ceramic fillers (100:0, 60:40, 50:50, 40:60, 0:100) have been chosen with constant ceramic to polymer ratio (20:80). Well-crystallized particles of CCTO and BT are obtained using a conventional solid-state synthesis route. $CaCu_3Ti_4O_{12}$ - $BaTiO_3$ – EpoxyComposites are fabricated using hand lay-up and compression moulding process. Later on,theeffect of frequency on the dielectric property of the composites has studied at room temperature by taking frequency variation from 100 Hz to 1 MHz range. Besides, phase and microstructure of the composites are also analysed.

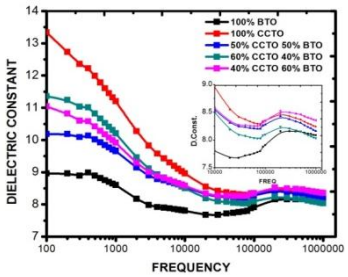

Figure-1. Dielectric constant versus frequency graph for [(CCTO-BT)-Epoxy] composites at room temperature

The present study summarizes that [(CCTO-BT)-Epoxy] compositesare verysuccessful material for a capacitor and other electronic applications as compared to single filler epoxy composites. XRD patterns of [(CCTO-BT)-Epoxy] composite samples show the presence of both CCTO and BT ceramic samples separately. [(CCTO60-BT40)-Epoxy] composite samples show the highest value of εr~ 11.35 at 100 Hz, which is three-time larger than the dielectric constant of epoxy without any ceramic filler (εr~ 4). However,[(CCTO50-BT50)-Epoxy] composite sample shows the lowest dielectric loss tanδ~ 0.07 and the highest conductivity in contrast to other compositions.

References

[1] D. S.Saidina, M. Mariatti, and M. J. Julie. "Dielectric properties and thermal properties of calcium copper titanate and barium titanate hybrid fillers filled epoxy thin film composites for electronic packaging applications." Journal of Materials Science: Materials in Electronics 26, no. 8, pp. 6245-6251,2015.

[2] C. J. Dias and D. K. Das-Gupta, in Ferroelectric Polymer and Ceramic-Polymer Composites, edited by D. K. Das-Gupta ~Trans Tech Publications Ltd., Switzerland, p. 217,1994.

[3] C. J. Dias and D. K. Das-Gupta,"Inorganic ceramic/polymer ferroelectric composite electrets." IEEE Transactions on dielectrics and electrical insulation, 3(5), pp. 706-734, 1996.

[4] PedroDuran, Dionisio Gutierrez, Jesus Tartaj, and Carlos Moure. "Densification behaviour, microstructure development and dielectric properties of pure BaTiO3 prepared by thermal decomposition of (Ba, Ti)-citrate polyester resins." Ceramics international 28, no. 3, pp. 283-292, 2002.

[5] Zhong-Feng Zhang, Xiao-FeiBai, Jun-Wei Zha, Wei-Kang Li, and Zhi-Min Dang. "RETRACTED: Preparation and dielectric properties of BaTiO3/epoxy nanocomposites for embedded capacitor application."100-105, 2014.

[6] M. A.Subramanian, Dong Li, N. Duan, B. A. Reisner, and A. W. Sleight."High dielectric constant in ACu3Ti4O12 and ACu3Ti3FeO12 phases." Journal of Solid State Chemistry 151, no. 2, pp. 323-325, 2000.

[7] C. C. Homes, T. Vogt, S. M. Shapiro, S. Wakimoto, and A. P. Ramirez. "Optical response of high-dielectric-constant perovskite-related oxide." science 293, no. 5530, pp. 673-676, 2001.

[8] Elizabeth K.Michael, and Susan Trolier-McKinstry. "Cubic pyrochlore bismuth zinc niobate thin films for high-temperature dielectric energy storage." Journal of the American Ceramic Society 98, no. 4, pp. 1223-1229, 2015.

[9] LalithaSirdeshmukh, K. Krishna Kumar, S. BalLaxman, A. Rama Krishna, and G. Sathaiah. "Dielectric properties and electrical conduction in yttrium iron garnet (YIG)." Bulletin of Materials Science 21, no. 3,pp. 219-226, 1998.

[10] Ying-Ling Liu, Yu-Lo Lin, Chih-Ping Chen, and Ru-Jong Jeng. "Preparation of epoxy resin/silica hybrid composites for epoxy molding compounds." Journal of applied polymer science 90, no. 14, pp. 4047-4053, 2003.

[11] Yu-Mao Chen, and Jyh-Ming Ting. "Ultra high thermal conductivity polymer composites." Carbon 40, no. 3, pp. 359-362, 2002.

[12] Behzad. Kord"Effect of calcium carbonate as mineral filler on the physical and mechanical properties of wood based composites." World applied sciences journal 13, no. 1, pp. 129-132, 2011.

[13] D. S. Saidina, M. Mariatti, and M. J. Julie. "Dielectric properties and thermal properties of calcium copper titanate and barium titanate hybrid fillers filled epoxy thin film composites for electronic packaging applications." Journal of Materials Science: Materials in Electronics 26, no. 8, pp. 6245-6251, 2015.

1st International Online Conference on Emerging Smart Materials in Applied Chemistry(ESMAC-2020)
10-12 August 2020

Paper ID:26

Synthesis and charecterization ofAl-Fly ash composite via powder metallurgy method

Dinesh Kumar Mishra[1a]*and R.P. Dalai[2b]

[a]Department of Metallurgical and Materials Engineering, Veer SurendraSai University of Technology, Burla, Odisha, India, E-mail id: dinesh.igit@gmail.com

[b]Department of Metallurgical and Materials Engineering, Veer SurendraSai University of Technology, Burla, Odisha, India, E-mail id: dalai.renu@gmail.com

***Abstract*—The objective of this present study is about the microstructures, hardness and wear characteristics of fly ash reinforced aluminum matrix composites. The composites of varying fly ash content from 15-20 wt% are prepared by powder metallurgy route. The synthesized composites are sintered at three different temperatures as 575, 600, and 625 ^{0}C. Then, the SEM micrographs are revealed the non-homogeneous distribution and clustering of fly ash particles along with porosities in the Al matrix. The measured Vickers hardness value is increased with the increase in fly ash content from 15 to 20%. However, it is also observed that for both 15 and 20% reinforcement, with increase in the sintering temperature from 575 to 625^{0}C, hardness of the composites increases by 9.23%, 10.58% and 11.37% respectively. The observed wear resistance of the composited are increased with the increase in both sintering temperature and fly ash content.**

Keywords—Aluminum, Fly Ash, Composite, Sintering temperature, Hardness

Aluminium has a wider number of potential applications in the field of aerospace, automotive industries, and in the design of various structural components like doors, windows, complex sections, and solar panels, etc. due to its excellent machinability, high strength to weight ratio, greater malleability, and ductility [1, 2]. In the meantime, they are failing to provide enough wear resistance, hardness, tensile and compressive strength that limits its wider applicability [3, 4]. So to improve those properties in particular hardness and wear resistance, various reinforcement materials such as SiC [5], Al_2O_3[6, 7], TiC [4], TiO_2[8] and B_4C [9],etc. have been used earlier. However, the current researchesare more concerned on the utilization of waste and inexpensive materials preferably fly ash (FA) [5, 10, 11].Apart from low cost, FA also has excellent wettability and low density [10, 11]. Earlier several researchers have been reported on synthesis of Al-FA composites using different methods [12-14]. In the present study, we have been synthesized Al-FA composite using powder metallurgy route and further have done the scanning electron micrography, hardness test, and wear test to reveal the effect of FA composition and sintering temperature on the developed composites' behavior.

A fine mixture of Al-FA mixture is prepared usinga planetary ball mill (Model-Retsch PM 200) at a constant speed of 250 rpm for 30 min. Then the milled powders are compacted inKBrhydraulic press to prepare the pellets which are undergone for sintering in a muffle furnace at three different temperatures as 575, 600, and 625 ^{0}C for 1 hr. The SEM micrographs are obtained by SU3500, Hitachi model. The Vickers hardness test is conducted ina universal hardness tester. The wear test is done with the help of a pin on disc set-up.

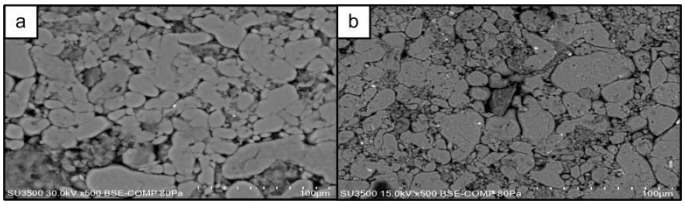

Fig-1. SEM micrographs of Al reinforced with (a) 15% (b) 20% FA before sintering.

Fig. 1 is shown the SEM micrographs of Al-FA composites before sintering. The increase in FA content, there a decrease in porosity content is observed (refer to **Fig. 1**). Then after sintering the SEM analysis is revealed the appearance of a more compact structure due to the development in intermolecular bonding along with non-uniform distribution. The measured Vickers hardness value is increased with the increase in fly ash content from 15 to 20%. However, for the both 15 and 20% FA reinforcement, the Vickers hardness value increases by 9.23%, 10.58% and 11.37% with an increase in the sintering temperature from 575 to 625^0C respectively.Eventually, the wear test results arealso shown a similar trend as hardness, and maximum wear resistance is observed for Al-20% FA at 625 ^{0}C.

So from the present study, the following conclusions can be drawnas the SEM micrographs of sintered composites are revealed the non-uniform distribution and clustering of fly ash particles along with porosities in the Al matrix. Further, the observed hardness trend is increased for both the increase in sintering temperature and FA content. The wear resistance of the compositesisalso increased in a similar trend as hardness with the increase in both sintering temperature and fly ash content. The optimum wear resistance is obtained for Al-20% FA composite that is sintered at 625 ^{0}C temperature.

References

[1] P.Shanmughasundaram, R. Subramanian, and G. Prabhu. "Some studies on aluminium–fly ash composites fabricated by two step stir casting method." European journal of scientific research, vol. 63, pp. 204-218, 2011.

[2] I.Adeqoyin, F. A. Mohamed, and E. J. Lavernia. "Particulate reinforced MMCs-A review." J. Mat Sci, vol. 26, pp. 1137-1156, 1991.

[3] Y.Sahin, and S. Murphy. "The effect of fibre orientation of the dry sliding wear of borsic-reinforced 2014 aluminium alloy." Journal of materials science, vol. 31, pp. 5399-5407, 1996.

[4] S.Gopalakrishnan,and N. Murugan. "Production and wear characterisation of AA 6061 matrix titanium carbide particulate reinforced composite by enhanced stir casting method." Composites Part B: Engineering, vol. 43, pp. 302-308, 2012.

[5] M. M. Boopathi, K. P. Arulshri, and N. Iyandurai. "Evaluation of mechanical properties of aluminium alloy 2024 reinforced with silicon carbide and fly ash hybrid metal matrix composites." American journal of applied sciences, vol. 10, pp. 219, 2013.

[6] A.Wagih, "Synthesis of nanocrystalline Al 2 O 3 reinforced Al nanocomposites by high-energy mechanical alloying: microstructural evolution and mechanical properties." Transactions of the Indian Institute of Metals, vol. 69, pp. 851-857, 2016.

[7] K.Kanthavel, K. R. Sumesh, and P. Saravanakumar. "Study of tribological properties on Al/Al2O3/MoS2 hybrid composite processed by powder metallurgy." Alexandria Engineering Journal, vol. 55, pp. 13-17, 2016.

[8] M. Ravichandran, M. Meignanamoorthyand S.Dineshkumar."Microstructure and Properties of Hot Extruded Al-TiO2 Powder Metallurgic Composites."In Applied Mechanics and Materials, vol. 852, pp. 130-135, 2016.

[9] H. Guo, Y. Zhao, S.Xu, J. Li, N. Liu, Y. Zhang, and Z. Zhang. "Influence of high B4C contents on structural evolution of Al-B4C nanocomposite powders produced by high energy ball milling." Ceramics International, vol. 45, pp. 5436-5447, 2019.

[10] R. Palanichamy, J.Lakshmipathy, B.Kulendran, and M. Vairavel. "Mechanical Characteristics of Fly Ash Reinforced Aluminium Metal Matrix Composite-Art of Review." International Journal of Advanced Research in Engineering and Technology, vol. 10, pp. 122-129, 2019.

[11] B.Admile, S. G. Kulkarni, andS. A. Sonawane, Review on mechanical & wear behavior of aluminum-fly ash metal matrix composite. International Journal of Emerging Technology and Advanced Engineering, vol. 4, pp. 863-866, 2014.

[12] S.Sarkar, S. Sen, S. C. Mishra, M. K. Kudelwar, and S. Mohan. "Studies on aluminum—fly-ash composite produced by impeller mixing." Journal of reinforced plastics and composites, vol. 29, pp. 144-148, 2010.

[13] E.Marin, M.Lekka, F.Andreatta, L.Fedrizzi, G.Itskos, A.Moutsatsou, N.Koukouzas, and N.Kouloumbi, "Electrochemical study of Aluminum-Fly Ash composites obtained by powder metallurgy." Materials Characterization, vol. 69, pp. 16-30, 2012.

[14] K. N. P.Prasadand M. Ramachandra, "Determination of abrasive wear behaviour of al-fly ash metal matrix composites produced by squeeze casting." Materials today: proceedings, vol. 5, pp. 2844-2853, 2018.

Department of Chemistry
School of Applied Sciences,
KIIT Deemed to be University, Bhubaneswar-751024,
Odisha